An assessment of the impacts of space heating electrification and future space cooling in the buildings of UK

Meng Zhang

Submitted in fulfilment of the requirements for

the Degree of Doctor of Philosophy

James Watt School of Engineering

College of Science and Engineering

University of Glasgow

February 2024

Abstract

This thesis provides a comprehensive examination of the space heating and cooling demand modelling in the UK, linking crucial issues in energy policy with the practicalities of demand forecasting. At its core, the research develops a cohesive methodology that marries the deterministic accuracy of physical models with the predictive agility of ANNs, setting a new standard for energy demand estimation. The research marks a departure from conventional methods, embracing advanced modelling techniques that enhance the prediction and management of energy requirements.

Key findings from this integrated approach reveal that the UK's transition to a decarbonised heating sector will significantly increase electricity demand, highlighting the
essential role of energy storage in reducing pressure on the power grid. The work demonstrates that precise and expedient modelling is crucial for providing robust data support to energy policymakers and operators, helping to create quick and well-informed energy strategies. Moreover, the thesis conducts a comprehensive analysis of future cooling demands and the corresponding requirements for diverse cooling technologies. In doing so, it charts potential scenarios for cooling equipment needs, preparing stakeholders for shifts in consumer demand patterns. Additionally, the thesis delves into the performance of neural networks within the context of energy prediction, illustrating their efficacy and potential to transform the landscape of energy demand forecasting.

Through this investigation, the thesis contributes to a nuanced understanding of energy demand, aiding the development of energy policies and infrastructures that are not only sustainable but also adaptive to the pressing demands of climate change and technological evolution. This work lays a foundational blueprint for future research initiatives aimed at optimising energy systems and underscores the importance of integrating varied modelling techniques to achieve greater accuracy and efficiency in energy demand forecasting.

Acknowledgements

Dedicated to my dearly beloved father, a beacon of strength in my darkest times. His battle against death following a tragic accident has imparted lessons of perseverance and hope that resonate through every page of this thesis. Though he can no longer read my words, his silent encouragement deeply infuses this work, guiding me through each step of this journey.

I would like to express my deepest gratitude to my supervisor, Prof. Zhibin Yu, for the unwavering support and guidance. At many points along this journey, the end seemed distant, not solely due to the academic rigor, but more so because of the personal tribulations that arose from a significant family ordeal. Prof. Yu's profound empathy and steadfast support provided a steadying force amidst the chaos. Without his generous academic guidance, compassionate ear, and the personal time he offered for me to work through life's unexpected challenges, I might have relinquished my pursuit. Undoubtedly, I count myself incredibly fortunate to have encountered supervisor who excel not only in academics but also in character. I would also like to extend my deepest gratitude to my industrial supervisor, Prof. James Yu, from Scottish Power, whose guidance has been a constant thread throughout my academic and professional journey. In many ways, he has not only served as an academic and career mentor but a life mentor as well, and his guidance and support have been invaluable, especially during pivotal moments. Prof. Zhibin Yu and Prof. James Yu have played an instrumental role in shaping both my academic and personal growth. For them, it may be a daily routine to extend their kindness and help to every young individual facing challenges, but for me, it has been a rekindling of the light. Their willingness to stand by me, ready to help at any turn, was a beacon of hope that illuminated my path forward.

I would also like to extend my heartfelt gratitude to my co-supervisor Dr Jing Yang, whose invaluable insights and assistance in the field of integrated energy system have been greatly appreciated. His valuable insights and willingness to provide assistance have left an indelible mark on my academic path. I am also profoundly thankful to the senior colleagues during the early stages of my academic career, Dr Guopeng Yu and Prof. Youcai Liang, who have since left our group and risen to associate professors and professors. Their guidance was particularly invaluable during moments of doubt and uncertainty in my doctoral studies. Their unwavering support and encouragement not only bolstered my confidence but also shaped my approach to academic challenges. I would also like to extend my

heartfelt thanks to Dr Michael-Allan Millar whose guidance in building simulation and energy optimization was invaluable. A special thanks goes to Dr Si Chen and Dr Yaxing Ren for their guidance in neural networks and paper writing, skills crucial for my research. My gratitude extends to every member who has joined or is still part of our group, including Dr Ruiping Zhi, Dr Hongyang Li, Dr Andrew Mckeown, Dr Geng Chen, Dr Saif Fraih K Alshammari, Dr Nan Zhang, Dr Zahra Hajabdollahi Ouderji, Dr Kadam Sambhaji, Dr Sarath Babu Kaki, and many others whose support and collaboration enriched my research experience.

I must also express my deep appreciation for Dr Qingwen Pang, a dear friend from my undergraduate days and my former class leader. Although she has never been officially involved in my academic career by now, her private support and academic advice have been immensely helpful. I am particularly grateful to Ms Heather Lambie, Ms Julia Deans, and the entire administrative team at Glasgow University for their extraordinary support, especially during the challenging period following my father's incident. Their compassion, understanding, and efficiency during that difficult time were more than just professional courtesy. I am grateful to everyone I have encountered during my academic journey. Each person has left an indelible mark on my path, contributing to my growth both as a researcher and as an individual. This journey has been enriched by your diverse perspectives, support, and camaraderie.

Beyond the journey of academia, my personal life has been equally graced by countless individuals whose support and kindness have been pivotal. I would like to first and foremost thank my mother, whose support and sacrifices are beyond the power of any words to convey. Her relentless strength has not only provided me with a safe haven to pursue my studies but also absorbed many of the stresses and challenges that I should have faced. This journey is as much hers as it is mine, a shining tribute to her unwavering love and sacrifice. Clearly, reaching this point in my journey would have been impossible without the unwavering support of my extended family. I am equally grateful to each and every member of my family for their invaluable encouragement, love, and belief in me and my mother.

Additionally, there are individuals who, though not connected by blood, have become cherished members of my heart's family. Their presence in my life has created bonds as strong and meaningful as any kinship. I must express my profound gratitude to Prof. James Yu’s wife, Dr Jie Zheng, a remarkable individual who has become more than just a mentor to me. During my time in the UK, her unwavering care and attention have been a source of comfort, infusing my days with the warmth

of a home away from home. I am profoundly grateful to Aunt Wang, Uncle Yang, and other close friends of my father for their extraordinary support during my most challenging times. Their belief in me, a continuation of my father's own trust and friendship, was a guiding light that helped me navigate through adversity.

Finally, I am deeply indebted to my friends who have been with me through different stages of my life. Together, we have navigated life's ups and downs, and their support has been a healing presence throughout these challenging years of my doctoral studies. I am grateful to friends Qing Yuan, Yachun Cao, and Keying Ji, whose unwavering friendship has been a source of comfort and strength since our childhood. I also extend my heartfelt gratitude to all my high school friends, whose memories have been a constant source of joy and support. And to Xiaoyu Chen, another cherished friend from my university days, whose companionship has been a profound source of solace, especially in times when both my father and I needed it most. I am also grateful to Shuang Sun, who provided unwavering support when I was in Shanghai accompanying my hospitalised father. Equally, I am grateful to Jiaxiu Xu, a special friend whose presence in my life has been nothing short of a blessing. Her support and understanding have provided not just comfort, but also a sense of belonging and strength during my most trying times. Each one of them has played a pivotal role in soothing my soul and accompanying me through life's key moments. Thank you for your steadfast friendship and for being the pillars upon which I lean.

Contents

List of Abbreviations

AC	Air Conditioning
ANN	Artificial Neural Network
BEIS	Department for Business, Energy and Industrial Strategy
BPNN	Back Propagation Neural Network
BPTT	Backpropagation Through Time
BUS	Boiler Upgrade Scheme
CaRB	Carbon Reduction in Buildings
CCC	Climate Change Committee
CCHP	Combined Cooling, Heat and Power
CDD	Cooling Degree Day
CDH	Cooling Degree Hour
CfD	Contracts for Difference
CHP	Combined Heat and Power
CIBSE	Chartered Institute of Building Services Engineers
CNN	Convolutional Neural Network
COP	Coefficient of Performance
COP21	Climate Change Conference
CRNN	Convolutional Recurrent Neural Network
CV-RMSE	Coefficient of Variation of the Root Mean Squared Error
DB	Design Builder
DHI	Diffuse Horizontal Irradiance
DNI	Direct Normal Irradiance
DNN	Deep Neural Network
DT	Decision Tree
EER	Energy Efficiency Ratio
EHS	English Housing Survey
ELM	Extreme Learning Machine
EMR	Electricity Market Reform

ESO	Electricity System Operator
ETYS	Electricity Ten Year Statement
FS	Feature Selection
GA	Genetic Algorithms
GB	Gradient Boosting
GDP	Gross Domestic Product
GGR	Greenhouse Gas Removal
GHI	Global Horizontal Irradiance
GRU	Gated Recurrent Unit
GSA	Gravitational Search Algorithm
HUG	Home Upgrade Grant
HVAC	Heating, Ventilation, and Air-Conditioning
IPCC	Intergovernmental Panel on Climate Change
KDE	Kernel Density Estimation
KNN	K Nearest Neighbor
LAD	Local Authority Delivery
LASSO	Least Absolute Shrinkage and Selection Operator
LMSR	Linear Model Stepwise Regression
LPG	Liquid Petroleum Gas
LR	Linear Regression
LSTM	Long Short-Term Memory
MAE	Mean Absolute Error
MAPE	Mean Absolute Percentage Error
MASE	Mean Absolute Scaled Error
MCD	Method of Characterization Decomposition
ML	Machine Learning
MLR	Multiple Linear Regression
MSE	Mean Squared Error
MSPD	Method of Spatial Homogenization Decomposition
NB	Naive Bayes
NETS	National Electricity Transmission System
NIHCS	Northern Ireland House Condition Survey
NMBE	Normalised Mean Bias Error
PB	Proposed Benchmark

ReLU	Rectified Linear Unit
RF	Random Forest
RMSE	Root Mean Square Error
RNN	Recurrent Neural Network
SAP	Standard Assessment Procedure
SHCS	Scottish House Condition Survey
sMAPE	Symmetric Mean Absolute Percentage Error
SVM	Support Vector Machine
TMY	Typical Meteorological Year
UKCS	UK Continental Shelf
WHCS	Welsh Housing Conditions Survey
WMO	World Meteorological Organization
WRF	Weather Research and Forecasting
XGB	Extreme Gradient Boosting Techniques

List of Figures

List of Tables

List of publications

Meng Zhang, Michael-Allan Millar, Zhibin Yu, James Yu, An assessment of the impacts of heat electrification on the electric grid in the UK, Energy Reports, Volume 8, 2022, Pages 14934-14946

Meng Zhang, Michael-Allan Millar, Si Chen, Yaxing Ren, Zhibin Yu, James Yu, Enhancing hourly heat demand prediction through artificial neural networks: A national level case study, Energy and AI, Volume 15, 2024, 100315

Declaration

I hereby declare that this thesis, conducted at the James Watt School of Engineering, University of Glasgow, is predominantly my own work. Except for cited references, all research and writing are my original efforts. I acknowledge and adhere to the University of Glasgow's policy on plagiarism, ensuring academic integrity in this submission.

Meng Zhang

January 2024

Chapter 1

Introduction

1.1 Background

The World Meteorological Organization (WMO) has released a report stating that there is a 66% chance that the average global temperature near the Earth's surface will exceed pre-industrial levels by at least 1.5°C for a year between 2023 and 2027. Additionally, there is a 98% probability that one of the next five years, as well as the entire five-year period, will be the hottest ever recorded [1]. Global warming is causing extreme weather events across the world, resulting in significant negative impacts on the environment, economy, and people.

Europe is experiencing the most rapid increase in temperatures compared with other continents. In 2022, Europe endured extreme heat, droughts, and wildfires. In addition, sea surface temperatures around Europe reached record highs, accompanied by marine heatwaves. Meanwhile, Asia has also faced increasing occurrences of extreme weather and the effects of climate change, including alternating periods of drought and floods in 2022, leading to immense human suffering and economic losses [2]. The melting of ice and glaciers, and rising sea levels, further pose a threat to future socio-economic disruptions. Recent

reports by the WMO confirm these alarming trends [3]. Therefore, the Paris Agreement was embraced by 196 Parties during the Climate Change Conference (COP21) held in Paris, France, on December 12, 2015. Its primary objective is to address the issue of global climate change. Additionally, it establishes objectives for reducing worldwide greenhouse gas emissions in order to keep the global temperature increase below 2℃ and strives to limit it to 1.5℃ [4].

The Intergovernmental Panel on Climate Change (IPCC) has found that emissions from fossil fuels are the dominant cause of global warming [5]. In 2018, 89% of global CO2 emissions came from fossil fuels and industry [6]. Coal, as a fossil fuel, is the most polluting energy source, contributing more than 0.3 ℃ to the 1 ℃ increase in global average temperatures. When oil is burned, it releases a significant amount of carbon, accounting for approximately one-third of the world's total carbon emissions. While natural gas is often touted as a cleaner alternative to coal and oil, it is still a fossil fuel and contributes to a fifth of the world's total carbon emissions [7]. According to the IPCC, to limit global warming to 1.5°C above pre-industrial levels, fossil fuel emissions must be reduced by half within the next 11 years [8]. The Glasgow Climate Pact was adopted by nations in 2021 with the goal of transforming the 2020s into a decade focused on climate action and support. This agreement urges nations to gradually reduce the use of unchecked coal power and eliminate ineffective subsidies for fossil fuels [9].

The UK government has committed to achieving Net Zero Carbon by 2050 [10]. This target, based on the latest scientific evidence and recommended by the Climate Change Committee (CCC), is the first of its kind in a major economy. The government is fully committed to implementing ambitious decarbonisation measures across various sectors. However, it is also mentioned by the government that achieving net zero does not mean eliminating emissions by 2050. Some sectors pose challenges in terms

of complete decarbonisation. To compensate for the residual emissions from these difficult-to-decarbonise sectors, it is crucial to employ greenhouse gas removal (GGR) techniques or indirect approaches [11].

While steady progress has been made in other sectors, heat poses a unique challenge. The Department for Business, Energy and Industrial Strategy (BEIS) acknowledged in their 2018 report "Clean Growth - Transforming Heating" that decarbonising the heating sector poses a unique challenge compared to other significant energy-consuming sectors of the economy [12]. In 2016, heating accounted for 37% of the total greenhouse gas emissions in the UK, making heat a critical energy sector for decarbonisation [12]. The heat demand of the building accounts for the majority. The UK has approximately 30 million buildings, collectively contributing roughly 30% of its national emissions. The primary source of these emissions is heating, accounting for 79% of buildings' emissions and approximately 23% of all emissions in the country [13].

Energy consumption in buildings is essential for various purposes such as heating, cooling, cooking, and providing hot water. Although the electricity used for lighting and appliances is rapidly becoming cleaner, most buildings still depend on fossil fuels for heating, hot water, and cooking [14]. Space heating for buildings accounts for approximately 25% of the UK’s energy demand, while this proportion is higher in high-latitude regions, such as Scotland [15].

Delivering low-carbon residential heating is widely regarded as a formidable challenge due to its significant scale and substantial costs. In 2019, the CCC reported that there are around 29 million households in the UK. The magnitude of the challenge is made more complex due to the UK's housing stock is among the oldest and least insulated in Europe. Approximately only 15% of the existing stock

has been built since 1990 [16]. In 2017, the gas grid provided heating to the majority (85%) of residential buildings through a boiler and wet-based central heating system. The remaining 15% of homes relied on alternative heating fuels such as oil, liquid petroleum gas (LPG), or electric heating, as they were not connected to the gas grid [17].

According to projections from the UK Energy Research Centre in October 2020, it is anticipated that most homes will remain standing in 2050. To achieve the net zero target by 2050, it is estimated that one million homes will need to undergo retrofitting annually for the next three decades [18]. To achieve decarbonization of household heating, the UK is focusing on three eco-friendly technologies: heat pumps, hydrogen, and district heating [19]. The 6th Carbon Budget Report by the CCC predicts that by 2050, all residential heating will be sourced from low-carbon options. This will primarily involve 52% utilization of heat pumps, 42% reliance on district heating, around 5% utilization of hydrogen boilers, and approximately 1% adoption of new direct electric heating [20].

As heating accounts for one-third of the UK's total emissions, researchers have been working for years to mitigate the impact of the nation's cold winters. Historically, buildings in the UK have been designed to be warm and airtight, thus providing effective insulation during winter months. However, this approach has inadvertently led to overheating during summer [21].

The recent "State of the UK Climate 2020" report reveals that the effects of global warming are already being experienced in the UK, with the average temperature between 2011 and 2020 being 1.1°C higher than the 1961-1990 average [22]. Space cooling accounts for approximately 20% of the electricity demand in buildings worldwide. Residential cooling is currently the largest contributor to global cooling

demand[23]. A 2016 study found that air conditioning (AC) is responsible for about 10% of the total electricity demand in the UK, mostly in non-residential buildings such as offices. The usage of AC in the UK has been estimated to increase by around 2% per year from 2012 to 2019. However, due to the limited availability of regular data collection, the demand for cooling is often estimated using modeling techniques [24].

A POST note issued by the UK Parliament states that around 20% of homes in the UK are currently overheated, even in mild summers, resulting in increased heat-related illnesses and deaths [25]. The emergence of extreme weather events undoubtedly indicates that overheating will become a widespread throughout the UK, posing significant health risks [26]. The global electricity demand for space cooling will have doubled, with cooling energy demand likely to equal heating energy demand by 2060 [27].

1.2 Problem Statement and Research Scope

A number of technologies (e.g. low carbon heat networks, hydrogen and heat pumps) have been proposed to support the decarbonisation of heat to 'net zero' by 2050. Considering the rapid uptake of renewable electricity generation, electrification is likely to be the dominant method for the decarbonisation of heat in the future [28]. The most promising low-carbon heating technologies are all electrical based, which can place significant strain on local electricity infrastructure. As the Boiler Upgrade Scheme (BUS) project moves forward, more heat pumps will be installed in domestic buildings [29]. However, there is currently very little understanding of how the electrification of heat will affect the resilience of the electrical grid in the lead to 2050. This makes the predictions of heat demand an important milestone on the path to the net-zero emission targets. In particular, a high-resolution and rapid response model for heating demand prediction is necessary to provide policymakers with essential data support.

Many research methods for heating demand estimation for different purposes or scenarios have been proposed. Annual energy demand estimation is commonly used in the UK for general economic analysis. However, annual energy demand estimation does not assess the dynamic nature of power networks. In addition, the annual estimation cannot achieve the analysis of a short time horizon, which is incapable of capturing the daily or even hourly peak demand. A higher level of granularity (a high-resolution model) is necessary for analysing the power system operation. A high-resolution model allows stakeholders to assess the impact of shorter changes (e.g., 30 minutes) on a network, which becomes increasingly important as heat is electrified due to the large portion of demand that heat makes up. If electricity is not correctly managed, the increased load can lead to infrastructure damage (e.g., network overload) and power outages.

Most energy policy research in the UK has traditionally focused on space heating, reflecting the country's cooler climate. This focus has resulted in a substantial gap in understanding and policymaking regarding cooling, especially within the domestic sector. The oversight of cooling in energy policy and research is stark, with data on cooling demand in the UK being particularly scarce. This lack of data can be primarily attributed to the historical absence of widespread cooling systems in residential buildings, as opposed to commercial structures, where such systems are more prevalent.

However, the situation is rapidly evolving due to climate change. As global warming leads to increasingly warmer temperatures, the need for effective cooling solutions in residential areas is becoming more obvious and urgent. This shift necessitates an evaluation of energy policies to include the growing importance of domestic cooling. Estimating and understanding domestic cooling demand is no longer a

peripheral issue but an issue of vital importance. The future of UK energy policy must pivot to recognise the growing importance of residential cooling. This includes investing in research to fill data gaps, revising building regulations to improve energy efficiency in cooling, and considering the health and social implications of increased temperatures. Addressing these challenges is vital for a sustainable and resilient energy future despite global warming.

1.3 Major Contributions

This thesis integrates physical and data-driven models in the specific context of predicting heating and cooling demands, with a significant focus on the application of Artificial Neural Networks (ANNs). This confluence represents a pivotal development in the realm of energy forecasting, marrying the established principles of physical models with the sophisticated analytical prowess of data-driven methodologies. Central to this thesis is an examination of how this integration enhances the accuracy and efficiency of heating and cooling demand predictions. Physical models, which are rooted in the understanding of thermodynamics and building physics, provide a fundamental framework for capturing the intricacies of heat and cooling dynamics in various environments. The incorporation of ANNs introduces a new dimension of predictive capability, leveraging their ability to process vast datasets and identify complex, nonlinear relationships inherent in energy usage patterns.

This thesis investigates the dynamic and adaptive nature of these integrated models, emphasising their critical role in navigating the challenges of energy forecasting in an era marked by climate change, urbanization, and evolving energy practices. The ability of these models to adjust to varying environmental conditions and predict heating and cooling demands with heightened precision is underscored as being particularly valuable. A substantial portion of the thesis is devoted to exploring the

wider implications of this integrative approach in the field of energy forecasting. This includes its impact on developing more accurate and efficient energy policies, its utility in urban planning for designing energy-efficient buildings and infrastructures, and its significance in the development of sustainable energy systems that can adapt to future needs and constraints. This integrated approach not only elevates the precision and depth of understanding in energy demand forecasts but also holds considerable promise in shaping energy strategies and infrastructure to meet the demands of an increasingly complex and variable energy landscape.

Moreover, the thesis highlights the potential of these predictive models to inform the development and deployment of energy storage technologies. By understanding the peaks and valleys of energy demand, particularly in heating and cooling, energy storage systems can be utilised more effectively. This not only aids in balancing the load on the grid but also ensures that renewable energy can be stored and used when it is most needed, thereby enhancing overall grid reliability and sustainability.

In essence, the thesis presents a comprehensive view of how the fusion of physical and ANN-based models in heating and cooling demand forecasting is vital not only for precision in predictions but also for advancing the goals of grid stability and sustainable energy usage. This holistic approach is key to addressing the multifaceted challenges of modern energy management, paving the way for a more sustainable, efficient, and environmentally friendly energy future.

Advanced Forecasting Models for Heating and Cooling Demands

i. High-Resolution Heat Demand Forecasting Model:

This model is pivotal in revolutionising the way heating demands are forecasted on a national scale. By offering hourly predictions, it captures intricate fluctuations in heat demand with unprecedented accuracy. This level of detail is essential for tailoring energy distribution strategies and effectively managing peak loads, particularly during high energy usage seasons. The model's nuanced understanding of energy requirements plays a crucial role in the broader context of electrification of heating systems. As nations move towards greener energy solutions, this model provides the necessary insights to facilitate this transition, ensuring energy efficiency and minimizing carbon footprint.

ii. Urban Cooling Demand Model:

Similarly, the cooling demand model brings a high level of detail and specificity to city-wide cooling assessments. This model integrates diverse data sources, including physical building characteristics and economic factors, to provide a multifaceted analysis of urban cooling needs. This is particularly relevant considering increasing urban heat island effects and global temperature rises. By accurately forecasting cooling demands, this model aids city planners and policymakers in developing strategies to mitigate the strain on electricity grids during peak periods. It also informs the design of energy-efficient buildings and urban layouts that naturally reduce cooling needs.

Innovative Use of ANNs in Energy Forecasting

i. ANN-Based Heating and Cooling Demand Prediction Model:

The use of ANNs in this model represents a significant stride in the field of energy forecasting. These networks excel in processing large, complex datasets, learning from them, and making accurate predictions about future heating demands. The adaptability of the ANN model to various climatic and geographic conditions makes it a versatile tool. Its predictive power is not limited by regional variations, making it an invaluable asset in global energy management.

ii. Weather Data-Driven Predictions:

Reliance on weather data as a primary input for the ANN model significantly streamlines the forecasting process. It circumvents the challenges associated with gathering and processing large amounts of building-specific data, thereby enhancing the model's scalability and applicability.

Enhancing Grid Stability through Sustainable Energy Solutions

i. Energy Storage Systems for Balanced Demand Management:

The critical role of energy storage systems, as highlighted in the studies, addresses the challenge of matching energy supply with fluctuating demands. These systems are essential for stabilising the grid, particularly during periods of peak demand, which are becoming more frequent and intense due to climate change. These systems facilitate the use of renewable energy by storing excess energy generated during periods of low demand (such as solar energy during sunny days) and releasing it during high-demand periods (like cold winter evenings), thereby ensuring a consistent and stable energy supply.

ii. Scenario Analysis for Future Energy Planning:

The scenario analysis provided in the heat demand study is a key tool for future-proofing energy infrastructure. By considering a range of future scenarios, including the potential impacts of extreme weather events and the move towards full electrification, this analysis helps prepare for a range of eventualities, ensuring that energy systems remain resilient and adaptable despite future challenges.

1.4 Thesis Outline

Chapter 2: Literature review

Chapter 2 starts with a detailed literature review, dissecting the current and prospective energy scenarios in the UK, thereby setting a pertinent stage for subsequent analyses. This study is supplemented

by an exploration of physical and statistical modeming techniques in space heating demand, with a particular emphasis on the application of ANNs, thereby bridging the gap between theoretical modelling and practical application. The chapter concludes with a comparative analysis of the modelling techniques employed for both heating and cooling demands, showcasing the nuances and intricacies inherent in each approach.

Chapter 3: Theory and methodology

Chapter 3 focuses on the basic theories and methods used in this research. It starts by explaining the basics of building simulation, showing how this approach helps predict heating and cooling demand in buildings. Then, the chapter introduces theory of different types of neural networks, and discusses how they improve the accuracy and efficiency of predicting energy demands. Each method is clearly explained, showing how it is applied and why it is effective. This chapter links the theories discussed to the practical tools that will be used in the later analysis.

Chapter 4: Building Simulation for Space Heating Demand

The third chapter transitions to a pragmatic examination of building simulation for space heating demand. It meticulously analyses the regional classification and building typologies pertinent to the UK's heating demand, integrating meteorological data, building construction parameters, and heating system dynamics into the simulation process. The chapter culminates in a comprehensive "Results and Discussion" segment, where simulation outcomes are critically analysed and interpreted, highlighting their implications in the context of energy forecasting.

Chapter 5: ANN for Space Heating Demand

In Chapter 5, the focus is on the utilization of ANNs for space heating demand forecasting. A thorough exposition of ANN methodologies, including backpropagation networks and feature selection strategies, sets the stage for a detailed case study. This case study meticulously delves into the specifics of ANN topology, training data, and model evaluation techniques, culminating in a results and discussion section that critically evaluates the ANN's predictive performance.

Chapter 6: Building Simulation for Space Cooling Demand

Chapter 6 mirrors the structure of Chapter 3, albeit with a concentrated focus on building simulation for space cooling demand. It scrutinises the building stock specific to London's cooling demand, incorporating detailed discussions on meteorological data and building features, culminating in a results and discussion section that rigorously analyses the cooling demand simulations.

Chapter 7: ANN for Space Cooling Demand

Chapter 7 explores the application of ANNs in space cooling demand forecasting. This chapter distinguishes itself by its in-depth examination of various neural network architectures, including recurrent neural networks and long short-term memory networks. A case study is presented, focusing on the parameterization, training, and evaluation of these networks, followed by a results and discussion section that critically assesses the networks' performance in the context of cooling demand forecasting.

Chapter 8: Conclusion and Future Works

The final chapter succinctly synthesises the key findings of the research, presenting a cogent conclusion that encapsulates the thesis's contributions to the field. It also proposes avenues for future research, thus extending the scope and applicability of the current study.

Chapter 2

Literature review

2.1 Energy in the UK

This section provides an analysis and summary of the current state of energy in the UK based on government data, reports, policies, and other literature. As the aim of this research is to provide future energy scenarios, a literature review of the current state of energy in the UK as well as policy is necessary.

2.1.1 State of UK’s energy

Energy in the UK is derived from a various source and serves different purposes. It is used for electricity, heating, and transportation across various sectors, including domestic, business, and industrial. The production of energy in the UK involves the use of different fuels and technologies. The UK is both a producer and a consumer of energy. It extracts oil and gas, which are pivotal to its energy portfolio, and generates electricity from various of sources [30]. Despite this production in the UK, the UK's demand for energy surpasses what it can produce, leading to the importation of energy to fill the gap, thus making the UK a net importer of energy [31].

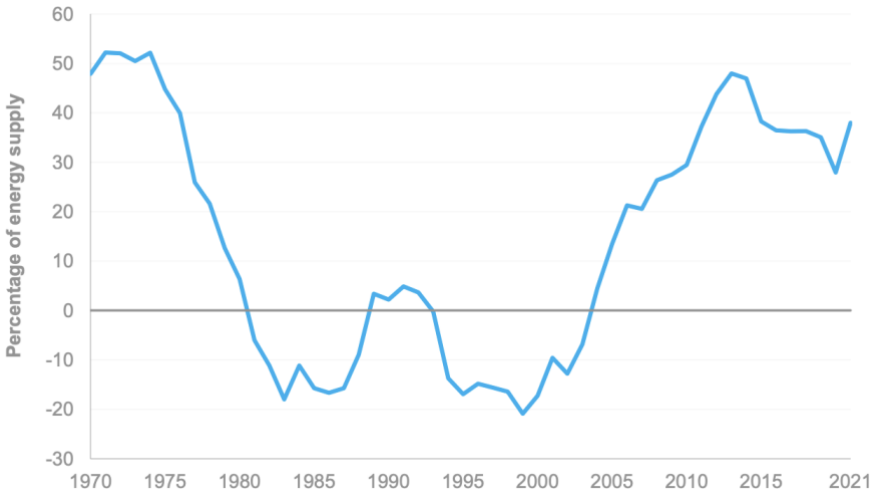

Figure 2-1 Import dependency of UK energy from 1970 to 2021 [32]

As shown in Figure 2-1, in the historical context of the UK's energy sector, the 1970s marked the nation's status as a net importer of energy [32]. This paradigm shifted dramatically with the exploitation of North Sea oil and gas resources, catapulting the UK to a net exporter position in 1981. However, this trend experienced a downturn in the late 1980s due to of the Piper Alpha disaster, causing a temporary reversion to net importer status until a resurgence in the mid-1990s. The zenith of North Sea production was attained in 1999, after which a decline ensued, leading to the UK's reversion to a net importer of energy by 2004. A notable shift occurred in 2013, when the UK began importing more petroleum products than it exported, primarily due to the cessation of operations at the Coryton refinery. Despite this, the UK managed to re-establish itself as a net exporter of primary oils in 2020 for the first time since 2004, while also continuing to export certain petroleum products like petrol and fuel oil [33]. By 2021, imported energy would account for 38% of the UK's consumption, a significant increase from the previous year and the highest proportion since 2015. This escalation was largely attributed to the relaxation of COVID-19 restrictions, which spurred an uptick in energy demand, and was compounded by diminished production from the UK Continental Shelf (UKCS) due to maintenance activities, necessitating increased

imports to satisfy the heightened demand [32]. The energy that the UK should import is mainly petroleum and natural gas, but it also includes a small proportion of electricity.

The specific fuels used for energy consumption in the UK are diverse. Natural gas, for instance, is predominantly used for heating purposes, taking advantage of its efficiency and availability. Petroleum, on the other hand, remains a staple in the transportation sector, powering vehicles, airplanes, and ships. The electricity that powers everything from homes to factories in the UK is generated through a mix of technologies—traditional fossil fuels, nuclear power, and a growing array of renewable sources such as wind and solar energy.

Table 2-1 Final energy consumption in the UK in 2021[34]

2021					Million tonnes of oil equivalent
	Industry	**Domestic**	**Transport**	**Services[1]**	**Total**
Coal & manufactured fuels	1.3	0.5	0.0	0.0	**1.8**
Gas	9.2	27.4	0.1	7.9	**44.6**
Oil	2.6	2.5	41.0	3.7	**50.3**
Electricity	7.3	9.4	0.5	7.4	**24.6**
Bioenergy and heat	2.4	1.4	1.5	1.7	**7.0**
Total	**22.8**	**41.1**	**43.6**	**20.7**	**128.2**

As shown in Table 2-1, in 2021, the final energy consumption across various sectors in the UK will be presented in million tonnes of oil equivalent. The industry sector consumed 22.8 million tonnes, with the majority being gas at 9.2 and electricity at 7.3. The domestic sector had a higher total consumption of 41.1 million tonnes, predominantly from gas at 27.4 and electricity at 9.4. The transport sector, with the highest oil consumption at 41.0 million tonnes, had a total energy consumption of 43.6 million tonnes. The services sector used 20.7 million tonnes, mainly from gas (7.9) and electricity (7.4). Overall, the total UK energy consumption was 128.2 million tonnes of oil equivalent, with oil and gas being the most consumed energy sources at 50.3 and 44.6 million tonnes, respectively. Specifically, electricity

consumption totalled 24.6 million tonnes across all sectors and constituted approximately 19.2% of the total energy consumption [34].

2.1.2 Energy policies in the UK

Indeed, while electricity accounts for a smaller fraction of the UK's total energy consumption, it is crucial to highlight that approximately 30% of the natural gas consumption in 2021 was allocated to electricity generation [32]. This represents a significant share of gas usage, second only to its role in heating. Furthermore, the decarbonization of the transport system in the UK is increasingly reliant on electric vehicles, which are considered to be one of the most promising avenues for reducing carbon emissions in the transportation sector. The transition to electric vehicles is a key component of the UK's broader strategy to achieve net-zero emissions, reflecting the pivotal role of electricity in the country's sustainable energy future. Therefore, the UK's energy policy is centreed on electricity, extending across various sectors, progressively subdividing into detailed strategies. It starts with decarbonising each sector and moves towards establishing a robust and secure energy infrastructure.

The decarbonization of electricity and its utilization as a lever to decarbonise other sectors has been a cornerstone of the UK's energy policy frameworks in recent times. The Electricity Market Reform (EMR) was introduced ten years ago [35]. Launched with the Energy Act 2013, the EMR aims to address the energy trilemma by introducing the Capacity Market and Contracts for Difference (CfDs) mechanisms to balance energy supply and support low carbon infrastructure [36]. The "energy trilemma" is a pivotal concept in energy policy, encapsulating the challenge of simultaneously achieving three key objectives: sustainability, security, and affordability. It emphasises the need for a balanced approach in transitioning to environmentally friendly energy sources (decarbonising energy) while ensuring that energy supplies

remain reliable and secure against disruptions. At the same time, it underscores the importance of keeping energy costs manageable for consumers, ensuring that the transition to sustainable energy does not impose undue financial burdens. The Energy Act 2013 was enacted to ensure the smooth progression of decarbonization while guaranteeing the reliability and affordability of energy supplies. In 2016, BEIS and Ofgem proposed the establishment of a smart, flexible energy system, which included the integration of smart homes. This includes the implementation of time-of-use pricing, which encourages energy consumption during off-peak hours, and the establishment of appliance standards that facilitate automation [37]. The 2017 Clean Growth Strategy, a government report required under the Climate Change Act of 2008, aimed at decarbonising all economic sectors. It announced a series of energy sector-related policies, including those enhancing energy efficiency and backing new technologies, which were pivotal to progressing toward carbon budget goals. The document mentions the necessity to improve housing by reducing carbon emissions in homes and introducing low-carbon heating technologies such as heat pumps. This includes the implementation of time-of-use pricing, which encourages energy consumption during off-peak hours, and the establishment of appliance standards that facilitate automation [38]. The Energy White Paper, initially planned for 2019 but delayed due to the coronavirus pandemic, was eventually published by the UK government in December 2020 [39]. This refers to the detailed policy outlined by the Secretary of State for BEIS, Greg Clark, in his 2018 Trilemma speech [40]. Recognising electricity as crucial for decarbonising the economy, the government has set ambitious targets for offshore wind (40GW by 2030) and floating offshore wind (1GW), alongside the expansion of other low-cost renewables. The commitment also includes support for at least one large-scale nuclear project and investment in innovative technologies such as fusion power. The White Paper reiterates existing policies such as the Future Homes Standard and aims for a significant number of homes to reach EPC (Energy Performance Certificates) Band C by 2035. It also extends existing schemes for energy

efficiency and sets heating targets. This includes promoting diverse sustainable heating technologies such as heat pumps and biomethane and exploring innovative options such as hydrogen as a potential heating source [39].

In addition to the aforementioned policies, there are many other policy reports in the energy sector concerning the economy or energy security. The Cost of Energy Review was launched by BEIS in August 2017 and was overseen by Professor Dieter Helm. The aim of this study was to provide suggestions on reducing consumer energy expenses and limiting state involvement in the energy market [41]. In November 2020, the government introduced the Ten Point Plan for a Green Industrial Revolution. This comprehensive strategy highlights government funding for multiple green initiatives, with the goal of generating employment opportunities and reducing carbon emissions [42]. The Interim Report by HM Treasury on Net Zero focuses on the financial consequences of the UK's shift towards achieving net-zero emissions. It sheds light on the economic worries related to public expenditure and maintaining competitiveness [43]. Powering up Britain in 2023 is a comprehensive strategy by the UK Government, focusing on enhancing energy security, exploiting economic opportunities in the energy transition, and achieving net-zero emissions. The initiative emphasises the diversification of energy sources, investment in renewable technologies, and fostering economic growth through sustainable practices [44].

The government has also implemented numerous schemes for the decarbonization of buildings. The Energy Company Obligation (ECO) scheme allows obligated energy suppliers to install energy efficiency measures, such as insulation or replacement heating systems, in low-income and vulnerable households [45]. The Home Upgrade Grant (HUG) and the Local Authority Delivery (LAD) schemes in England are designed to fund energy efficiency upgrades and low-carbon heating for low-income households.

Currently, homes off the gas grid are eligible for funding under HUG Phase 1, while those on the gas grid can receive funding through LAD Phase 3 [46], [47]. Previous phases of LAD catered to both on- and off-gas grid homes. The Boiler Upgrade Scheme (BUS) provides grants to assist with the installation of renewable heating systems in domestic and small non-domestic properties in England and Wales. Under this scheme, property owners can receive a grant of £5,000 towards the cost and installation of biomass boiler, £7,500 for an air source heat pump or a ground source heat pump [48].

2.1.3 Summary

The UK's energy policy is progressively advancing, focusing on the decarbonization of energy, energy economy, and energy security. Electricity decarbonization, as the forefront sector, is becoming the backbone of the future energy network. With the increasing use of electricity in decarbonization efforts, the security and stability of electric power supply are becoming increasingly significant. The Electricity System Operator (ESO) has addressed grid upgrade plans in its Electricity Ten Year Statement (ETYS), presenting a perspective on future transmission needs and the capacity of Great Britain's National Electricity Transmission System (NETS) over the next decade [49].

In the context of heating, the UK government has been actively promoting the adoption of low-carbon heating technologies such as heat pumps, which are more energy-efficient and have a lower carbon footprint than traditional fossil fuel-based heating systems. This transition is particularly pertinent given the high demand for heating during the winter months, which historically contribute significantly to the nation's carbon emissions and energy consumption. As residential heating shifts towards electrification, there is a growing need to ensure that the electricity grid can handle the increased load, especially during peak demand.

On the other hand, cooling systems, which are essential for comfort during warmer months, have not been prominently featured in energy policy discourse. However, as climate change leads to warmer average temperatures, the demand for cooling is expected to rise, potentially increasing electricity use and peak demand during summer months. Efficient and sustainable cooling solutions, such as passive cooling design, energy-efficient air conditioners, and the use of renewable energy sources for cooling, will become increasingly important. Moreover, the integration of cooling systems with smart energy management technologies could contribute to a more flexible and demand-responsive grid. Evaluating the UK's energy policy regarding heating and cooling is vital for future research and development. Understanding how these technologies affect the capacity and function of the electricity grid is crucial for maintaining energy security and achieving the nation's goals for net-zero emissions.

2.2 Modelling of the Space Heating Demand

2.2.1 Physical and economic data-based models

There are many methods for estimating heating demand in different sectors. Physical models based on the conservation of heat are a common method for predicting heat. Outdoor temperature, indoor temperature, building heat loss, etc. would be taken into account in the physical model. Cholewa et al. developed a method for short-term forecasting of heat power for space heating, which may be easily applied in existing buildings [50]. Hietaharju et al. proposed a physical model for urban heat demand based on Newton's cooling law [51]. Clegg et al. adopted building simulation to obtain the GB half-hourly heat demand profile in high-quality [52]. Mavrogianni et al. infer the characteristics of London buildings through the geographic information system and then estimate the heat demand using a unified approach [53]. The Scottish government’s heating demand map uses a similar method to forecast the annual heating

demand in different regions in Scotland [54]. In addition, EE-Delta also presents research on the heating demand estimation in Scotland [55]. In this study, Scotland was divided into six regions and the building stock of each region was estimated. This method can realise heat estimation in large areas, however, the granularity of the EE- delta study also focuses on the annual heating demand. Heat demand can also be related to social metrics. Watson et al. developed a half-hourly domestic heat demand model for the UK by considering the outdoor air temperature and the effects of the socioeconomic status of customers [56]. McCallum et al. investigated the long-term UK energy demand, and the model takes into account physical information as well as human behaviour [57]. The conclusion drawn from the paper is that energy demand can be influenced by human behaviour while policy can affect human behaviour during the long term. The importance of scenario analysis in energy demand estimation was highlighted by Eggimann et al. In addition to the classification of scenarios, scenario analysis includes changes in population, improvement in technologies and so on[58]. Research on the heat demand of low-energy dwellings shows that building fabric can affect building performance[59]. Six key factors suggested by Beckmann et al. to affect heat demands are population and stock of building, building size and type, physical characteristics of the building, weather conditions, customer status and heating choice[60].

In practice, there are now several well-established building simulation software based on energy conservation that can provide more accurate heat predictions for buildings. Building simulation is one of the primary methods to estimate heat demand due to the significant role the built environment plays in demand balancing. Using computational building models requires the collection of environmental and building parameters (e.g., external air temperature, glazing ratio, construction type). This method can be difficult to scale nationally due to the limitless number of variations found in practice. Therefore, it is most often used to solve heat estimation in a small-scale area e.g., a small number of buildings. These

areas could be several buildings or groups of buildings, such as a university campus or hospital. For large-scale heat demand estimation (e.g. across a town or city), building simulation is seldom used.

Another commonly used method is to break down the energy consumption for space heating and hot water based on fuel usage. The UK government considers the end use of energy for four scenarios each year: domestic, service, industry and transport[61]. Natural gas accounts for 80% of the heating energy in the UK, and the data on natural gas consumption are complete and easy to obtain. Based on this, Sansom et al. estimated the hourly heat consumption of the UK in 2010[62]. They used the collected gas consumption data from 19 condensing gas boilers and 52 micro-Combined Heat and Power (CHP) systems every half hour as a database, and plotted the curve related to hourly heat demand and temperature. The daily consumption of national natural gas is broken into every half hour. This method is simple and easy to operate, and the estimated results include the influence of personnel activities. Watson et al. collected the gas data from 6000 dwellings around the UK. The temperature-heat curve is obtained and extended nationwide [56].

2.2.2 Machine learning method

In energy demand estimation methods, machine learning (ML) based models can make fast and accurate predictions after being trained using large amounts of data. ML can make more reliable predictions than other statistical or physical methods, which can significantly reduce labour costs and time consumption [63]. Therefore, the application of ML in the energy sector has grown exponentially over the past decade, especially in forecasting electricity demand and renewable power generation, such as solar and wind power[64], [65]. ML energy prediction has also been increasingly applied to building energy consumption [66]. Singaravel et al. designed a data-driven model for the design stage of buildings,

in which specific data from similar circumstances can be reused [67]. Singh et al. proposed that enrichment is more effective than increment in decreasing the generalization for early-stage building energy prediction and developing an efficient data collection approach [68]. Kurek et al. analysed heat demand forecasting for district heating (DH) systems using various ML methods [69], [70]. Deng et al. compared the statistical and ML prediction model with publicly available building energy data from US commercial buildings [70]. Chen et al. used the University of Glasgow campus as a case study, using ML in place of physical models to predict the heat demand of the campus quickly and accurately [71]. The Extra-Trees Regressor and Extreme Learning Machine algorithms were used individually and coupled in a heat prediction model for district heating systems [72]. Olu-Ajayi et al. developed an annual prediction model for residential buildings in the design stage using ANN, Gradient Boosting (GB), Deep Neural Network (DNN), Random Forest (RF), Stacking, K Nearest Neighbor (KNN), SVM, Decision tree (DT) and Linear Regression (LR) [73].

The ANN-based method is one of the most popular forecasting methods for energy planning models, and it has been used to predict energy consumption at both the district level and national levels [74]. ANNs have extensive applications at the district level and are renowned for their high accuracy. Conversely, national-level predictions typically concentrate on forecasting annual demand based on economic data. Geem et al. developed an ANN model based on population, Gross Domestic Product (GDP) and energy consumption data to predict the annual energy demand for South Korea [75]. Liu et al. proposed an annual energy prediction model for different sectors in Spain with an ANN and grey neural network according to three different GDP growth scenarios (optimistic, baseline and pessimistic) [76]. Luo et al. designed a prediction framework for multiple building energy loads with different machine-learning methods and the ANN-based model has the best accuracy and is less time-consuming [77].

Elbeltagi et al. designed a user-friendly interface based on the ANN algorithm to calculate the heating and cooling consumption of any building with the need for building physical characteristics and location [78]. Li et al. proposed an ANN-based model using the method of characterization decomposition (MCD) and the method of spatial homogenization decomposition (MSHD), which can be used to predict buildings with complex architectural forms [79]. Kannari et al. developed prediction models based on ANN for different types of buildings [80]. Bünning et al. enhanced the accuracy of a daytime ANN model using online corrections [81]. Parfenenko et al. forecasted the daily heat demand of district-heated public sector buildings based on an ANN model [82]. Li et al. designed an ANN-based building energy model with transfer learning for one hour ahead energy prediction based on the data from the Building Genome Project, which has a better performance for information-poor buildings by taking advantage of rich data from other buildings [83]. Seyedzadeh et al. proposed that choosing the right method for building energy prediction is important by analysing methods of ANN, SVM, Gaussian-based regressions and clustering [84]. Singaravel et al. proposed a faster and more accurate model for predicting heating demand based on Energy Plus model data using a component-based ML algorithm [85]. Nutkiewicz et al. proposed a Data-driven Urban Energy Simulation framework that combines ML with building simulation [86]. Algorithm application or development of ML is the most attractive topic in building load prediction, but it is still a challenge to realise automation in the industry. In the meantime, more research on the effects of climate change on buildings' energy performance using ML approaches is necessary [87].

Monitoring heating demand is not as simple as using electricity meters and the meter for heat is not widely used today. As mentioned in many pieces of research, the real demand data for heat are not easily accessible. It can be found that not all buildings have advanced building automation systems. In addition, the heating is always provided by different technologies and multiple sources, which increases the

difficulty of measurement. As real data on the heating demand of district heating systems are more accessible than those in a national area, forecasts of heating demand are mostly concentrated on district heating systems. The availability of high-resolution data at the district level is a contributing factor to this phenomenon. In addition, construction data of buildings, such as wall and window insulation, are comparatively easier to collect at the district level. Nonetheless, it should be noted that not all district-level heating systems have monitoring systems installed, leading some studies to rely on the construction of physical models to obtain high-resolution data. Therefore, in many investigations training data are derived from building simulations, especially for the early design of a building.

2.2.3 Feature selection

However, a lack of data exists not only in the case of heat demand data or building data but also in the case of meteorological data. That is also the reason why ML is used less for heating demand forecasting in reality. The meteorological data of recent years are more complete and include more data types. However, there are fewer data types in the historical meteorological database. This gap would result in ML methods built on current meteorological data types not being able to train with historical meteorological data that misses some data types. Therefore, feature selection methods are used to extract more sensitive meteorological data from the database to train ML models. In this way, the trained ML model can use fewer types of meteorological data and incorporate historical data into the training dataset. The complexity of predicting future meteorological conditions and heat demand can also be reduced, thus making heat demand forecasting more reliable and achievable. In particular when applied to ML models, some inputs can bring perturbation to the system. Seyedzadeh et al. made specific tunings to several popular ML algorithms and compared the performance of the tuned model with that of the original model through sensitivity analysis [88]. Potočnik et al. combined feature extraction and various ML methods to

develop a multi-step short-term heat demand forecasting model for district heating (DH) systems [89]. Zhang et al. proposed a new approach for feature selection by combining three global sensitivity analyses, Pearson, Sobol' and PAWN, with RF. The Gravitational Search Algorithm (GSA) based feature selection method is significantly better than the feature extraction method principle component analysis in predicting settlement in tunnel applications [90]. Shen et al. proposed a feature selection method based on sensitivity analysis that is applicable to SVM. This method assesses the importance of a selected feature by calculating the total value of the absolute difference between the probability output of an SVM on the feature space with or without the feature [91]. Hana et al. developed a wrapper feature selection method for supervised learning based on Sobol' global sensitivity analysis. RF and a set of published data were used to validate this feature selection method and the proposed feature selection significantly improved the accuracy of the predictions [92]. Becker et al. applied global sensitivity analysis to select variables in Regression Models and a competitive novel model selection method based on the 'Pantula-principle' was obtained [93]. Guo et al. combined correlation analysis with the Least Absolute Shrinkage and Selection Operator (LASSO) method to select optimised feature sets for a building energy prediction model which includes four different ML methods: MLR, SVR, BPNN and Extreme Learning Machine (ELM) [94]. Eseye et al. also combined ML with feature selection to develop a model for predicting the heating demand of a specific building [95], [96]. Li et al. developed a prediction model with support vector regression (SVR), linear model stepwise regression (LMSR), distance-weighted K-nearest neighbours (KNN) and Naive Bayes (NB) for electricity and heating demand on campus and select the optimised feature set to improve the model by using Particle Swarm Optimization and Genetic Algorithms (GA) [96]. Salcedo-Sanz et al. improved the accuracy of wind energy predictions with a new packaging method for feature selection [97]. Ahmad et al. designed a prediction model for district energy consumption by comparing several different feature selection methods [98], [99].

2.2.4 Summary

Physical models are well-established and based on energy conservation principles, providing accurate heat predictions for buildings. The model is used primarily for small-scale estimations due to the significant role of the built environment in demand balancing. It requires detailed environmental and building parameters, making it difficult to scale nationally due to the vast variability in building types and characteristics. Machine learning models require substantial and accurate data and can efficiently create demand profiles using training datasets from physical models or building simulations, but their effectiveness is contingent on data availability. The heating demand monitoring system calculates heat demand by monitoring supply and return temperatures. It provides real demand data but not widely used due to the lack of widespread heat metering, The high-resolution data necessary for such monitoring is more accessible at the district level, where data are easier to collect. However, not all heating systems have the required monitoring systems in place， especially in the UK. Consequently, the effectiveness of these models at a national level is constrained by the limited data, which impedes the ability to conduct. For large-scale heat demand estimations encompassing cities or entire countries, economic data-based models are commonly employed due to their capacity to handle extensive datasets over broad geographic areas. These models typically draw from economic data, such as fuel prices, income levels, and historical consumption patterns, to project annual heat demand. economic data-based models also do not account for micro-level variations such as individual building characteristics or local climate conditions, all of which can significantly influence actual heat usage. As decarbonization progresses and different energy sectors become more interconnected, there is a clear need for long-term forecasting beyond what economic data-based models can offer, indicating a gap in current modelling capabilities for national-scale, high-resolution heat demand forecasting.

2.3 Modelling of the Space Cooling Demand

2.3.1 Data driven model

The most popular data-driven method is the use of machine learning to predict cooling demand. Geekiyanage et al. analysed data from 30 buildings, including factors such as shape and orientation, and correlated it with the building cooling demand, to construct a regression model predicting cooling demand for Sri Lankan flats [100]. Vaghef et al. proposed an advanced Cochrane-Orcutt estimation approach, merges multiple linear regression with a seasonal autoregressive moving average model for precise Combined Cooling, Heat and Power（CCHP）system load demand forecasting[101]. Aghdaei et al. developed linear regression models to predict annual thermal loads in residential buildings across three major climates in New South Wales, Australia [102]. Waite et al developed a simple and general regression model based on electricity consumption, cooling degree hour (CDH) and population to predict cooling demand in different regions of the world [103]. Wang et al. used sensors to collect environmental data from a project studio in a university in Hong Kong and estimated cooling demand using a traditional model, which was then trained into an ANN model [104]. Dulce-Chamorro et al. employed ANN, support vector machines (SVM), and extreme gradient boosting techniques (XGB) algorithms to forecast hospital chiller energy consumption using data from the hospital's Building Management Systems (BMS) [105]. Leung et al. applied the Levenberg-Marquardt algorithm to predict the electrical demand for building cooling at a Hong Kong university, incorporating meteorological data, air unit schedules, and occupancy power demand into the model [106]. Huang et al. used back propagation neural network (BPNN), long-short term memory (LSTM), and encoder-encoder LSTM dynamic models to predict residential cooling demand in the U.S, comparing their performances using data from smart Wi-Fi thermostats [107].

Another data-based model employs traditional statistical or mathematical methods for cooling demand prediction, although these studies have been less frequent recently compared with machine learning. Koo et al. developed a mathematical model that can be used for building cooling and heating requirements using a four-node-based Lagrangian finite element method to simplify the physical model-based building simulation approach to a mathematical model. Thefinite element method converts continuous problems into discrete problems using a numerical-analysis method such as algebraic or polynomial equations [108]. Koo et al. also developed a nine-node-based Lagrangian finite element model for estimating the heating and cooling demand of a residential building with a different envelope design. The results show that the performance of the nine-node model outperforms that of the four-node model for both cooling and heating predictions [109]. Since all large cooling systems are on record in Geneva, Chambers et al. extracted the office building address, area, and Coefficient of Performance (COP) of the cooling system, electricity consumption, and average annual operating hours from publicly available data provided by the government. A mathematical model was constructed using a Monte Carlo approach to estimate the cooling demand of Swiss offices to verify the effect of glazing on cooling demand [110]. Chambers et al. also utilised the Monte Carlo method to estimate Swiss service sector's cooling demand considering climate change, differentiating their model by categorising buildings by type and age. They also incorporated new parameters such as the presence of active cooling equipment and cooling area, and simulated climate change by altering the cooling degree day (CDD) [111].

2.3.2 Economic data-based model

With the effects of global warming, the impact of climate on cooling demand is a hot research area, with increasing numbers of studies combining the CDD methodology with economic factors to predict cooling demand in future scenarios. Various models based on the CDD approach are the most common

of theeconomic data-based models. Jakubcionis et al. studied the correlation between cooling demand and meteorological conditions in the US due to insufficient European data, identified cooling indicators, and estimated the space cooling demand for European domestic buildings accordingly [112]. The same methodology was applied to forecast the European service sector's space cooling demand, with Jakubcionis et al. refining the estimate by classifying buildings based on usage due to the sector's increased complexity [113]. Falchetta et al. determined CDD distribution by analysing historical sub-Saharan climate and data and calculating overall energy demand from household cooling equipment use and CDD [114]. Laine et al. developed a model to forecast and analyse the global demand for cooling based on socio-economic and climatic inputs under different scenarios, the core of which is the CDD method [115]. Morakinyo et al. investigated the cooling demand during extreme hot weather in Hong Kong using the CDD method [116]. Day et al. used the CDD approach to annually estimate London's cooling demand, considering the city's building sizes, cooling system efficiency, and potential future scenarios [117]. Bezerra et al. employed CDD calculations to evaluate Brazil's cooling demand by combining regional and population data and analysed its variations under different global warming scenarios [118].

Another economic data-based model estimates future cooling demand by collecting regional or national data on energy consumption, efficiency, economic growth and so on. The model can be bottom-up such as estimating the cooling demand per square meter and the total floor area, or top-down such as breaking down the total energy usage to different scenarios. Rehfeldt et al used a bottom-up model to estimate industrial space heating in Europe, where the final energy demand for space heating and cooling results from the activity, employees and specific energy demand per square meter of floor area [119]. Werner et al. evaluated the cooling demand for service and residential buildings in eight European

countries, using average specific demands, building floor areas, and saturation rates for space cooling [120]. Pardo et al. determined Europe's heating and cooling demands in domestic, services, and industrial sectors using published official data. They continuously break down the total data based on sector-specific energy consumption percentages and energy source efficiencies [121]. Sachs et al. introduced a GIS-based approach that generates global heat density maps from data such as total energy consumption, population density, and weather conditions. These maps help identify energy consumption of each end-user within the energy density bands determined by K-means clustering [122].

2.3.3 Physical model

Physical models based on heat conservation principles are essential tools in engineering. Parameters such as outdoor temperature, indoor temperature, and building heat loss are variables that are factored into the physical model, which can influence the heat exchange between a building and its environment. Therefore, there are many building simulation software developed based on physical principles which can be used to estimate the energy consumption of a building. In addition, other factors affecting the energy demand of a building have been studied. Pappaccogli et al. used TRNSYS to simulate an Italian building's cooling demand, integrating the Weather Research and Forecasting/Urban (WRF/Urban) approach for enhanced meteorological data accuracy [123]. Xiong et al. utilised DeST software to forecast China's future cooling demand, employing a bottom-up model that represents various climate types and dwellings through selected typical Chinese cities and buildings. Like most similar software, DeST requires meteorological data, building structures, and Heating, Ventilation, and Air-Conditioning (HVAC) system operation information [124]. Cox et al. utilized TAS software to analyse the impact of varying future weather files on the accuracy of building cooling energy demand predictions. The study found that despite coarse weather files being sufficient for annual energy demand predictions, their accuracy diminishes for

daily or monthly predictions when air temperatures approach the heating or cooling balance point [125]. Allegrini et al. suggested an enhancement to building energy modelling methodology. This study measures the impact of urban radiation balance, urban heat island effect, and urban convective heat transfer coefficients on space cooling demands [126]. De Rosa et al developed a new steady state model incorporating the thermal inertia of the building envelope and monthly averaged climatic data based on the lack of accuracy of existing steady state models [127]. The model proposed by Li et al. considers the effect of window-to-wall ratio on indoor temperature, and the model is coupled with Envi-met and TRNSYS to obtain a model with better accuracy [128].

2.3.4 Summary

Several methodologies exist for prediction of cooling demand, paralleling the strategies used in heating demand projection. These methods can be primarily classified into three categories. The initial approach is the data-driven Method, followed by economic data-based modelling, and finally, physical modelling. It is worth noting that a significant portion of heating forecasting research has been centred around physical modelling. This is due to the diverse sources of heating energy, which makes data collection a challenging task. Conversely, in regions with high cooling demand, the majority of the energy required for cooling is derived from electricity. Given the easier accessibility of electricity data, the data-driven method is more commonly used in such regions. Economic data-based modelling based on economic and demographic data is common in both areas.

For data-driven models, whether traditional statistical models or machine learning models, historical cooling demand data are essential. These models establish a mathematical correlation between inputs and outputs, necessitating a substantial dataset. The cooling data could be sourced from sensors, substituted

with electricity data, or derived from a physical model. However, it is evident that this methodology is not viable for present cooling estimates in many UK regions due to the scarcity of cooling data. This issue is one of the primary challenges that this paper intends to address. In contrast, the economic data-based model demands significantly fewer data than its data-driven counterpart. The advantage of this model lies in its computational efficiency and speed, making it suitable for forecasting cooling demand across large-scale regions. Nevertheless, this model is typically a steady state, spanning years, and is primarily employed to investigate future cooling scenarios in the context of climate change. Therefore, it is unable to study the dynamics of the cooling profile over shorter periods. On the other hand, physical models are developed based on the principles of heat balance and possess a robust capability for dynamic predictions. These models require a more comprehensive set of environmental data. They take into account the details of the building, such as floor area, materials, cooling system, ventilation, etc. Building simulation software is the most commonly used in prediction, often yielding highly accurate predictions. Despite their accuracy, the application of physical models on a city or country scale presents a significant challenge.

The study of future cooling scenarios is not sufficiently supported by large-scale steady-state models, such as economic data-based models and small-scale physical models in the context of the net-zero objective. The importance of realising a dynamic prediction for a large-scale region in the absence of data cannot be overlooked. This not only shows the future cooling demand and scenarios but also analyses the impact of the dynamic changes in cooling on the future power or energy sources.

2.4 Energy Technologies

2.4.1 Technologies of heat electrification

In the transition towards more sustainable energy systems, heat electrification technologies play a pivotal role. Among these, heat pumps, electric boilers, and electric resistance heaters are identified as the three most promising applications [129].

Heat pumps are particularly notable for their ability to provide flexibility to power systems while delivering efficient heating solutions. They operate by transferring heat between a low-temperature source and a high-temperature sink using a refrigerant cycle and insulated pipes, serving not only for space and water heating but also for air conditioning and various industrial applications. The technology is favoured for its high efficiency, low operational costs, ease of installation, minimal maintenance requirements, and high safety standards. This technology is widely adopted not just for domestic heating and water heating purposes, but also in air conditioning and diverse industrial processes. Within the heat pump category, two primary types stand out due to their efficiency and application diversity: ground-source heat pumps (GSHPs) and air-source heat pumps (ASHPs). GSHPs, also known as geothermal heat pumps, operate by extracting heat from the ground or below-ground water. This method is highly efficient due to the stable thermal properties of the earth, which remain constant regardless of the air temperature fluctuations. They are ideally suited for climates with significant seasonal temperature variation. However, the initial installation cost of GSHPs can be quite high due to the need for extensive excavation or drilling. ASHPs extract heat from the outside air and are more common due to their easier installation and lower upfront costs compared to GSHPs. While not as efficient as GSHPs in extreme conditions, modern ASHPs have improved significantly and can operate effectively even in temperatures as low as -15°C. They offer a good balance of cost, ease of installation, and operational efficiency, making them a versatile option for

moderate climates. However, their efficiency can decrease in extremely cold weather, and they may require a supplementary heating system under such conditions [130].

Electric boilers, including types like electric resistance boilers and electrode boilers, are crucial for heat electrification, primarily used in utilities for generating hot water and steam. These boilers are preferred due to their low upfront cost, compact and sturdy build, and versatility in operation. They are environmentally friendly, especially when powered by renewable energy, as they emit no carbon, making them suitable for industrial uses. Additionally, their quiet functionality and easy maintenance enhance their practicality and user-friendliness. Electric resistance boilers and electrode boilers are two specialised types of electric boilers, each serving distinct needs in heating applications. Electric resistance boilers operate by passing electricity through resistance elements that heat up and transfer this energy to water or other fluids. This type is widely used in residential and commercial settings for space heating and providing hot water, favoured for its simplicity, reliability, quiet operation, and flexibility in installation. However, resistance heating is generally less efficient in terms of energy consumption compared to other technologies like heat pumps [131]. On the other hand, electrode boilers generate heat by passing electricity through water, using the water's own conductivity to facilitate the heating process. This method is highly efficient, nearly reaching 100% efficiency, and is particularly useful in industrial settings where large volumes of high-pressure steam or hot water are required quickly. Electrode boilers are valued for their compact design, quick response to demand changes, and scalability. Despite their higher initial costs and strict water quality requirements to avoid fouling of electrodes, when powered by renewable sources, both boiler types offer environmentally friendly heating solutions with zero emissions [132].

Electric resistance heaters provide fast heating and are simpler and cheaper to install compared to more complex systems. These heaters efficiently convert electricity directly into heat and often come with sophisticated controls like internal thermostats or programmable timers, improving their effectiveness and user-friendliness. However, despite their ability to heat up quickly and their compact size, electric resistance heaters are generally less energy-efficient than heat pumps [133].

2.4.2 Technologies of cooling supply

Conventional vapor compression systems are the most widely used technology for air conditioning and refrigeration. These systems operate based on the vapor compression refrigeration cycle, which involves four key components: the compressor, the condenser, the expansion valve, and the evaporator. Conventional Vapor Compression (VC) air-conditioning systems are categorised primarily into two distinct types: Centralised Air-Conditioning Systems (CACs) and Room Air-Conditioners (RACs), each designed to cater to different environmental and spatial cooling requirements. CACs are engineered to efficiently manage and distribute cooled air throughout multiple rooms or entire buildings from a single, central location. This category encompasses various system types such as Chillers, which utilize chilled water circulated to air handling units or fan coil units to absorb heat from the air, thus cooling it effectively. Variable Refrigerant Flow (VRF) systems provide an advanced solution by enabling precise temperature control across different zones within a building through varying the refrigerant flow, offering flexibility and enhanced energy efficiency. Rooftop Units, another subset of CACs, are large HVAC systems installed on building roofs, designed to condition air at a centralised point and distribute it through ductwork, making them ideal for commercial buildings with large, open spaces.

In contrast, RACs are typically employed for cooling individual rooms or smaller, localised areas and are characterised by their decentralised nature. Among RACs, Split Systems are prevalent, consisting of an outdoor unit (housing the compressor and condenser) and one or more indoor units that distribute cooled air, connected by refrigerant piping. This setup is favoured for its operational efficiency and quieter performance. Multi-Split Systems expand on this by connecting multiple indoor units to a single outdoor unit, allowing for individual temperature control in different rooms, thus providing a versatile cooling solution suitable for residential and small commercial applications. Packaged Units, which encase all components in a single assembly, are commonly installed through walls or windows and are straightforward to install, serving as a practical option for small commercial spaces or supplementary residential cooling. Lastly, Single Duct Systems offer the ultimate in flexibility with their portability and ease of installation, ideal for temporary cooling needs or locations where traditional systems are impractical.

CACs are generally more energy-efficient in larger buildings or spaces due to their ability to centrally control and distribute air. Systems like VRF are particularly notable for their high efficiency. VRF systems can adjust the amount of refrigerant flowing to different indoor units based on the specific cooling needs of each zone or room. This tailored approach minimises energy waste, as the system operates at varying capacities rather than a constant full capacity. Chillers, another type of CAC, also offer high efficiency, especially in scenarios where large volumes of air need cooling. They can be integrated with energy recovery systems to further enhance their efficiency, capturing waste heat and using it for other building needs like heating water.

On the other hand, RACs, such as split and multi-split systems, are typically more energy-efficient for smaller or residential spaces. These systems provide the advantage of cooling specific areas only when needed, which reduces the energy consumption compared to cooling an entire building constantly. Split systems have the added benefit of having the heat-generating components (like compressors and condensers) located outside, which reduces the heat load inside and thus lowers energy use. Multi-split systems share these advantages and add the flexibility of controlling temperatures in multiple rooms independently, which can lead to further efficiencies if some zones do not require constant cooling.

Each type of system within the CAC and RAC categories is tailored to specific applications, from extensive, large-scale cooling in commercial and industrial settings to precise and flexible cooling solutions in residential or smaller commercial environments. The selection between CACs and RACs depends on several factors including the scale of the area to be cooled, installation implications, energy efficiency considerations, and the specific cooling needs of the space. As the technology evolves, these systems continue to improve in terms of energy efficiency, environmental impact, and user adaptability, ensuring they remain integral to modern climate control solutions [134][135].

2.4.3 Technologies of Energy storage

Thermal Energy Storage (TES) systems are engineered to store thermal energy through the processes of cooling, heating, melting, condensing, or vaporising a substance, storing it at controlled temperatures within insulated repositories. The stored energy is later utilised for various residential and industrial applications, such as space heating or cooling, hot water production, or electricity generation. TES systems are categorised into Low Temperature Energy Storage (LTES) systems, used for applications like industrial cooling below -18 °C and building cooling between 0 and 12 °C, and High Temperature Energy

Storage (HTES) systems, suitable for heating buildings between 25 and 50 °C and for industrial heat storage above 175 °C.

Mechanical Energy Storage (MES) systems efficiently manage energy flow by storing electrical energy as mechanical energy, either as potential or kinetic energy, and converting it back when needed. These systems include Pumped Hydro Energy Storage (PHES), Gravity Energy Storage (GES), Compressed Air Energy Storage (CAES), and Flywheel Energy Storage (FES). PHES, GES, and CAES primarily store potential energy, while FES focuses on kinetic energy storage. The process involves storing energy during low-demand, off-peak hours and converting this stored mechanical energy back to electrical energy during peak times. This quick conversion capability is one of MES systems' significant advantages, allowing for responsive energy management to meet demand surges effectively.

Chemical Energy Storage (CES) systems are primarily utilised in the generation of electricity and the transportation sector, where they store energy long-term within the chemical bonds of materials. Key fuels such as coal, gasoline, diesel, natural gas, liquefied petroleum gas (LPG), propane, butane, ethanol, and hydrogen is integral to these systems. These fuels undergo chemical reactions that change their composition, breaking old bonds and forming new ones to release energy. This released energy is then converted from chemical to mechanical and finally to electrical energy. CES systems commonly include options for storing hydrogen, synthetic natural gas, and solar fuels, highlighting their importance in global energy strategies.

The Electrochemical Energy Storage (EcES) system is a pivotal element in modern energy storage, with widespread applications across various industries. It predominantly encompasses two distinct types:

Battery Energy Storage (BES) systems and Flow Battery Energy Storage (FBES) systems. In BES systems, the electrical charge is stored directly within the electrodes, allowing for efficient and rapid energy release. Conversely, FBES systems store the charge in a liquid fuel which is then externally transferred to the electrode surfaces, offering unique advantages in scalability and rechargeability. Alongside these traditional technologies, there is a surge of innovative research aimed at pushing the boundaries of electrochemical storage. In residential settings, EcES systems, particularly Battery Energy Storage (BES) systems, provide homeowners with the capability to store excess energy generated from rooftop solar panels or the grid during off-peak hours. At the utility scale, EcES systems, including both BES and Flow Battery Energy Storage (FBES) systems, are integral in stabilising the grid, managing peak load demands, and integrating renewable energy sources [136], [137], [138].

Chapter 3

Theory and Methodology

3.1 Theory of building simulation

In this study, Design Builder is used for building simulation and the core algorithm of Design Builder for heating and cooling demand prediction is EnergyPlus. EnergyPlus is also an open-source software combined different algorithms. The primary modules of the EnergyPlus algorithm are showcased in Figure 3-1 [139]. The entirety of the system is under the centralised management of the EnergyPlus control system called EnergyPlus simulation manger, which is not the central topic of this chapter. The algorithm is segmented into three principal categories: the surface heat balance, the air heat balance, and the building system simulation.

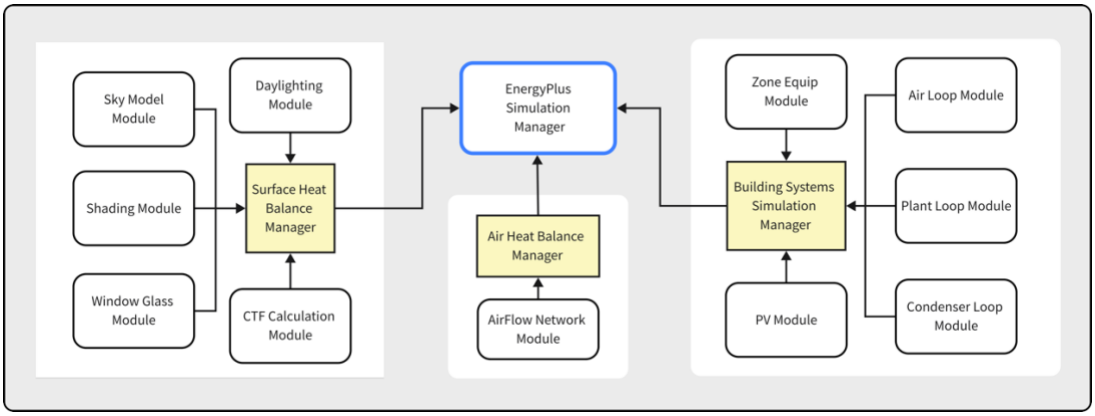

Figure 3-1 EnergyPlus Program Schematic [139]

The surface heat balance serves as the algorithm's foundation, dealing with the building's outer layers—walls, floors, ceilings—and their role in heat and moisture movement. This module is crucial because it determines how these surfaces interact with the indoor temperature and humidity, factoring in variations in materials and their properties. Additionally, it incorporates environmental influences through the sky model and daylighting model to simulate the impact of weather on indoor conditions. For air movement and temperature control within the building, the air heat balance is responsible. It calculates the overall air temperature and humidity, critical for maintaining comfortable indoor conditions. Zones within this module act as interfaces for the HVAC system, ensuring that heating, cooling, and ventilation. The building system simulation module is centreed around the HVAC system, aiming to proactively manage the building's climate. This includes specific components like the plant loop module and the space equipment module, which collectively maintain and adjust the building's heating, cooling, and air circulation to achieve the desired indoor environment. The formulas presented in the following section are taken from the Engineering Reference manual provided by EnergyPlus [140].

3.1.1 Surface heat balance

3.1.1.1 Conduction Through the Walls

At the core of time series analysis for building thermal performance is the response factor equation. This equation connects the heat flow on one side of a building element to past temperatures on both sides. The equation looks like this:

$$q''_{ko}(t) = \sum_{j=0}^{\infty} X_j T_{o,t-j\delta} - \sum_{j=0}^{\infty} Y_j T_{i,t-j\delta} \quad (1)$$

Where,

q'' = heat flow per area,

T = temperature,

i is for inside, o is for outside,

t = the current time step,

δ = time interval between steps

X and Y are constants based on the material's response to temperature changes.

Simplifying the equation by replacing later terms with the history of heat flow, a more practical set of equations involving conduction transfer functions (CTFs) is obtained:

$$q''_{ki}(t) = -Z_o T_{i,t} - \sum_{j=1}^{nz} Z_j T_{i,t-j\delta} + Y_o T_{o,t} + \sum_{j=1}^{nz} Y_j T_{o,t-j\delta} + \sum_{j=1}^{nq} \Phi_j q''_{ki,t-j\delta} \quad (2)$$

For the heat flow inside

$$q''_{ko}(t) = -Y_o T_{i,t} - \sum_{j=1}^{nz} Y_j T_{i,t-j\delta} + X_o T_{o,t} + \sum_{j=1}^{nz} X_j T_{o,t-j\delta} + \sum_{j=1}^{nq} \Phi_j q''_{ko,t-j\delta} \quad (3)$$

For the heat flow outside $\left(q'' = \frac{q}{A}\right)$

Where,

$X_j =$ Outside CTF coefficient,

Y_j = Cross CTF coefficient,

Z_j = Inside CTF coefficient,

Φ_j = Flux CTF coefficient,

T_i = Inside face temperature,

T_o = Outside face temperature,

q''_{ko} = Conduction heat flux on outside face,

q'' = Conduction heat flux on inside face,

3.1.1.2 Outside Surface Heat Balance

The heat balance on the outside face is

$$q''_{\alpha sol} + q''_{LWR} + q''_{conv} - q''_{ko} = 0 \quad (4)$$

Where,

$q''_{\alpha sol}$ = absorbed solar radiation heat flux, encompassing both direct and diffuse solar gains on the surface

q''_{LWR} = net long-wavelength radiation heat flux, accounting for thermal radiation exchange with the ambient air and other external surfaces

q''_{conv} = convective heat flux between the surface and the external air

q''_{ko} = Conduction heat flux $\left(\frac{q}{A}\right)$ into the wall.

3.1.1.3 Inside Surface Heat Balance

$$q''_{LWX} + q''_{SW} + q''_{LWS} + q''_{ki} + q''_{sol} + q''_{conv} = 0 \quad (5)$$

Where,

q''_{LWX} = net longwave radiation exchange flux that occurs between surfaces within a zone or an enclosure.

q''_{SW} = net shortwave radiation flux received by the surface from artificial lighting sources.

q''_{LWS} = longwave radiation flux emitted by equipment and other heat-generating items within the zone or enclosure.

q''_{ki} = conductive heat flux traversing the wall from the external environment to the interior.

q''_{sol} = Transmitted solar radiation flux absorbed at surface.

q''_{conv} = convective heat flux exchanged with the indoor air.

3.1.1.4 Solar radiation from sky

IR_H is defined as the rate of infrared radiation emitted from the sky falling on a horizontal upward-facing surface, in $\frac{W}{m^2}$.

$$IR_H = \sigma T_{sky}^4 \quad (6)$$

Where,

σ = Stefan-Boltzmann constant,

T_{sky} = effective average sky temperature, measured in kelvin (K).

The Direct Normal Irradiation on a clear day at Earth's surface is defined as:

$$\text{Direct Normal Irradiation} = \frac{A}{\exp\left(\frac{B}{\sin\beta}\right)} \quad (7)$$

Where:

A = apparent solar irradiation at air mass $m = 0$,

B = atmospheric extinction coefficient,

β = solar zenith angle.

The global solar radiation value:

$$I = \frac{[I_0 \cdot \sin(h) \cdot (c_0 + c_1 \cdot CC + c_2 \cdot CC^2 + c_3(T_n - T_{n-3}) + c_4 \cdot \varphi + c_5 \cdot V_w) + d]}{k} \quad (8)$$

Where,

$I =$ estimated hourly solar radiation, (W/m²)

$I_0 =$ global solar constant, (1355 W/m²)

$h =$ solar altitude angle,

$CC =$ cloud cover,

$\varphi =$ relative humidity percentage,

T_n and $T_{n-3} =$ dry-bulb temperatures at the current hour and three hours prior,

$V_w =$ Wind speed (m/s),

$c_0, c_1, c_2, c_3, c_4, c_5, d, k =$ regression coefficients.

3.1.1.5 Shadow Projection

Solar position is the first value should be determined. The fractional year in radians (γ) is computed using the day of the year:

$$\gamma = \frac{2\pi}{366}(\text{ day of year }) \quad (9)$$

Using this fractional year, the equation of time and the solar declination angle are calculated. The hour angle for each time step, which is a fractional hour, is then derived from: The TimeZoneMeridian corresponds to the standard meridian of the location's time zone (GMT +/-).

$$Hour\ Angle =$$

$$(15 * \big(12 - (TimeValue + EquationOfTime)\big) + (TimeZoneMeridin - Longitude)) \quad (10)$$

Pixel Counting is a method for calculating sunlit fractions and determination of surface shading.

$$A_s \approx \frac{N \cdot A_p}{\cos\theta} = \frac{PSSA}{\cos\theta} \tag{11}$$

Where,

$A_s =$ Sunlit area,

$N =$ Number of visible pixels,

$A_p =$ the projected area of a single pixel,

$\theta =$ solar incidence angle of the surface,

$PSSA =$ Projected Sunlit Surface Area.

The total solar gain (Q_{so}) on an exterior surface is the sum of absorbed direct and diffuse solar radiation:

$$Q_{so} = \alpha \cdot \left(I_b \cdot \cos\theta \cdot \frac{S_s}{S} + I_s \cdot F_{ss} + I_g \cdot F_{sg}\right) \tag{12}$$

Where,

α is the solar absorptance of the surface,

θ is the angle of incidence,

S is the surface area,

S_s = sunlit area,

I_b = beam radiation intensity,

I_s = sky diffuse radiation intensity,

I_g = ground reflected diffuse radiation intensity,

F_{ss} and F_{sg} are angle factors for the sky and ground, respectively.

For a building surface on a featureless plain, the sky and ground angle factors are given by:

$$F_{ss} = \frac{1+\cos\phi}{2},\ F_{sg} = \frac{1-\cos\phi}{2} \quad (13)$$

Shading corrections may be applied to F_{ss} based on sky radiance distribution, while ground diffuse solar radiation shading is not calculated by the program and must be estimated by the user to adjust F_{sg} accordingly.

3.1.1.6 Daylighting

Daylight factors are established to quantify the efficiency of indoor lighting conditions. These factors are defined as the ratios between the amount of light inside a space (illuminance or luminance) and the amount of light available outside.

$$d_{sun} = \frac{\text{Illuminance at reference point due to sun} - \text{related light}}{E_{h,sun}} \quad (14)$$

$$d_{sky} = \frac{\text{Illuminance at reference point due to sky} - \text{related light}}{E_{h,sky}} \quad (15)$$

$$w_{sky} = \frac{\text{Average window luminance due to sky} - \text{related light}}{E_{h,sky}} \quad (16)$$

$$w_{sun} = \frac{\text{Average window luminance due to sun} - \text{related light}}{E_{h,sun}} \quad (17)$$

$$b_{sky} = \frac{\text{Window background luminance due to sky} - \text{related light}}{E_{h,sky}} \quad (18)$$

$$b_{sun} = \frac{\text{Window background luminance due to sun} - \text{related light}}{E_{h,sun}} \quad (19)$$

$E_{h,sky}$= Exterior horizontal illuminance due to light from the sky

$E_{h,sun}$ =Exterior horizontal illuminance due to light from the sun

d_{sky}, d_{sun}= Interior illuminance factor due to sky, sun related light

w_{sky} , w_{sun} =Window luminance factor due to sky, sun related light

b_{sky} , b_{sun} = Window background luminance factor due to sky, sun related light

3.1.1.7 Window model

The window model process begins with the calculation of glass-to-glass resistance, which includes the thermal resistances of both the interior and exterior surface heat transfer coefficients, in addition to the resistance of the window material itself. This total resistance inversely relates to the U-value, or the overall heat transfer coefficient of the window. Mathematically, it's represented as:

$$\frac{1}{U} = R_{i,w} + R_{o,w} + R_{l,w} \quad (20)$$

Where,

$R_{i,w}$ = resistance of the interior film coefficient under standard winter conditions

$R_{o,w}$ = resistance of the exterior film coefficient under standard winter conditions and

$R_{l,w}$ = resistance of the bare window under winter conditions (without the film coefficients)

The thickness of the equivalent layer in units of meters is calculated using,

$$\text{Thickness} = \begin{cases} 0.002 & \text{for } \frac{1}{R_{l,w}} > 7.0 \\ 0.05914 - \frac{0.00714}{R_{l,w}} & \text{for } \frac{1}{R_{l,w}} \leq 7.0 \end{cases} \quad (21)$$

The effective thermal conductivity, λ_{eff}", of the equivalent layer is calculated using,

$$\lambda_{eff} = \frac{\text{Thickness}}{R_{l,w}} \quad (22)$$

Window angular properties are a critical factor in building energy simulations due to the typically high angles at which sunlight strikes windows. These incidence angles are measured from a perpendicular line to the window's surface. The modeling of simple glazing systems incorporates correlations based on overall heat transfer coefficient (U-values), which measure heat transfer efficiency, and Solar Heat Gain Coefficient (SHGC), which indicates how much solar heat is admitted. These correlations align with

expected performance for various window types. A matrix categorising potential U-value and SHGC combinations has been organised into 28 distinct categories, as illustrated in Figure 3-2. In addition, it is also necessary to determine the Layer Solar Transmittance, Layer Solar Reflectance, and Layer Visible Properties, which will not be specifically elaborated.

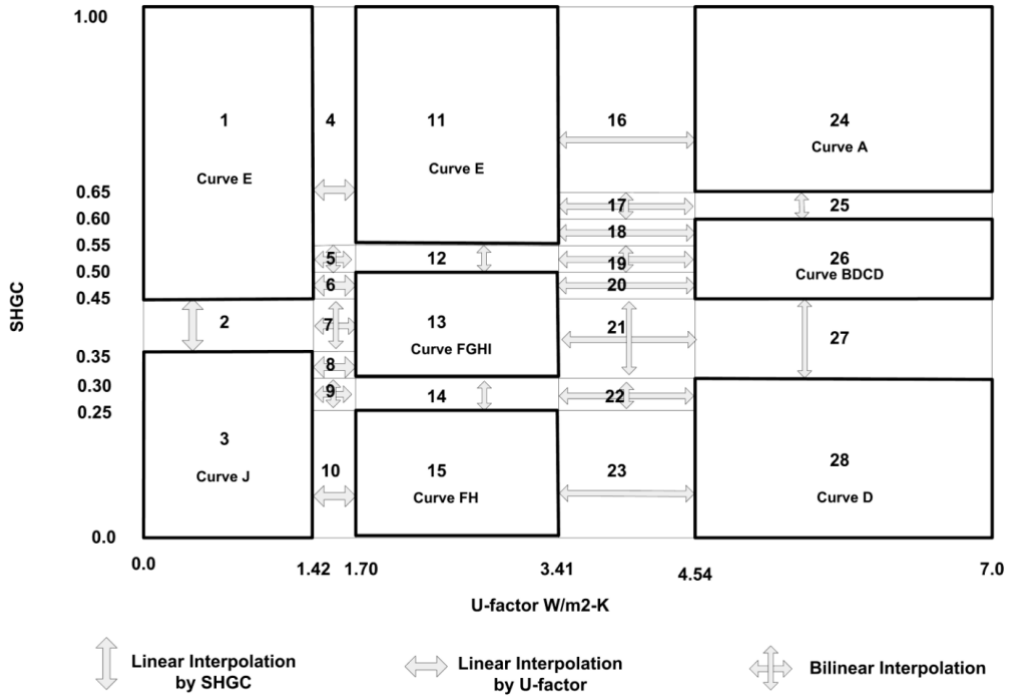

Figure 3-2 Diagram of Transmittance and Reflectance Correlations Used based on U and SHGC

3.1.2 Air heat balance

3.1.2.1 Infiltration by Effective Leakage Area

In the domain of building energy simulation, the air heat balance involves quantifying the air exchange between the indoors and outdoors due to factors like temperature differences and wind. A critical aspect of this air heat balance is the infiltration rate.

$$\text{Infiltration} = (F_{\text{Schedule}}) \frac{A_L}{1000} \sqrt{C_s \Delta T + C_w (\text{WindSpeed})^2} \qquad (23)$$

where,

$F_{schedule}$ = value from a user-defined schedule,

A_L = effective air leakage area in

C_s = coefficient for stack-induced infiltration in $(L/s)^2/(cm^4 \cdot K)$,

ΔT = absolute temperature difference between zone air and outdoor air,

C_w = coefficient for wind-induced infiltration in $(L/s)^2/(cm^4 \cdot (m/s)^2)$,

WindSpeed = local wind speed.

3.1.2.2 Infiltration by Flow Coefficient

$$\text{Infiltration} = (F_{\text{Schedule}})\sqrt{(cC_s\Delta T^n)^2 + (cC_w(s * \text{WindSpeed})^{2n})^2} \quad (24)$$

where,

$F_{schedule}$ = value from a user-defined schedule,

c = flow coefficient in $m^3/(s \cdot Pa^n)$,

C_s = coefficient for stack-induced infiltration in $(Pa/K)^n$,

n = pressure exponent,

C_w = coefficient for wind-induced infiltration in $(Pa \cdot s^2/m^2)^n$

s = shelter factor.

3.1.2.3 Ventilation by Wind and Stack with Open Area

For natural ventilation, the flow rate is determined by a schedule that multiplies the open area and is regulated by temperature limits that can be constant or change over time.

$$Q_w = C_w A_{opening} F_{schedule} V \quad (25)$$

where

$Q_w =$ Volumetric air flow rate driven by wind (m^3/s)

$C_w =$ Opening effectiveness (dimensionless)

$A_{opening} =$ Opening area (m^2)

$F_{schedule} =$ Open area fraction

$V =$ Local wind speed (m/s)

3.1.2.4 Zone Air Balance Outdoor Airflow

Unbalanced supply or exhaust ventilation in a zone can cause pressure differences that affect infiltration, this part defines how to account for the total outdoor airflow entering a zone.

$$Q = \sqrt{Q_n^2 + Q_{u,v}{}^2 + \left(Q_{u,l}{}^2\right)} + Q_{b,v} \quad (26)$$

where,

$Q =$ Combined outdoor airflow with infiltration, balanced and unbalanced outdoor air flows, and unbalanced duct leakage (m^3/s)

$Q_n =$ Natural infiltration airflow (m^3/s)

$Q_{b,v} =$ Balanced ventilation airflow, excluding infiltration (m^3/s)

$Q_{u,v} =$ Unbalanced ventilation airflow, excluding infiltration (m^3/s)

$Q_{u,l} =$ Unbalanced duct leakage: the difference between supply and return leaks (m^3/s)

3.1.3 Building system simulation

3.1.3.1 Zone Mixer

The Zone Mixer component within EnergyPlus plays a pivotal role in simulating the behaviour of HVAC systems in buildings. By integrating multiple air streams from different zones, it ensures a harmonised output that maintains the desired environmental conditions across the building. The component's functionality is crucial in complex HVAC systems where air from various sources must be mixed before being supplied to conditioned spaces.

Mass Balance: Ensures the conservation of mass by equating the total mass of the combined outlet air stream to the sum of all inlet air streams.

$$\dot{m}_{\text{air, out}} = \sum_{i=1}^{n} \dot{m}_{\text{air , in ,i}} \quad (27)$$

Humidity Balance: Balances the moisture content of the air, ensuring the combined outlet air stream's humidity ratio matches the sum of the inlet streams' humidity ratios.

$$\dot{m}_{air,\text{ out}} \cdot W_{air,out} = \sum_{i=1,n} \dot{m}_{air,in,i} \cdot W_{air,in,i} \quad (28)$$

Enthalpy Balance: Maintains energy conservation by equating the total enthalpy (a measure of heat content in the air) of the outlet stream with the sum of the enthalpies of the inlet streams.

$$\dot{m}_{air,out} \cdot h_{air,out} = \sum_{i=1,n} \dot{m}_{air,in,i} \cdot h_{air,in,i} \quad (29)$$

Pressure Balance: Ensures the pressure of the mixed outlet air stream is consistent with the sum of the pressures of the inlet air streams.

$$\dot{m}_{air,out} \cdot P_{air,\text{ out}} = \sum_{i=1,n} \dot{m}_{air,in,i} \cdot P_{air,in,i} \quad (30)$$

Temperature Calculation: Employs a psychrometric function to calculate the dry bulb temperature of the outlet air stream based on its enthalpy and humidity ratio.

$$T_{air,out} = PsyTdbFnHW\left(h_{air,out}, W_{air,out}\right) \quad (31)$$

Where,

$\dot{m}$ = air mass flow rate,

W = humidity ratio,

h = specific enthalpy,

P = pressure,

T = temperature,

$PsyTdbFnHW$ is an EnergyPlus psychrometric function to determine dry bulb temperature based on enthalpy and humidity ratio.

3.1.3.2 Plant Calculation Model

The calculation can be expressed with the equation:

$$T_{\text{out}} = T_{\text{in}} - \frac{Q_{\text{load}}}{m^{\cdot} c_p} \quad (32)$$

where

T_{out} = the outlet water temperature,

T_{in} = the inlet water temperature,

Q_{load} = the scheduled plant load,

$m^{\cdot}$ = the water mass flow rate,

c_p = the specific heat of water,

It's important to note that the actual flow rate in the calculation is constrained by the plant's capability and may be less than the user's requested rate. For tracking energy use, the object calculates energy consumption as follows:

$$E = Q_{\text{load}}\,\Delta t \tag{33}$$

where

$E =$ the energy consumption

$Q_{\text{load}} =$ the scheduled plant load

$\Delta t =$ the time step interval

This model serves as a fundamental tool within EnergyPlus, allowing users to simulate and analyse the energy performance of plant loops with precision, aiding in the optimization of system operation and energy usage.

3.2 ANN theory

3.2.1 Neuron in ANN

As an information processing unit, there are three basic elements in a model of neuron: connections links with weights w, an adder for summing the input signal u and an activation function φ. The bias b in the model is applied to increase or decrease the net input of the activation function. It also can be considered as a threshold of the system [3]. The neuron k can be described by mathematical equation while x_j is the input of neuron and y is the output of neuron.

$$u_k = \sum_{j=1}^{m} w_{kj}\, x_j \tag{34}$$

$$y_k = \varphi(u_k + b_k) \tag{35}$$

Note that bias is an external parameter of the neuron, but it can be added as a new connectionist link of neuron with its input $x_0 = +1$, and weight $w_{k0} = b_k$.

The new equations for neuron k

$$v_k = \sum_{j=0}^{m} w_{kj}\, x_j \tag{36}$$

$$y_k = \varphi(v_k) \tag{37}$$

Threshold function (Equation 38) and Sigmoid function (Equation 39) are wo basic activation functions which are always applied in the neuron.

$$\varphi(v) = \begin{cases} 1 & if\ v \geq 0 \\ 0 & if\ v < 0 \end{cases} \tag{38}$$

$$\varphi(v) = \frac{1}{1+\exp(-av)} \tag{39}$$

3.2.2 Back propagation network

A BPNN is a multi-layer feedforward neural network, which is characterised by the forward propagation of signals and backward propagation of errors. The BP neural network propagates forward layer by layer to obtain a result, and this result o is compared with the expected result d to obtain an error e. The neural network passes the error from the back to the front using the 'gradient descent' strategy to adjust weights and thresholds until a selected stopping criterion is met.

The specific analysis of the working process of the BP neural network can be divided into five steps. The first step initialization refers to setting the initial values of weights and thresholds, which are generally set to zero without prior information. An error equation such as MSE and an activation function such as sigmoid are used to be choose in BP network. The settings for the learning rate η, the number of iterations, the target error, and so on are also decided. The second step is briefly summarised as input training data, which contains the desired output in this paper. The third and fourth steps are forward computation and

backward computation, which are the most important processes for BP to adjust $\Delta\omega$. Suppose that the training input of a BP network is $x(n)$, the expected output is $d(n)$, and there are L layers in total of the network. According to equation (36) and equation (37), the neuron k which relates to neuron j in previous layer of BP network can be denoted as:

$$v_k(n) = \sum_{j=0}^{m} w_{kj}(n) y_j(n) \tag{40}$$

$$y_k(n) = \varphi_k\big(v_k(n)\big) \tag{41}$$

If the k is in first hidden layer,

$$y_k(n) = x_k(n) \tag{42}$$

If the k is in output layer,

$$y_k(n) = o_k(n) \tag{43}$$

The correction is defined by the delta rules:

$$\Delta\omega_{kj}(n) = \eta\delta_k(n) y_j(n) \tag{44}$$

If the neuron k is in output layer L, local gradient δ is defined by equation (45)

$$\delta_k(n) = e_k(n)\varphi_k'\big(v_k(n)\big) \tag{45}$$

$$e_k(n) = d_k(n) - o_k(n) \tag{46}$$

If the neuron k is in hidden layer and connected to neuron i in next layer, local gradient δ is represented by equation (47)

$$\delta_k(n) = \varphi_k'(v_k(n)) \sum_i \delta_i(n)\omega_{ik}(n) \tag{47}$$

The fifth step is the iterative forward and backward computations with the training data [141].

3.2.3 Feature selection

The Morris method is a global sensitivity analysis method developed based on the local derivative-based sensitivity method, which incorporates the advantages of both local and global sensitivity analyses. Morris method approximates this derivative using a finite difference scheme[142].

The elementary effect EE_i of the ith factor is

$$EE_i = \frac{f(X_1,X_2,\ldots+\Delta,\ldots,X_n,)-f(X_1,X_2,\ldots+X_i,\ldots,X_n,)}{\Delta} \quad (48)$$

where Δ is step size, n is the number of factors.

$$\mu_i = \sum_{k=1}^{r} \frac{EE_i^k}{r} \quad (49)$$

μ_i is the mean of these elementary effects, r is the repetition time.

$$\mu_i^* = \sum_{k=1}^{r} |EE_i^k|/r \quad (50)$$

μ_i^* is absolute values of μ_i and this value is used to reflect the significance of the input.

A kth-order polynomial model in one variable can be represented by the following equation, where x is the independent variable y is the dependent variable, β is the regression coefficient, and ε is an unobserved random error.

$$y = \beta_0 + \beta_1 x + \beta_1 x^2 + \cdots + \beta_k x^k + \varepsilon \quad (51)$$

In regression models, the Coefficient of determination is usually used to indicate the strength of the variable association. The coefficient of determination R^2 is defined by the following equation.

$$R^2 = 1 - \frac{SSE}{SST} \quad (52)$$

SST is the total sum of squares,

$$SST = \sum(y_i - \bar{y})^2 \quad (53)$$

y is the real value of data set, $y = [y_1, y_2 \ldots y_i \ldots y_n]$, $\bar{y}$ is the mean value of the data set.

$$\bar{y} = \frac{1}{n}\sum_0^n y_i \quad (54)$$

SSE is the error sum of the square,

$$SSE = \sum(y_i - \hat{y}_i)^2 \quad (55)$$

$\hat{y}$ is the fitted value, $\hat{y} = [\hat{y}_1, \hat{y}_2 \ldots \hat{y}_i \ldots \hat{y}_n]$

3.2.4 Convolutional Neural Network

The process of initialising a Convolutional Neural Network (CNN) begins by setting the network parameters, such as weights and biases, to small random numbers. This initialization allows for the optimization process to commence. The CNN then processes input data that is multidimensional in nature. The data is carefully analysed by convolutional layers, which utilise learnable filters to extract local features and create feature maps. To introduce non-linearity and enable the network to learn complex patterns within the data, these feature maps undergo a nonlinear activation function, commonly Rectified Linear Unit (ReLU). To improve computational efficiency and enhance the network's ability to detect features despite variations in position, subsequent pooling layers down sample the feature maps, reducing their spatial dimensions. Following the convolutional and pooling layers, the architecture of the network leads to fully connected layers. These layers synthesise the localised features into a global understanding that is necessary for decision-making. The final step of this process occurs in the output layer. For classification tasks, a Softmax function is typically employed. This function provides a probabilistic distribution over various class. For regression tasks, a single neuron is used to provide continuous variable predictions.

During the training, the network's predictions are evaluated against actual targets using a designated loss function. Optimization algorithms, specifically variations of gradient descent, then iteratively adjust the weights and biases of the network in an attempt to minimise this loss. Backpropagation plays a crucial role in this optimization process by efficiently computing gradients for each weight. This guides the network towards better performance. This iterative process of forward passes, loss computation,

backpropagation, and weight updates continue until the network achieves satisfactory accuracy or meets a stopping condition. This allows CNNs to autonomously learn from data and excel in various domains.

CNNs differ from basic feedforward neural networks, like BPNN, in that CNNs include specialised layers known as convolutional layers and pooling layers. This discussion focuses on the convolutional and pooling layers, omitting the explanation of the forward pass and backpropagation algorithm, which are common in neural networks.

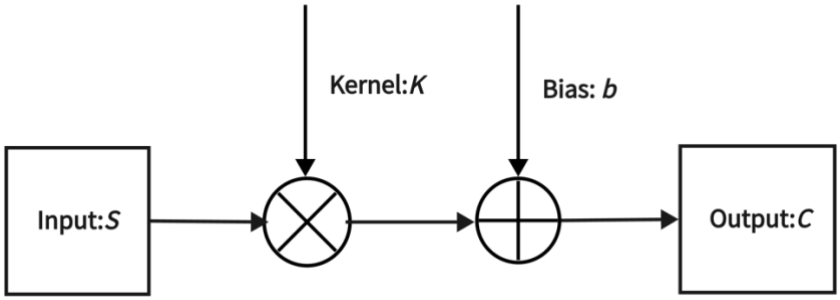

Figure 3-3 Diagram of convolution and pooling layer

The process from the input layer to the pooling layer is demonstrated in the Figure 3-3. After convolution, the output can be expressed as follows [143]:

$$C_q^l = \left(\sum_{p=1}^{n} S_p^{(l-1)} * k_{p,q}^l\right) + b_q^l \tag{56}$$

Where:

l denotes the layer number within the neural network.

C_q^l represents the output of the q-th feature map at layer l.

$S_p^{(l-1)}$ signifies the p-th feature map of the previous layer $(l-1)$.

The asterisk (*) symbolises the convolution operation.

$k_{p,q}^{l}$ denotes the convolutional kernel (or filter) between the p-th and q th layers.

b_q^l represents the bias term for the q-th feature map at layer l.

Assuming the spatial location within the feature map is denoted by (i, j), the convolution operation is more precisely defined as:

$$C_q^l(i,j) = \left(\sum_{p=1}^{n} \sum_{u=-x}^{x} \sum_{v=-x}^{x} S_p^{(l-1)}(i-u, j-v) \cdot k_{p,q}^{l}(u,v)\right) + b_q^l \quad (57)$$

Where,

x represents the size of the filter/kernel.

The double summation over u and v accounts for the spatial dimensions of the kernel, applying it over the appropriate elements of the input feature map to produce the output feature map.

Following the convolution operation, a pooling layer is typically applied. Pooling, also known as subsampling or down-sampling, reduces the dimensionality of each feature map while retaining the most important information. Pooling layers help to make the detection of features invariant to scale and orientation changes and also reduce the computational complexity for the upcoming layers.

One common approach to pooling is using the equation:

$$S_q^l(i,j) = \frac{1}{4} \sum_{u=0}^{z} \sum_{v=0}^{z} C_q^l(2i-u, 2j-v) \quad (58)$$

Where,

$S_q^l(i,j)$ is the pooled feature map.

C_q^l represents the output of the convolution operation from the previous layer.

i and j denote the spatial location in the feature map.

z is the size of the pool window, which is the area over which the pooling operation is applied. The factors $2i$ and $2j$ suggest a stride of 2, meaning that the pooling window skips every other pixel, a common setting for pooling layers. The equation indicates that the pooling operation takes the average value of the pixels in the pool window, essentially down sampling the input feature map by a factor of four (hence the $\frac{1}{4}$ factor). This form of pooling is known as average pooling. The process of convolution followed by pooling is repeated a significant number of times within a CNN architecture, depending on the complexity and depth required by the task at hand.

3.2.5 Recurrent Neural Networks

Recurrent Neural Networks (RNNs) start by initialising weights and biases with random values to aid in subsequent learning. They then receive a sequence of inputs, often ordered over time, such as consecutive time series data points. For each input, the RNN updates its hidden state based on the current input and the previous time step's hidden state. The sharing of weights and bias parameters across layers allows RNNs to adapt to sequences of different lengths. After processing each input, the RNN can generate an output, which often depends on the current hidden state. The RNN continues to process the entire input sequence, receiving one input at a time and updating its hidden state. The recurrence in RNNs is evident in the interaction between the hidden state and input data. At each time step, the RNN combines the current input data with the hidden state from the previous time step to update the current hidden state. This interactive mechanism enables RNNs to maintain a state while processing sequential data, allowing them to capture temporal dependencies within the data.

During training, the RNN's outputs are compared to the ground truth values, and a loss function computes the total loss for the entire sequence. To train RNNs, Backpropagation Through Time (BPTT) is used, where the gradients of the loss function are propagated backward through the network to update weights and biases. These steps collectively enable RNNs to effectively capture temporal dependencies in sequential data, making them suitable for various applications. However, RNNs may encounter issues like vanishing or exploding gradients when handling long sequences, which is a significant limitation. To address this problem, variants of RNNs have been developed, such as Long Short-Term Memory (LSTM) and Gated Recurrent Unit (GRU). These variants introduce different architectures and mechanisms to better capture information and gradient flow in long sequences.

In RNNs, the unique aspect is the use of the BPTT algorithm, which adjusts the weights after computing the gradients. RNNs typically have three sets of weights: input-to-hidden (W_{xh}), hidden-to-hidden (W_{hh}), and hidden-to-output (W_{ho}). The hidden-to-hidden weight matrix (W_{hh}) is what creates the temporal dependency, as it connects the hidden state from one time step to the next.

Loss function with respect to outputs at each time step [144]:

$$L(O, Y) = \sum_{t=1}^{T} l_t(O_t, Y_t) \tag{59}$$

In the formula, L is the total loss over all time steps. O are the outputs from the network and Y are the target values. l_t is the loss at time step t, while O_t is the output of the network at time step t. Y_t is the target value at time step t.

Gradient of loss with respect to weight matrix W_{ho}

$$\frac{\partial L}{\partial W_{ho}} = \sum_{t=1}^{T} \frac{\partial l_t}{\partial O_t} \cdot \frac{\partial O_t}{\partial \phi_o} \cdot H_t \tag{60}$$

W_{ho} is the weight matrix from hidden layer to output layer, $\phi_o$is the activation function applied at the output layer. H_t is the hidden state of the network at time t.

Gradient of loss with respect to weight matrix W_{hh} and Gradient of loss with respect to weight matrix W_{xh} :

$$\frac{\partial L}{\partial W_{hh}} = \sum_{t=1}^{T} \frac{\partial l_t}{\partial O_t} \cdot \frac{\partial O_t}{\partial \phi_o} \cdot W_{ho} \cdot \frac{\partial H_t}{\partial \phi_h} \cdot \frac{\partial \phi_h}{\partial W_{hh}} \quad (61)$$

$$\frac{\partial L}{\partial W_{xh}} = \sum_{t=1}^{T} \frac{\partial l_t}{\partial O_t} \cdot \frac{\partial O_t}{\partial \phi_o} \cdot W_{ho} \cdot \frac{\partial H_t}{\partial \phi_h} \cdot \frac{\partial \phi_h}{\partial W_{xh}} \quad (62)$$

W_{hh} is the Weight matrix from the hidden layer at time $t-1$ to the hidden layer at time t. W_{xh} is the Weight matrix from input layer to hidden layer. ϕ_h is the Activation function for the hidden layer.

3.2.6 Long Short-Term Memory

The Long Short-Term Memory (LSTM) model introduces specialised memory cells to store and retrieve information. By utilising three gates (input gate, forget gate, and output gate), LSTM can control the flow of information, selectively remembering or forgetting specific pieces of information. This unique mechanism allows LSTM to effectively handle long sequences and overcome the issue of vanishing or exploding gradients.

LSTM follows a similar process to RNN, starting with the initialisation of internal states such as cell states and hidden states. These states are typically initialised with zeros or small random values to aid memory. At each time step, LSTM receives an input along with the previous time step's states, including cell states and hidden states. The difference lies in LSTM's employment of gating mechanisms, which consist of the forget gate, input gate, and output gate. The forget gate determines what information from the previous cell state should be retained or forgotten, considering the current input and previous hidden

state. The input gate decides which new information should be added to the cell state based on the current input and previous hidden state. The output gate controls which parts of the current cell state should be exposed as the hidden state. The cell state undergoes updates, including the calculation of a candidate cell state based on the current input and previous hidden state. Subsequently, the cell state is updated by merging the old state (after forgetting some parts) with the newly calculated information. The hidden state is computed using a hyperbolic tangent (tanh) activation function based on the cell state and output gate. This hidden state represents LSTM's output for the current time step. At each time step, LSTM can generate an output, often dependent on the current hidden state. The entire input sequence is processed iteratively, one time step at a time, following the mentioned steps.

During training, the outputs are compared to the ground truth values, and the total loss for the entire sequence is computed using a loss function. LSTM is trained using the BPTT technique, which involves backward propagation of gradients through the network to update weights and biases.

Compared to a standard RNN, an LSTM includes additional structures: an input gate, a forget gate, an output gate, and a cell state. Consequently, the network possesses a greater variety of weight types. Specifically, these are W_{xi}, W_{hi} for the input gate, which manage weights for inputs and hidden states; W_{xf}, W_{hf} for the forget gate; W_{xo}, W_{ho} for the output gate; and W_{xc}, W_{hc} for the cell state weights.In an LSTM cell, three gates work together to update the cell state and the hidden state.

The forget gate (f_t) decides which information is to be discarded from the cell state. It applies a sigmoid function to the concatenated vector of the previous hidden state and the current input [145]:

$$f_t = \sigma\left(w_f \cdot \left[h_{(t-1)}, X_t\right] + b_f\right) \quad (63)$$

The square brackets $\left[h_{(t-1)}, X_t\right]$ represent the concatenation of two vectors: the hidden state from the previous time step $h_{(t-1)}$ and the current input X_t. σ is Sigmoid activation function, which maps the input values to a range between 0 and 1.

The input gate (i_t) determines which new information is added to the cell state. It processes the information through a sigmoid function:

$$i_t = \sigma\left(w_i \cdot \left[h_{(t-1)}, X_t\right] + b_i\right) \quad (64)$$

Alongside the input gate, a candidate cell state $\left(\tilde{C}_t\right)$ is created by processing the same concatenated vector through a tanh function:

$$\tilde{C}_t = \tanh\left(w_C \cdot \left[h_{(t-1)}, X_t\right] + b_C\right) \quad (65)$$

The output gate (o_t) decides what information the hidden state should carry to the next time step. It uses a sigmoid function to filter the cell state's information, which has been processed through a tanh function:

$$o_t = \sigma\left(w_o \cdot \left[h_{(t-1)}, X_t\right] + b_o\right) \quad (66)$$

These gates collectively influence the updates to the cell state (C_t) and the hidden state (h_t), with element-wise operations applied between their outputs and the current state values.

The outputs i_t and $\tilde{C}_t$ are then combined in an element-wise fashion to update the cell state C, thereby adjusting the long-term memory of the cell according to Equation (67):

$$C_t = f_t \odot C_{(t-1)} + i_t \odot \tilde{C}_t \quad (67)$$

The short-term memory, or the hidden state h_t, is updated through an operation involving the output gate o_t, as depicted in Equation (68):

$$h_t = o_t \odot \tanh\left(C_t\right) \quad (68)$$

The output gate o_t itself is governed by a sigmoid activation function, as indicated in Equation (8):

$$o_t = \sigma\left(w_o \cdot \left[h_{(t-1)}, X_t\right] + b_o\right) \quad (69)$$

In these equations, the symbol $\odot$ represents the element-wise (Hadamard) product.

3.2.7 Gated Recurrent Unit

The Gated Recurrent Unit (GRU) is another type of RNN architecture that aims to address gradient-related challenges. GRU combines memory units with hidden states and utilises update and reset gates to control the process of updating and forgetting information. Despite having a simpler architecture than LSTM, GRU still performs well in various tasks and shows resilience to gradient issues.

The update gate determines the extent to which the hidden state should be updated, deciding what information to retain or discard. It takes into account both the current input and the previous time step's hidden state to generate its output. On the other hand, the reset gate determines which information should be reset or disregarded, also based on the current input and the previous time step's hidden state. GRU updates the hidden state by leveraging the outputs of the update gate and reset gate. It selectively discards old information based on the reset gate's output and computes the update magnitude for new information using the update gate's output. These outputs work together to produce the updated hidden state. At each time step, GRU can generate an output, often relying on the current hidden state. GRU seamlessly continues processing the entire input sequence, following these steps iteratively.

During training, the model's outputs are compared to the ground truth values, and the total loss for the entire sequence is calculated using a loss function. To train GRU, backpropagation is utilised,

propagating gradients backward through the network to adjust weights and biases, ultimately minimizing the loss.

The GRU simplifies the LSTM model while retaining the ability to manage long-term dependencies. It accomplishes this with two gates: an update gate and a reset gate. The reset gate determines the amount of past information to forget and is defined at a specific time step t by the following equation[145]:

$$r_t = \sigma\left(w_r \cdot \left[X_t, h_{(t-1)}\right]\right) \tag{70}$$

Here, w_r represents the weight matrix for the reset gate, X_t is the current input vector, and $h_{(t-1)}$ is the hidden state from the previous time step.

The candidate hidden state $\tilde{h}_t$, which incorporates information from the current input and the past hidden state, is computed as:

$$\tilde{h}_t = \tanh\left(w \cdot \left[X_t, r_t \odot h_{(t-1)}\right]\right) \tag{71}$$

This candidate state is a blend of new input and the previous hidden state after it has been modulated by the reset gate.

The update gate functions to balance the old hidden state with the new candidate hidden state. Its role is expressed in the following equation:

$$z_t = \sigma\left(w_z \cdot \left[X_t, h_{(t-1)}\right]\right) \tag{72}$$

where w_z is the weight matrix for the update gate.

The final update of the current hidden state at time t combines the previous hidden state and the candidate hidden state, weighted by the output of the update gate:

$$h_t = (1 - z_t) \odot h_{(t-1)} + z_t \odot \tilde{h}_t \quad (73)$$

In this equation, z_t signifies how much of the past information needs to be forgotten, while $(1 - z_t)$ indicates the proportion of the past hidden state to retain.

3.2.8 Convolutional Recurrent Neural Network

The Convolutional Recurrent Neural Network (CRNN) is a neural architecture that combines the strengths of convolutional and recurrent neural networks. This integration allows CRNN to excel in tasks that require considering both spatial and temporal dependencies simultaneously.

CRNN utilises convolutional layers to extract spatial features from input data. These layers use convolutional kernels of different sizes to capture features at various scales. Depending on the network's architecture and the specific task, these features can include information about shapes, textures, edges, and more. Following the convolutional layers, CRNN incorporates recurrent layers like LSTM or GRU. These recurrent layers operate in the temporal dimension and handle sequential data. At each time step, they receive feature representations from the convolutional layers and the hidden state from the previous step, computing a new hidden state. This mechanism helps the network maintain state and memory while processing sequential data, allowing for a deeper understanding of patterns within the data. Convolutional layers focus on spatial features, while recurrent layers capture temporal dependencies. Together, these processes form the feature extraction and sequence modelling stage of CRNN, enabling it to consider both spatial and temporal information for a better understanding of the input data.

During training, CRNN optimises its parameters, including those in the convolutional and recurrent layers, to minimise prediction errors compared to target values. It employs BPTT to update model

parameters, capturing temporal dependencies. Training continues until predefined criteria are met, improving CRNN's accuracy and enabling it to analyse sequential data, identify patterns, and make accurate predictions.

3.3 Methodology of building simulation

3.3.1 Building simulation software

There are many building simulation software packages, such as BLAST, DOE-2, EnergyPlus, ESP-r and DeST. The model in this report was built by using DesignBuilder (DB), a commercial building energy modelling software. The calculation engine uses EnergyPlus, which has been widely documented elsewhere [146].

3.3.2 Classification of the buildings

The UK BEIS divides energy end consumption into four main sectors: domestic, industry, services, and transport [147]. This classification has been adopted to support the cross-comparison of the results. Representative buildings in each sector over the whole country are generated based on industry best practices, government building surveys, and consultation of local building standards regulations (e.g. Scottish Section six, Part L England and Wales, Part F Northern Ireland).

For the domestic sector, buildings are divided into four categories; detached, semi-detached, terraced, and apartment. For the service sector, buildings are divided into retail, office, and domestic-related categories. As the industrial sector accounts for less than 10% of the national space heating demand, it is assumed to have only one building form [61]. Transport is excluded because there is no associated heat demand.

Table 3-1 Selected buildings from different sectors [147]

Domestic	Service	Industry
Detached Semi-detached Terraced Apartment	Retail Office Domestic-related buildings	Industry buildings

3.3.3 Modelling of buildings

3.3.3.1 Construction of the buildings

Figure 3-4 shows the detached, semi-detached, terraced, and flat models in DB. After the construction of the buildings, many parameters need to be set in the software. As the key objective of the modelling is to obtain the heat profiles, the most important parameters are the U-values of building elements such as the external wall. The U-value is the rate of transfer of heat through a structure, which is also called thermal transmittance. The U-value is a measure of the effect of an insulator on the thermal performance of a building, and it can be calculated by finding the thermal resistance of all the materials that make up the building elements [148], [149], [150]. This means that the U-value is determined by basic building parameters such as thickness and material.

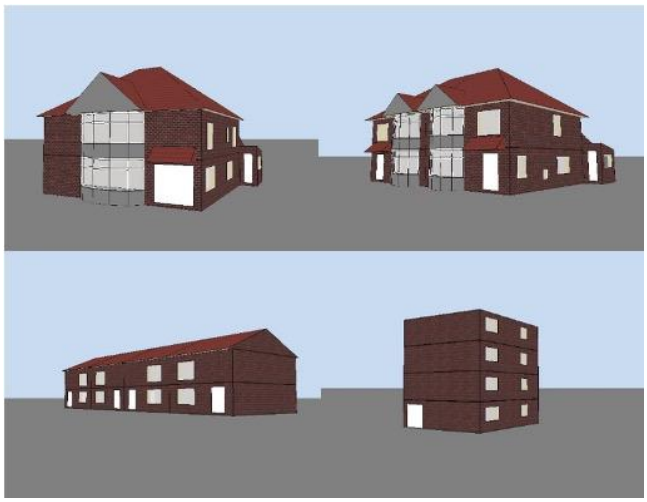

Figure 3-4 Models of domestic buildings in DB

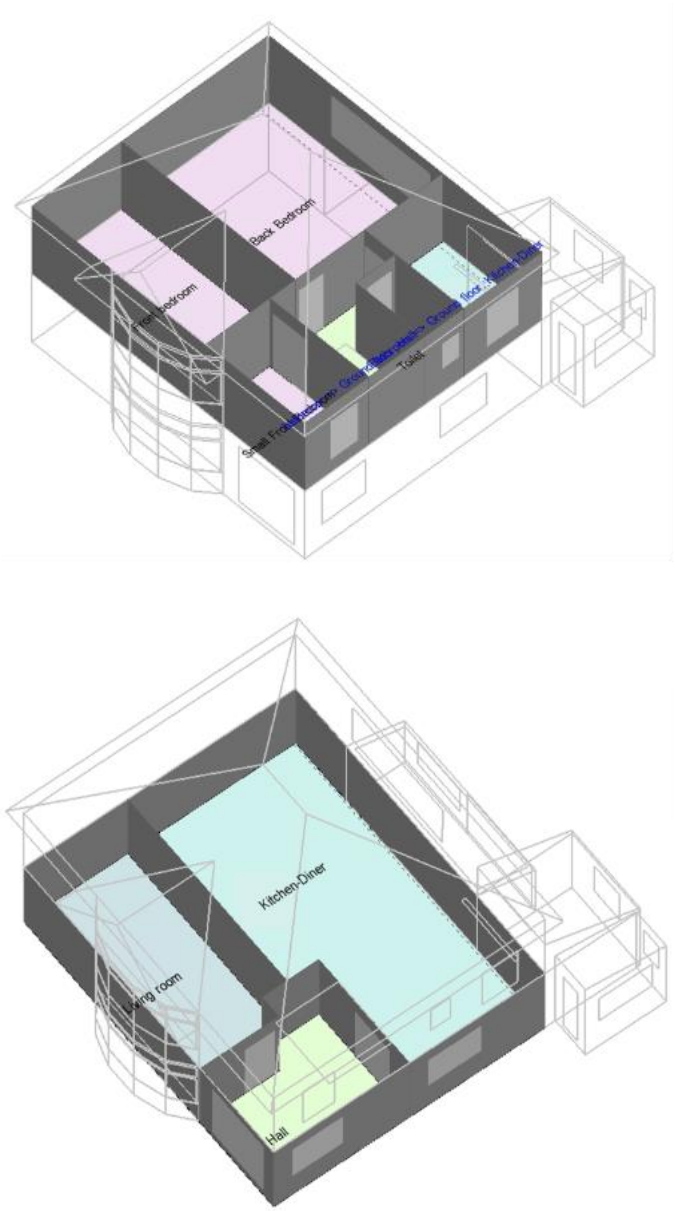

Figure 3-5 Floorplan of Detached house

As an example, the detached house is described in greater detail in Figures 3-5. This type of house features two stories with a total floor area of 140 m^2 and a sloping roof. The interior is divided into various sections including a living room, kitchen, bathroom, and bedrooms. In contrast, a semi-detached house shares one wall with another unit, also spans two stories, but has a smaller total area of 96 m^2. The figures also depict terraced houses and flats, each composed of four units. The terraced

houses have an area of 86 m^2 per unit, whereas the flats are smaller at 64 m^2 each.The population density for all building types is uniformly set at 0.0196.

The construction of the external wall in the model shown in Figure 3-6 is made up of the most common materials of brick and block, concrete, insulation, and plaster. Except for the exterior walls, other U-values that need to be considered in the model are roofs, ground floor and glazing. As standards vary across the UK and have evolved with time, there is a large mix of different standards and constructions. These have been aggregated into "good", "medium", and "poor" categories. According to the age of the building, the insulation level is divided into three levels. The U-value of each level is set as shown in Table 3-2. The solar transmission(G-value) of all windows is 0.69[52].

Figure 3-6 Construction of external wall in the DB model

Table 3-2 The setting U-value of different buildings [52]

		External wall	Roof	Glazing	Ground floor
		W/m^2			
Domestics	Good	0.43	0.15	2.7	0.25
	Medium	1.5	0.75	3.3	0.84
	Poor	2.1	2.5	6.2	1.1
Service and Industry	Good	0.42	0.19	2.7	0.32
	Medium	0.7	0.42	3.9	0.48
	Poor	3.4	2.9	6.2	1.9

3.3.3.2 HVAC module of the simulation

In addition to building construction, the heat gain inside the building affects the heat demand. The software can provide very detailed settings for parameters such as activity, HVAC and lighting modules. However, some detailed data such as population density, office equipment, and luminaire radiation are unpredictable and difficult to measure accurately, especially in older buildings. As such, a simplistic HVAC model has been adopted to exclude much of the detailed modelling which may be influenced by local system inefficiencies. The heating setpoint temperature is assumed to be 18°C and night-time setback temperature is 12°C[151]. It is assumed that natural ventilation is utilised above 22°C. This will influence the space cooling requirement, which is beyond the scope of this study. It may also have a slight dynamic impact when short, sharp spikes in temperature are modelled (e.g. at occupancy steps). The setting of the heating operation schedule varies according to the building type. The heating operation schedule on the weekdays of different buildings is shown in Figure 3-7. The office and

factory are closed during weekends and holidays, while retail and accommodation-related buildings are open on weekdays.

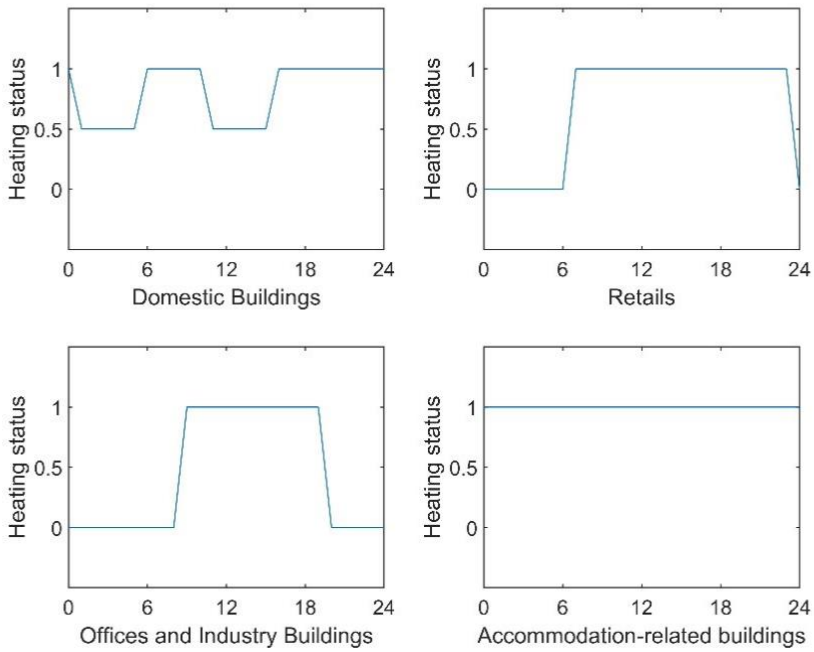

Figure 3-7 Heat schedule of different buildings

3.4 Methodology of ANN

Figure 1 describes the overall process of modelling. The meteorological data and the heat demand obtained from the physical model are used as training data to train the ANN network. At the same time, sensitivity analysis and correlation analysis are applied to select features for the models. ANN networks and feature selection have constituted the model in this chapter and are described further in this section.

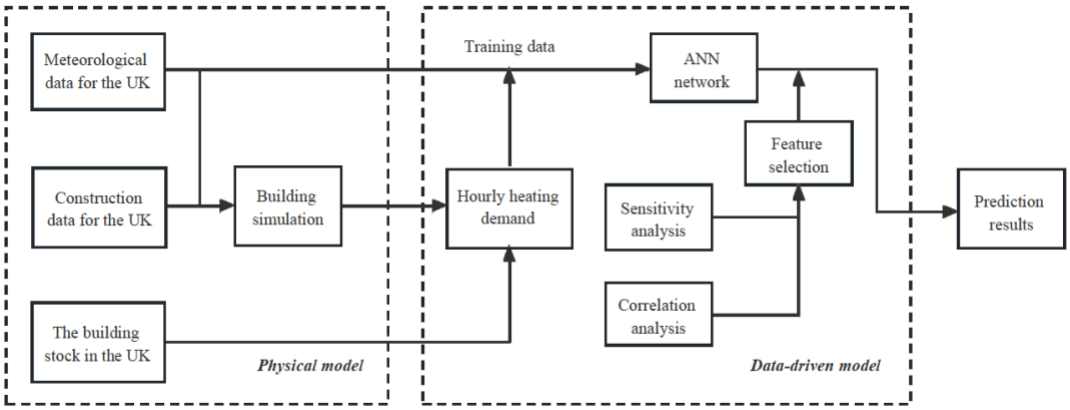

Figure 3-8 Block diagram of the prediction model

3.4.1 ANN topology

An ANN has input layers, hidden layers, and output layers, where the hidden layer can have one or more layers. In many ANN models for estimating building energy consumption, four different types of inputs will be included: time, meteorological data, building characteristics and human activity. Depending on the purpose of the model, time is generally quarterly, monthly, weekly, and hourly. Building characteristics mainly include floor area, volume, wall isolation and window area. ANN models built for a specific building will generally have building characteristics as interim parameters. The impact of human activities, such as heating schedules, numbers of occupants and heating setpoints, are also included in a particular building model. Different from most simplified models, the model used in this section is specific to an area. Therefore, building characteristics and human activities will not be counted. As inputs such as building construction parameters, heating schedules and set temperatures that have a significant impact on thermal demand are removed, it is more difficult to forecast heating demand for regions compared to forecasting for specific buildings. In the case study, the inputs are meteorological data and time while the output is the hourly heating demand in Scotland. Figure 2 shows the ANN topology used for the study. There are 13 inputs to the ANN model, two hidden layers with 40 and 1 neuron respectively,

and one output. After repeated training, a two-layer hidden layer gives more accurate results than a one-layer hidden layer, but more neurons in the second layer did not improve the accuracy but increased the computation time. The determination of the hidden layers and nodes of an ANN is still a research topic and there is no exact formula to give an optimal structure. The common approaches to determine the ANN structure are summarised in Rules of Thumb, Trial and Error, Exhaustive Search, Growing Algorithms, etc [152]. In the past, a number of works have summarised a formula based on experience or case studies to provide an approximate range for determining the number of hidden layers and nodes. In this chapter, the formula in [153]is used to determine the approximate range of hidden nodes for neural network layers, specifically calculating $\sqrt{(m+2)N}+2\sqrt{\frac{N}{m+2}}$ for the first layer and $m\sqrt{\frac{N}{m+2}}$ for the second layer. Here, m denotes the number of output neurons, and N represents the number of training samples. And the final number of layers and nodes is determined by manual adjustment.

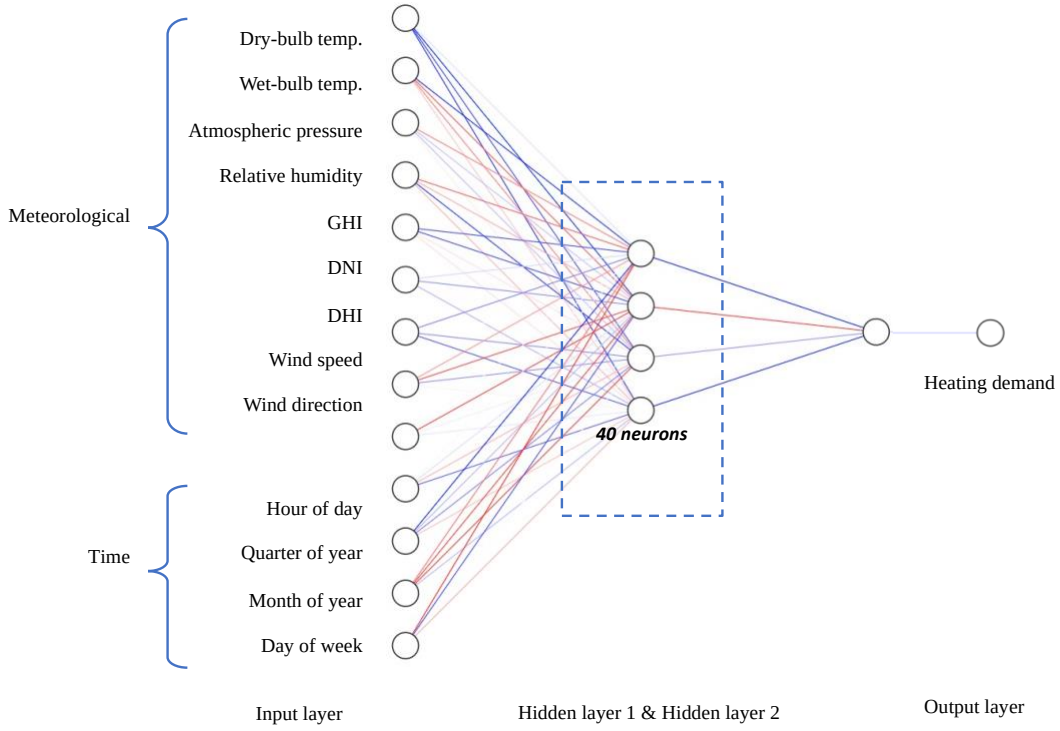

Figure 3-9 ANN topology used in the modelling

3.4.2 Model evaluation

In order to thoroughly compare the various neural networks, three metrics will be employed to assess their performance. One of these metrics is Root Mean Square Error (RMSE), which is commonly utilised to evaluate the accuracy of a model's predictions, especially in regression tasks. RMSE offers a standardised measure to quantify the disparities between predicted values and the actual observed values. The RMSE measures the average magnitude of errors between the actual and predicted values, making it a useful tool for assessing prediction accuracy. It is calculated by taking the square root of the average of squared differences, and this calculation is especially influenced by outliers, giving more weight to larger errors. The RMSE is commonly employed to compare the effectiveness of various models or the same model with different settings. In general, a lower RMSE value signifies a higher level of predictive accuracy for a model.

The formula for calculating RMSE is as follows:

$$\mathrm{RMSE} = \sqrt{\frac{1}{\mathrm{n}}\sum_{\mathrm{i}=1}^{\mathrm{n}}(\mathrm{y_i} - \hat{\mathrm{y}}_\mathrm{i})^2} \tag{74}$$

Where:

n is the number of samples.

y_i is the actual observed value for the ith observation.

$\hat{y}_i$ is the predicted value for the ith observation.

Mean Absolute Error (MAE) serves as a critical metric for quantifying the accuracy of model predictions. It is a measure of model performance that reflects the average magnitude of errors in the predictions, without considering the direction of the error. This makes it an intuitive measure to understand the model's accuracy. Unlike RMSE, MAE does not square the errors, which makes it less

affected by outliers. This robustness of MAE makes it suitable for datasets with anomalies that should not heavily impact the model evaluation. Additionally, since MAE is expressed in the same units as the data, it is easily interpretable and provides an indication of the expected magnitude of prediction errors. MAE is particularly useful in scenarios where the goal is to assess the typical error magnitude without giving excessive importance to larger errors, which is a characteristic of RMSE due to the squaring of errors. It is also advantageous for comparative model assessment, where a linear scale of error is preferred.

The formula for calculating MAE is as follows:

$$\mathrm{MAE} = \frac{1}{\mathrm{n}}\sum_{\mathrm{i}=1}^{\mathrm{n}} |\mathrm{y_i} - \hat{\mathrm{y}}_\mathrm{i}| \tag{75}$$

Where:

n is the number of samples.

y_i is the actual observed value for the ith observation.

$\hat{y}_i$ is the predicted value for the ith observation.

The Mean Absolute Percentage Error (MAPE) is a statistical measure that evaluates the accuracy of a model's predictions. It is expressed as a percentage and calculates the average absolute deviation of the predicted values from the observed values, relative to the observed values. MAPE provides insights into the relative size of the prediction errors by quantifying the average absolute error as a percentage of the actual values. This metric is useful for comparing forecast accuracy across different data scales and ranges, as it is independent of the scale. However, MAPE can be problematic when the actual values are zero or close to zero, as the formula involves division by the actual value. Additionally, the average of percentage errors may not accurately represent the true impact of individual errors in decision-making contexts.

The formula for calculating MAPE is as follows:

$$MAPE = \left(\frac{1}{n}\sum_{i=1}^{n}\left|\frac{y_i-\hat{y}_i}{y_i}\right|\right) \times 100\% \quad (76)$$

Where:

n is the number of samples.

y_i is the actual observed value for the ith observation.

$\hat{y}_i$ is the predicted value for the ith observation.

The Coefficient of Variation of the Root Mean Squared Error (CV-RMSE) is a statistical metric widely used to assess the accuracy of prediction models, particularly in fields such as energy efficiency and building performance simulation. By normalising the root mean squared error (RMSE) relative to the mean observed values, CV-RMSE presents errors as a percentage, offering a clear perspective on the proportion of error relative to actual measurements. A lower CV-RMSE indicates a model's predictions are close to observed values, suggesting better predictive performance. This standardised metric facilitates comparison across different datasets and models, making it valuable for model diagnosis and improvement across diverse applications like weather forecasting, financial analysis, and energy consumption prediction.

$$\text{CV-RMSE} = \frac{\sqrt{\frac{1}{n}\sum_{i=1}^{n}(y_i-\hat{y}_i)^2}}{\bar{y}} \times 100\% \quad (77)$$

Where:

y_i represents the actual observed value for the i-th observation.

$\hat{y}_i$ represents the predicted value for the i-th observation.

$\bar{y}$ is the mean of all observed values y_i.

n is the number of samples.

The Normalised Mean Bias Error (NMBE) metric evaluates the average percentage deviation of the predicted values from the observed values. This normalization by the observed values ensures that the bias is relative to the scale of the data, making it a robust measure regardless of the absolute magnitudes involved. The result expressed as a percentage enhances interpretability, allowing for a straightforward comparison across different models or datasets. A positive NMBE indicates a systematic overestimation by the model, whereas a negative NMBE points to a systematic underestimation. This metric is crucial for diagnosing the tendency of a model to bias its predictions in one direction, which can be particularly useful in applications where such biases can lead to significant practical implications. The goal in refining predictive models often involves minimising the NMBE to as close to zero as possible, indicating that, on average, the model neither significantly overestimates nor underestimates the observed values.

$$\mathrm{NMBE} = \frac{100\%}{n} \sum_{i=1}^{n} \frac{(\hat{y}_i - y_i)}{y_i} \tag{78}$$

Where:

- $\hat{y}_i$ represents the predicted value for the i-th observation.
- y_i represents the actual observed value for the i-th observation.
- n is the number of samples.

3.5 Meteorological data

The energy simulation requires weather files to perform the energy balance over each building. The weather files used are approved for use in UK government compliance calculations and are provided by the Chartered Institute of Building Services Engineers (CIBSE). Typical meteorological year (TMY) files were used for the analysis. The validation step uses files corresponding to 2010 to

be comparable to the validation set. This is because 2010 was the year that was studied by many researchers and had the most data that could be used to compare the results. The historical weather data for 2020 was used to represent the current climate characteristics and it was the year that the most government data could be obtained. Predictive TMY files were used for the 2050 forecasts as the zero-emission target will be achieved in this year. These are classified into “High”, “medium”, and “low” percentile scenarios based on the predicted severity of climate change. Due to the lack of data, the weather data of the same year of 2020 was used for the ANN as the training and testing data, and the specific details will be described in each chapter.

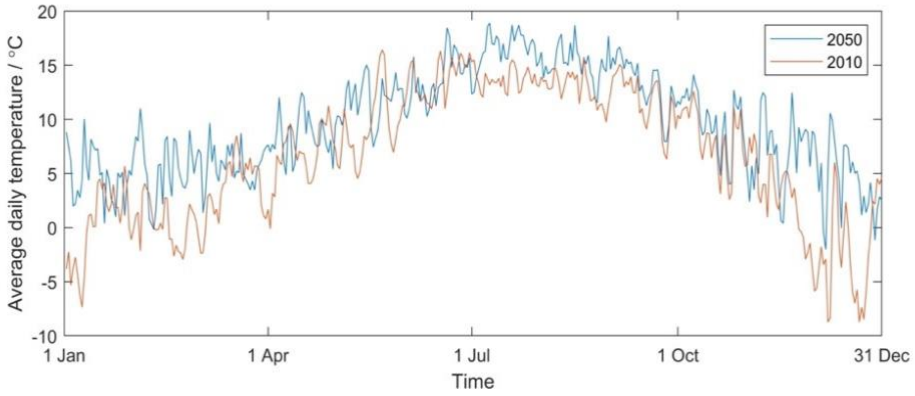

Figure 3-10 Temperature comparison of Scotland in 2010 and 2050 (high scenario)

Taking Scotland as an example, Figure 3-10 shows a comparison of temperatures over Scotland in 2010 and 2050 ("high" scenario). The average temperature of Glasgow in 2050 will be 9.71°C whereas the average temperature in 2010 is 6.81°C, and it rose by 2.9°C between 2010 and 2050. In December, the average temperature in 2010 was 6.56°C lower than the average temperature in 2050, whereas in June, the difference was only 0.01.

Chapter 4

Building Simulation for Space Heating Demand

4.1 Introduction

While the literature discussed above contributes interesting findings for their respective area, there are very few works that develop a high-resolution model for both the domestic and non-domestic sectors in the UK. Second, these studies almost exclusively focus on historic prediction, without focusing on the requirements of a Net Zero power network in future. Based on the research gap identified in the literature review, in this chapter, we present a bottom-up model to estimate hourly heat demand, using the UK in 2050 as a case study. Our approach is the first to be validated against published historic predictions. We then use probability-based weather information and building information for several locations in the domestic, service, and industrial environments to produce synthetic heat demand forecasts. We use this to discuss the potential impact and additional resilience needed in the UK electricity network to meet the demands of the electrification of heat as a recommendation to policymakers and energy distributors.

Computational modelling is necessary to generate thermal demand profiles associated with different sectors in the UK. While there are many validated methods for building energy simulations, there are few widely agreed methods for predicting heat demand at the national level. Therefore, our approach is to (1) generate a computational building thermal energy model for the UK building stock (2) validate this methodology against published literature data and (3) use the validated method to predict the thermal energy demand in 2050.

4.2 Building stock model of the UK

4.2.1Regional divisions

For this study, the UK is divided into six regions, as shown in Figure 4-1, based loosely on similarities in weather patterns. Eight different buildings from different sectors were used to represent the common building morphologies found in each sector, as shown in Table 1. This is based on building surveys of each respective nations. For each building morphology, three different levels of insulation are applied to create three different demand profiles per morphology so that 24 different half-hourly heat demand profiles can be obtained from 24 different building models in each region, giving a total of 144 different hourly heat demand profiles for the whole UK.

Figure 4-1 Regional divisions of the UK.

4.2.2 Stock of buildings

The UK non-domestic building stock model is proposed in [60] by the Bruhns in Carbon Reduction in Buildings (CaRB) project. In addition, the space heating demand of domestic households accounts for 70% of the total space heating demand. There are four housing surveys from governments: the English Housing Survey (EHS), the Scottish House Condition Survey (SHCS), the Welsh Housing Conditions Survey (WHCS) and the Northern Ireland House Condition Survey (NIHCS) [147], [154], [155]. Further studies have presented in detail the impact of different scenarios and policies on the model output [133], [134] [156]. We adopt a computational building model, using the stock of buildings in the commercial software DB for the UK hourly heat demand estimation based on the work presented by McCallum et al. [57].

The stock and classification data of buildings in the UK are limited to the domestic sector. There are contradictions between the different data sources, which also increases the difficulty of collecting

building stock data. The results of the building stock in this report are based on public government reports and many published pieces of literature [60], [147], [154], [155], [156], [157], [158], [159]. By 2050, 31.8 million dwellings will be needed in the UK, which will increase by 15% compared with 2010. Currently, the average EPC rating of the UK is band D. To meet the 2050 requirements, the EPC of new buildings will need to be band A. It is estimated that approximately 75% of buildings in use today will still be in use by 2050, and the remaining 25% will be composed of new buildings. From band D to band A, it is assumed that the efficiency improvement of new buildings in the UK is 30% [160], [161], [162], [163].

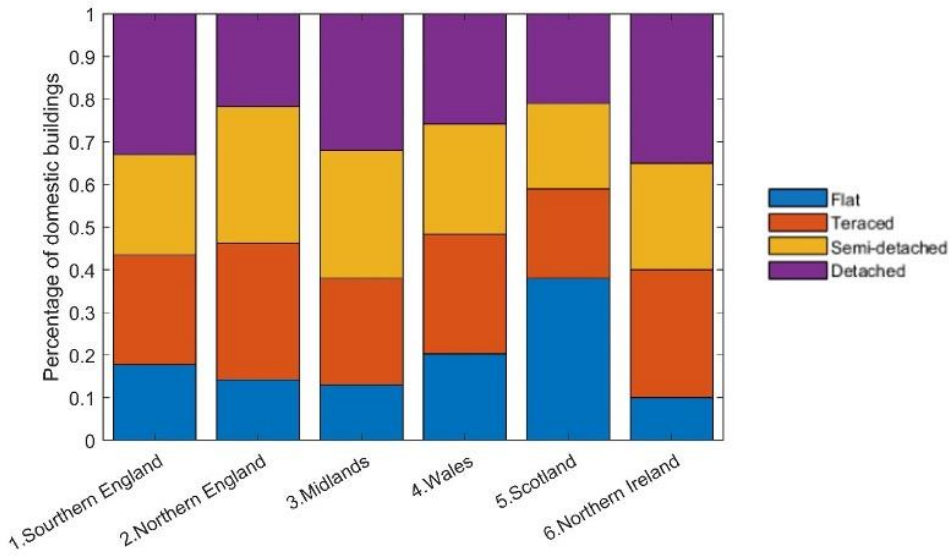

Figure 4-2 Percentage of different domestic buildings in the six regions

For the domestic sector, each national government has developed a housing survey that provides detailed and accurate data on non-domestic sector building conditions. The results of these four surveys provide the dwelling age, type of location and average size in the UK, which has been used in this model. The proportion of domestic buildings in the six regions is shown in Figure 4-2.

Office and retail are the most common types of service buildings. The domestic-service sector (e.g., healthcare, community centres etc.) accounts for less than 50% of the service sectors by floor area, and therefore a simplistic model has been used [164], [165]. For the industrial sector, the heat demand is mainly from heat processing, whereas space heating only accounts for a small part. Although the industrial sector is complex, the buildings are represented by a workshop because the demand profiles are similar. For service and industrial buildings, the total floor space is usually used for statistics rather than the number of buildings. Retail accounts for 16% of the total area, office accounts for 12%, domestic-related accounts for 34%, and industry accounts for 37% [60], [165]. Due to the lack of statistics on service and industrial buildings, the area of service and industrial buildings in each region is allocated according to the proportion of the population.

4.3 Model Validation

Once the model is established, we use it to calculate the hourly heat demand of the UK in 2010. The results of the model are then compared with those published work by Watson for validation [56]. After validation, the model is then used to predict the heat demand in the UK in 2050.

4.3.1 Comparison with Government Data

The UK's total energy consumption by end-use in 2010 is presented in Table 3-3 [61]. Hourly heat demand data are not available from government sources. The data in the first column are the estimated energy end-use for heat, where energy conversion efficiency also needs to be considered. Based on the percentage and efficiency of the four main types of heating in the UK (Gas boiler, Resistive heating, Oil-fired boiler, and Solid-fuel boiler), the average energy efficiency of all heating methods is estimated to be 84% [52]. The second column shows the heat demand after applying the average energy

efficiency. The comparison presented in Table 4-1 shows a good agreement between the prediction using our model and the government data, in terms of the annual total heat demand by each sector in 2010.

Table 4-1 Summary of modelled annual heat demand and government literature heat demand. The presented model is shown with a percentage deviation from the validation model.

Sector	Total Energy for Heat / TWh	Heat Demand / TWh	The present Model / TWh	Percentage Deviation / %
Domestic	402.7	338.3	350.6	3.6
Service	102.9	86.4	79.2	-9
Industry	37.6	31.6	31.5	-0.3

4.3.2 Comparison with Watson's Model

The heating demand data from the government is typically derived from economic data-based models based on GDP, population and industry that provide energy consumption for heating for a year. Hourly heating demand from the national grid or gas consumption as heat demand is not directly recorded in the same way as electricity due to the complexity of the sources and technologies of heating. Watson et al. present a temperature-heat model for domestic heating based on gas data collected from 8700 dwellings around the UK. The results are considered reliable compared with national daily non-daily metered gas consumption and official UK government annual domestic gas demand [166]. Watson's model involved several key steps to ensure robust and accurate estimation of half-hourly domestic heat demand in Great Britain. First, data were sourced from the Energy Demand Research Project (EDRP), which included over 8700 dwellings monitored between 2007 and 2010. The dataset was cleaned by replacing missing data and removing unreliable periods and erroneous readings, resulting in a reliable dataset from May 2009 to July 2010. A bottom-up statistical model was developed, relating daily gas

demand to effective outdoor temperature, while accounting for the spatial and socio-demographic differences between the sample and the national housing stock. The researchers then segmented daily gas demand into components for space heating, domestic hot water (DHW), and cooking. They created separate half-hourly profiles for different temperature bands and weekdays versus weekends. The model's predictions were validated against actual daily and annual gas consumption data, confirming its accuracy. Finally, the validated model was used to predict national half-hourly heat demand for space heating and DHW under various weather scenarios, providing detailed and reliable estimates that improved upon previous studies by using a larger dataset and incorporating temperature-dependent demand variations. Hence, Watson's domestic heat demand and hot water data in 2010 were used for validation. The demand for domestic hot water is added to the present model to compare with Watson's result. Since the approaches used by the two models are different, resulting in different daily peak periods, the average daily demand is used for comparison.

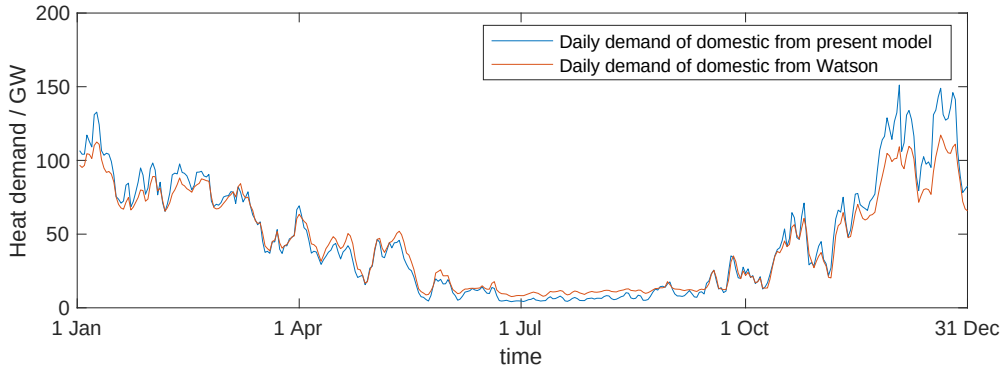

Figure 4-3 Comparison of daily heat demand between the present and Watson model.

Figure 4-3 shows the daily heat demand over 2010 using Watson's model and the presented model. In general, the distributions of heat demand throughout the year are similar, showing good agreement. Figure 8 shows that this result is strongly correlated with Watson's result when using linear regression.

According to the ASHRAE recommendations normalised mean bias error (NMBE) and coefficient of variation of the root mean squared error (CV-RMSE) were used to evaluate the performance of the model. The acceptable ranges of NMBE and CV-RMSE for daily building energy prediction is +/-7.5% and 22.5%[167]. The calculated value of NMBE is 5%, and the value of CV-RMSE is 20.5%. In addition, the symmetric mean absolute percentage error (sMAPE) of the two sets of data is 0.2 and the mean absolute scaled error (MASE) is 1.85. In winter, the daily demand of this model is greater than that of the Watson model, and the present heat demand in summer is smaller. In the presented model, the space heat demand in summer is negligible as the simulated room temperature does not drop below the set point temperature. The present model is more sensitive to temperature, resulting in a large difference between Watson's and present models in extremely hot and cold conditions. In practice however, human thermal comfort is subjective; therefore, it is likely that the Watson model may have considered the human aspects, while the presented model does not.

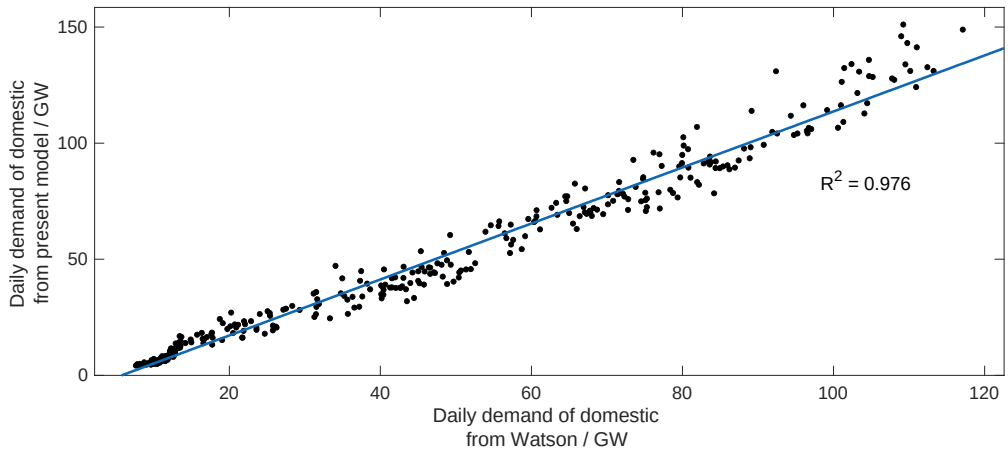

Figure 4-4 Comparison of the present model with Watson's model using linear regression.

Note that the key objective of this chapter is to approximately estimate the impacts of heat electrification on the grid in the future net zero, rather than developing a more accurate heat demand

forecasting model. Nevertheless, the comparison between our model and Watson's model showed a reasonably good agreement. Considering that Watson's model has been validated by the actual gas consumption data in 2010, such an indirect validation offers confidence that our model has captured the characteristics of the house stocks in the UK and is capable of estimating the hourly heat demand of the UK if a weather profile is given.

4.4 Results and Discussion

The weather file of 2050 used in our modelling is a 'high' scenario, which is a worst-case scenario of global warming, corresponding to the possible lowest heat demand. These weather data are based on climate change projections from the UK Met Office. Although weather data for the 'medium' scenario in 2050 were also provided, the average temperature of the medium scenario is only 0.5°C lower than that of the high scenario; therefore, the results are similar, and are omitted here. As the official department does not offer a weather file for the 'low' scenario in 2050, it is assumed that temperatures in 2050 will remain the same as those in 2020 in the case of no global warming to calculate the highest possible heat demand. In this way, we can calculate the range of possible heat demand in 2050.

4.4.1 Heat demand of the UK in 2050

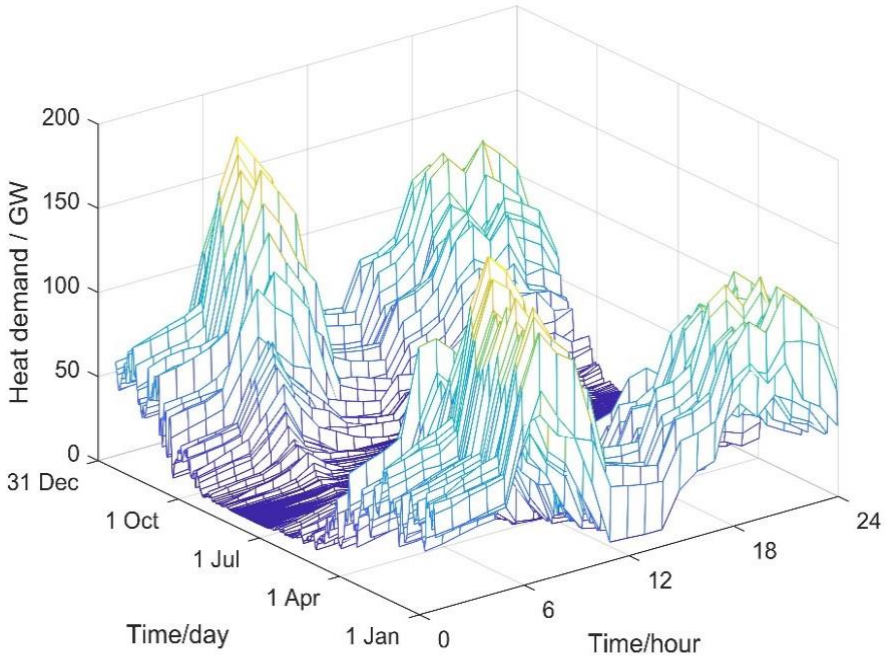
Heat demand / GW
200
150
100
50
0
31 Dec
1 Oct
1 Jul
1 Apr
1 Jan
Time/day
0
6
12
18
24
Time/hour

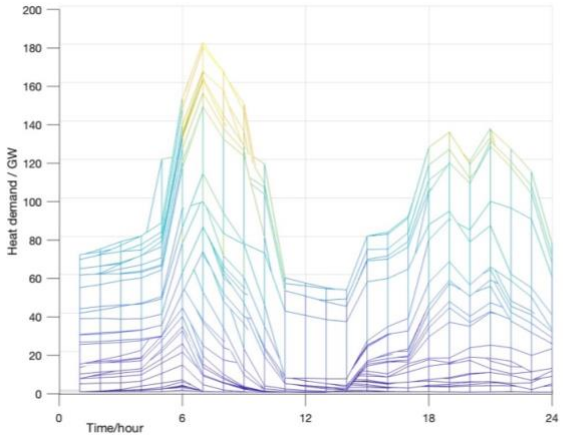
Heat demand / GW
200
180
160
140
120
100
80
60
40
20
0
0
6
12
18
24
Time/hour

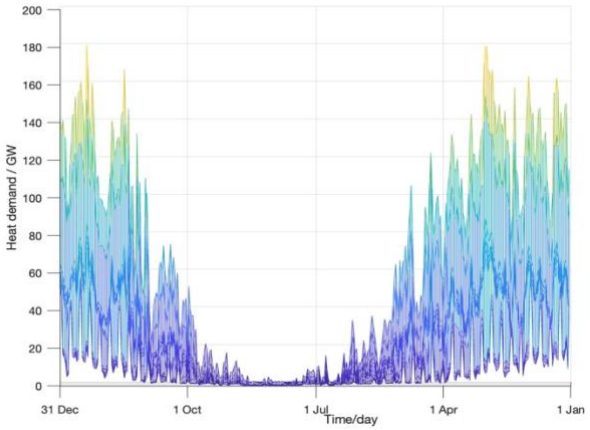
Heat demand / GW
200
180
160
140
120
100
80
60
40
20
0
31 Dec
1 Oct
1 Jul
1 Apr
1 Jan
Time/day

Figure 4-5 Mesh plot of modelled UK hourly heat demand of high scenario in 2050. (The daily profiles are shown on the X-axis and the monthly profiles on the y-axis, and the heat demand in GW is shown on the z-axis.)

Figure 4-5 is the mesh plot of the calculated UK hourly heat demand (i.e., heat demand for one hour) of the high scenario in 2050 which shows the variations of heat demand across a day (x-axis) and month (y-axis). For a given hour, the calculated heat demand reaches a peak in winter around December and January. For each day in winter, there are two distinct peaks in the heat demand profile (x-axis). The first peak occurs in the morning and the other in the early evening. The peak hourly heat demand of the high scenario in 2050 is 180.9 GW. The external temperature in 2050 is much closer to the set point temperature of the buildings; therefore, less energy is needed within the same time frame than in 2010. As the simulations are dynamic, the building will retain heat and therefore the peak demand will be reduced. The outdoor temperature in summer is higher than that in winter, and the setpoint room temperature is easier to reach, which can explain why the peak of the day arrives earlier in summer than in winter. It establishes that the actual peak demand over a year will be significantly underestimated if only the daily heat demand is calculated.

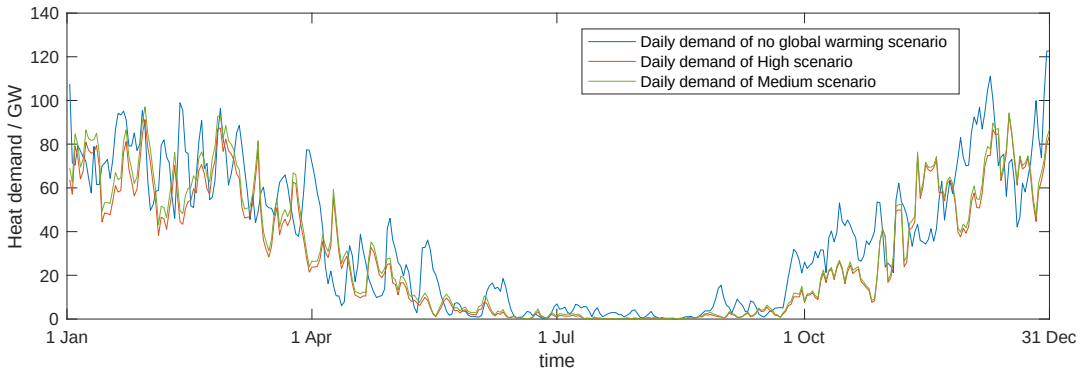

Figure 4-6 Comparison of daily heat demand of high scenario, medium scenario, and 2020

Figure 4-6 shows a comparison of daily heat demand (i.e., average hourly heat demand of the day) between the high scenario, the medium scenario and 2020 (no global warming scenario). The distributions of daily heat demand for the high and medium scenarios are similar throughout the year. The total annual demand for the high scenario is 256.5 TWh and the annual demand for the medium scenario is 275.6 TWh, the difference is only 19.1 TWh. Therefore, the medium scenario is not discussed further in this study. The high scenario implies the highest possible global warming, leading to the lowest heat demand. The no global warming scenario (using the 2020 weather profile) is the worst-case scenario for heat demand (i.e., highest demand case). The actual demand in 2050 will fall between these two extreme predictions. A comparison of the results for the two extreme cases is given in Table 4-2. The potential annual heat demand range for the UK in 2050 is from 256.5 TWh to 317.2 TWh. The possible hourly peak demand for heating in 2050 ranges from 180.9 GW to 201.9 GW and the possible daily peak demand is between 93.3 to 122.8 GW. For reference to see the scale of the problem, the 2020 peak electricity demand was only 45.9 GW[168].

Table 4-2 Heat demand for the high scenario and the no global warming scenario.

	Hourly peak demand / GW	Daily peak demand /GW	Total annual demand /TWh
High scenario	180.9	93.3	256.5
No global warming scenario	201.9	122.8	317.2

4.4.2 Electricity demand due to heat electrification in 2050

The comparison of hourly heat demand (high scenario) and electricity demand in the UK is shown in Figure 4-7(a). The national grid predicted that the electricity demand in the UK in 2050 would be 523TWh in the Steady Progression scenario[169]. As there is no hourly electricity demand data in the UK in 2050. We approximately broke down the annual electricity demand into hourly demand in 2050 according to the hourly electricity demand profile in 2020. We understand this approach is not accurate, but nevertheless, it can give us some indications of what the scale of the daily electricity demand without heat electrification would look like in 2050.

Compared with heat demand, the fluctuation in electricity demand throughout the year is not significant. For the whole year, hourly electricity demand is maintained at around 75 GW while heat demand could reach more than 150 GW in winter. In contrast, heat demand can be ignored during some summer days. There are many methods to achieve the electrification of heat. In this chapter, a heat pump is chosen to electrify the heat supply. If heat pumps can have an average COP of 2.9 (which is the threshold COP for qualifying renewable heat incentives in the UK) [170], the total electricity demand with 100% heat electrification is shown in Figure 4-7(b).

As shown in Figure 4-7, in 2050, the peak hourly electricity demand without heat electrification is around 96.1 GW while the peak hourly electricity demand with 100% heat electrification through electric heat pumps with a COP of 2.9 is around 135.8 GW. The same calculation was applied for the no-global warming scenario. In the case of 100% electrification of heat, the peak electrical demand is 146.7 GW, which requires the installed capacity of electricity to be increased by at least 50%. The potential range of electricity demand in 2050 is between 135.8GW and 146.7 GW after 100% heat electrification with heat pumps.

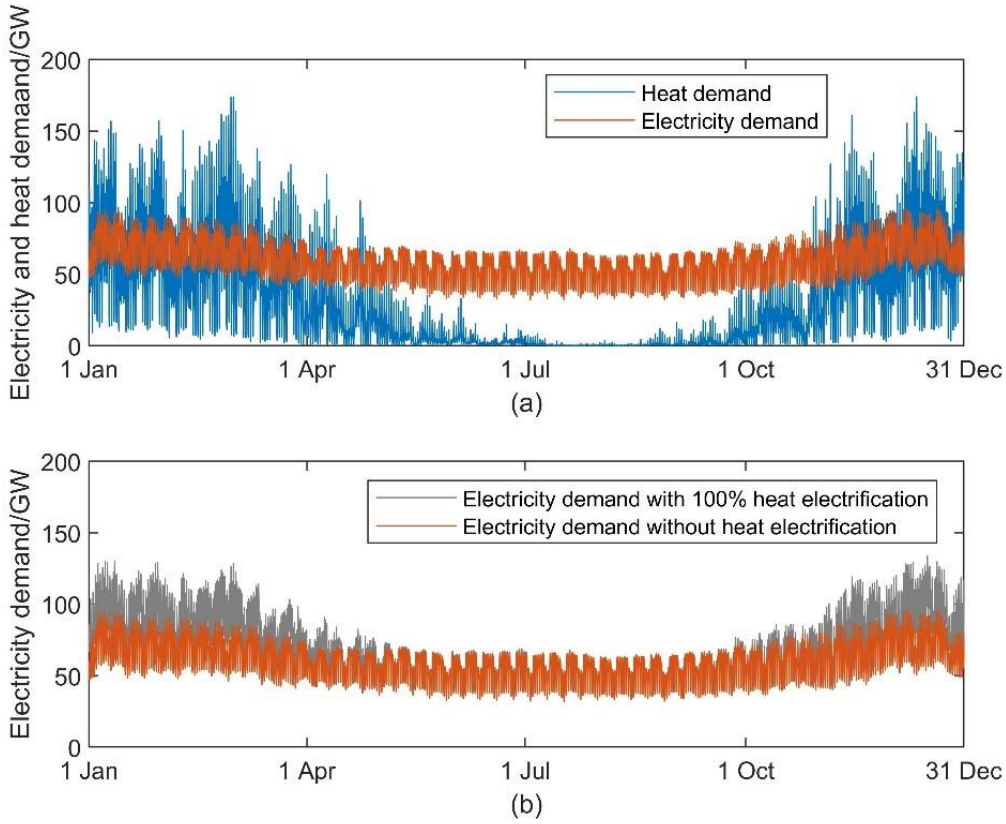

Figure 4-7 (a) Heat demand of high scenario and electricity demand in 2050; (b) Electricity demand with 0% and 100% heat electrification of high scenario in 2050

4.4.3 Peak demand analysis

It is worth noting that if all space heating needs are supplied by electric heat pumps with an average COP of 2.9, it will have a great impact on the power grid during the winter, but a small effect on electricity

demand in the summer. The imbalanced demand in summer and winter causes a dilemma in planning the investment of grid infrastructure. If the grid is not upgraded according to the daily peak demand in winter, it cannot supply enough power which causes overload. If the grid is upgraded according to the daily peak demand in winter, huge generation capacity will be wasted in summer. Furthermore, the insertion of a large number of heating equipment will aggravate the instability of the grid.

For domestic heating, people's activities are concentrated from 5 am to 10 am and from 3 pm to midnight. Figure 4-8 shows the hourly heat demand (high scenario) domestic heat demand (high scenario) and the whole UK's total heat demand in the day with the highest demand. For the UK, the two peaks occur in the morning and afternoon on the day of maximum demand, respectively. The first peak demand occurs between 6 am and 10 am. The second peak demand occurs between 6 pm and 10 pm. The two profiles in Figure 4-8 (a) are similar because the domestic demand is far greater than service and industrial demand. The predicted whole UK's heat demand is mainly decided by the domestic heat demand. For the day of minimum demand, the demand in the UK and domestic sectors is both lower than 1GW.

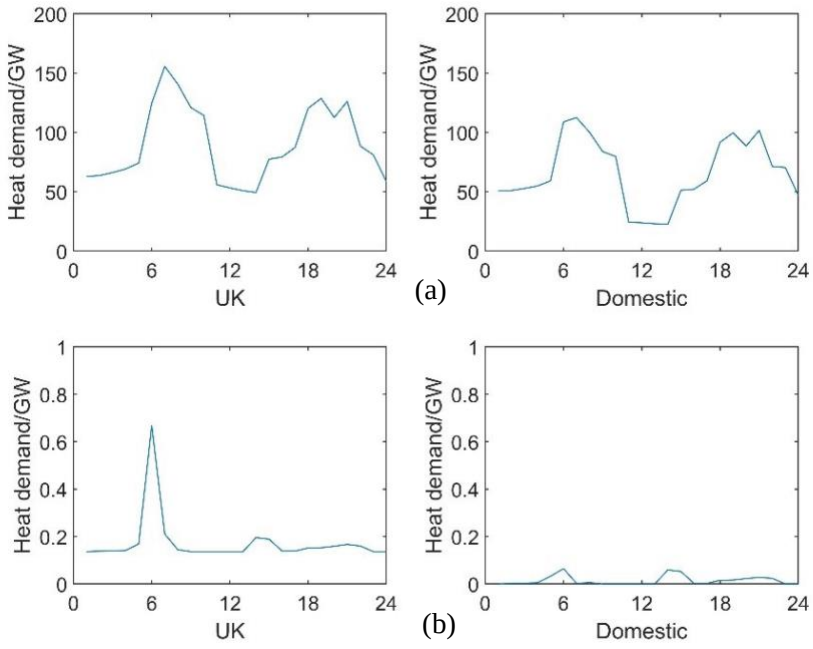

Figure 4-8 (a) Day of maximum demand in 2050 (high scenario); (b) Day of minimum demand in 2050 (high scenario)

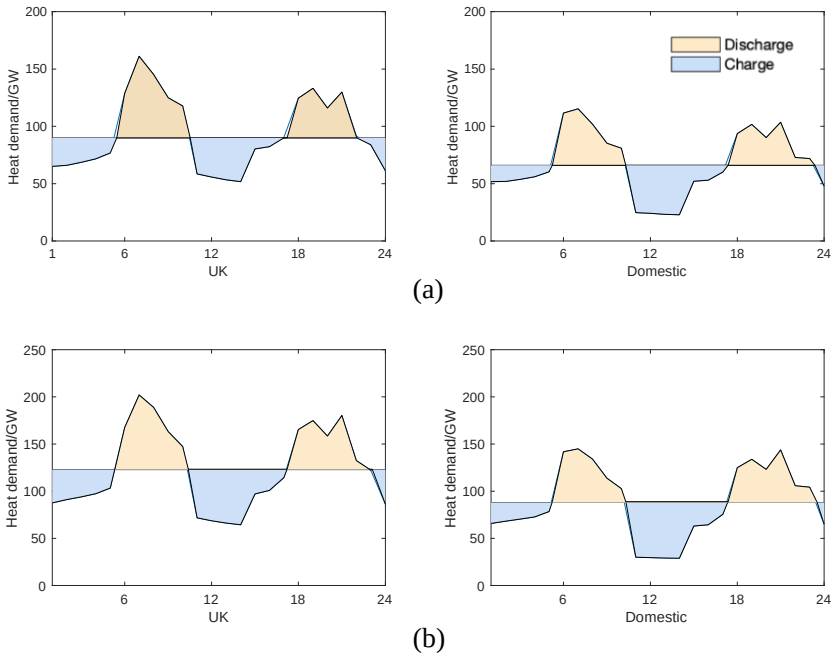

Figure 4-9 Storage demand of the maximum day:(a) The high scenario in 2050; (b) No global warming, i.e., using 2020 temperature profile for 2050.

Energy storage, such as short-term heat storage, is a possible solution to address the challenges caused by the high fluctuation of heat demand. It is therefore interesting to find out how much heat storage capacity would be required. Figure 4-9 shows a possible operational strategy to shave the daily peaks. All heat pumps operate at a daily average capacity of around 120 GW, the excessive heat production during periods of low demand can be stored in the heat storage. During a period of high demand, the stored heat can be released to top up the heat production from the heating systems that still operate at their average daily capacity. Take the whole UK as an example, according to Figure 4-9(a), around 333 GWh heat storage is required to shave the peak when the worst global warming happens in 2050. For the domestic sector, the required heat storage is around 282 GWh. In the case of no global warming in 2050, the

temperature profile in 2020 is used for calculation. The calculated results are shown in Figure 4-9(b). It can be found that the required heat storage capacity for the whole UK is 386.3 GWh, of which 344.7 GWh comes from domestic. Therefore, the total heat storage capacity could be between 333 GWh and 386.3 GWh for the whole UK in 2050.

For the domestic sector, it is predicted that around 31.8 million dwellings will be needed in the UK by 2050. Therefore, each dwelling on average will need a heat storage capacity between 8.8 kWh to 10.8 kWh, which seems feasible. There are various forms of heat storage, and it has been calculated that 8kWh requires roughly 0.347 cubic metres of hot water [171], so installing between 8.8kWh and 10.8kWh of heat storage would not be difficult for a household. As shown in Figure 13, coordinated heat storage could significantly shave the hourly peak power demand by 30-40% on the coldest day. This means wide installation heat storage could significantly reduce the required investment for new power generation capacity.

Similarly, inter-seasonal heat storage can also be utilised to reduce the winter peaks of heat demand by recovering heat in summer and storing it for winter use. In addition to heat storage, electricity storage will also play an important role in our future energy system, which is beyond the scope of this thesis.

For further peak demand analysis, the boxplot in Figure 4-10 shows the analysis of electricity demand for the high scenario during different hours in 2050. For each hour, there are 365 data points from different days during a year and the distribution of 365 data points in one hour can be analysed in the boxplot. The ‘red line’ in the box is Median (Q2) while the bottom of the box is the first quartile(Q1) and the top of the box is the third quartile(Q3). The upper and lower whiskers are represented in ‘-’. Upper

whisker = q3 + w × (q3 – q1) and lower whisker = q1 – w × (q3 – q1). The maximum and minimum values are around at upper whisker and lower whisker. If the values in the group exceed the upper and lower whisker, these values will be represented with red '+' and it is called outliers.

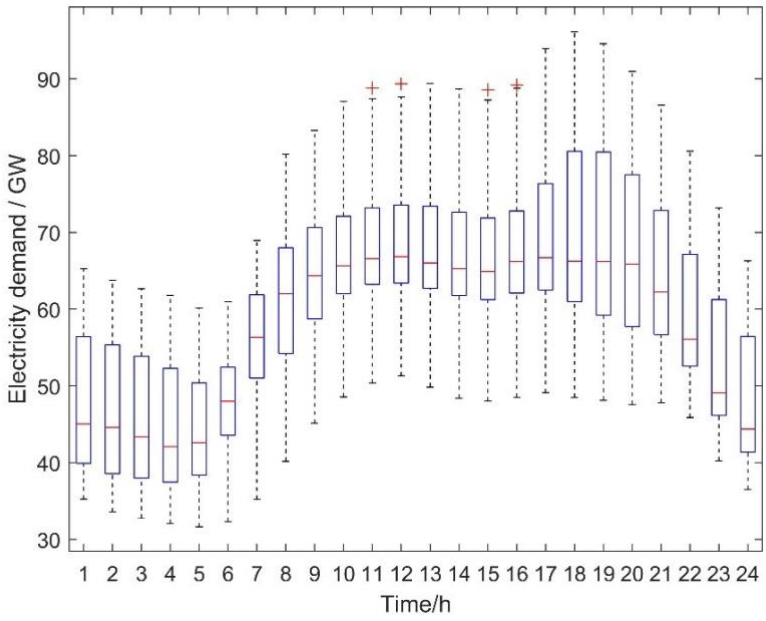

(a)

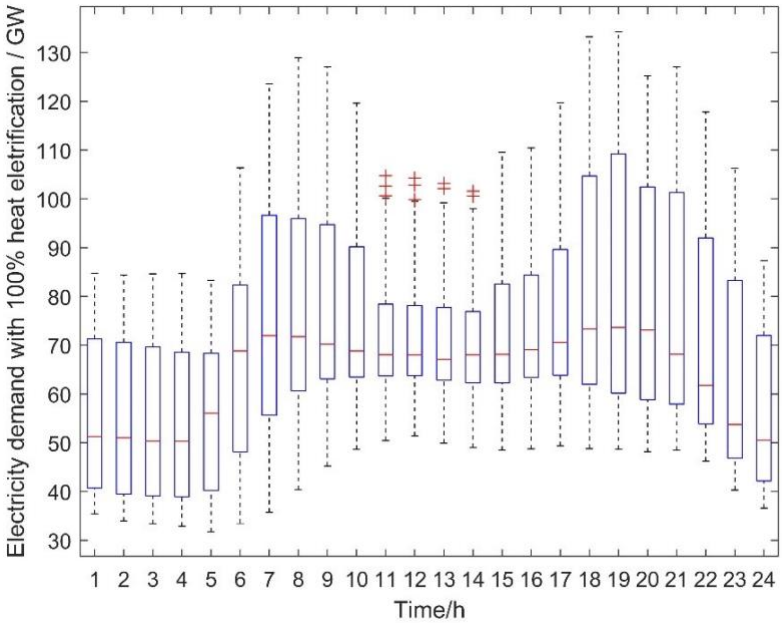

(b)

Figure 4-10 (a) Boxplot of the electricity demand of high scenario in 2050; (b) Boxplot of total electricity demand with 100% electrification of high scenario in 2050.

Figure 4-10 (a) shows the boxplot of the predicted electricity demand in 2050. The maximum value appears at 6 pm and the minimum value appears at 5 am. After 6 am, the electricity demand has been steadily increasing until it enters a stable period at 11 am. After four o'clock there is a second wave of growth, lasting for about three hours, and the demand peak is reached at 6 pm. Figure 4-10(b) shows the boxplot of total electricity demand with 100% electrification of heat. It is different from the profile in Figure 4-10 (a) that the electricity demand profile has two peaks. The first peak appears at around 7 am, and the second peak appears between 7 pm and 9 pm. Also, more outliers appear in Figure 4-10(b) during this period. It shows that demand from 11 am to 4 pm is greatly affected by the season. It is the same for the period from 0 am to 5 am, electricity demand remains stable and low in both figures. The results show that heat electrification not only affects the total electricity demand but also affects the shape of the profile. With the development of heat electrification, two peaks in the electricity demand profile will happen in a day. Meanwhile, the new electricity profile is very steep, which means the peak is reached in a very short time. There is no doubt that such changes will cause some difficulties in the operation of the grid and are a matter of concern in our further research.

4.4.4 Analysis of sections and regions

Figure 4-11 shows the heat demand of different sectors and regions of the high scenario in 2050. In the domestic sector, the annual demand for the high scenario is 195.5TWh, which is accounting for 76.2% of the total increase. The remaining 23.8% increase is from industry and service. The highest heat demand is in Southern England and is least in Northern Ireland. Regional heat demand is dependent on population rather than temperature or area. The heat demand in a region increases with its population density due to the larger total building area, resulting in the highest heat demand in Southern England. However, it is important to note that, for an identical building, the heat demand in Northern Ireland would be higher

than in Southern England. This is because the temperatures are generally higher in Southern England, reducing the heating needs for the same building in that region.

Figure 4-12 shows the hourly heating demand for domestic, service and industry of the high scenario in 2050. For domestic, the highest hourly demand is 132GW while the demand can decrease to 2GW during the same day. The profiles of the three scenarios have a subtle difference which is due to different building functions and different heating schedules. Many other unpredictable factors have not been considered. In terms of both total annual demand and hourly peak demand, heat demand for domestic will account for the largest share of space heating. Especially after the epidemic, flexible working will increase the demand for domestic heating. The government shall increase its concentration on domestic buildings such as upgrading the heating system in domestic or retrofitting domestic buildings.

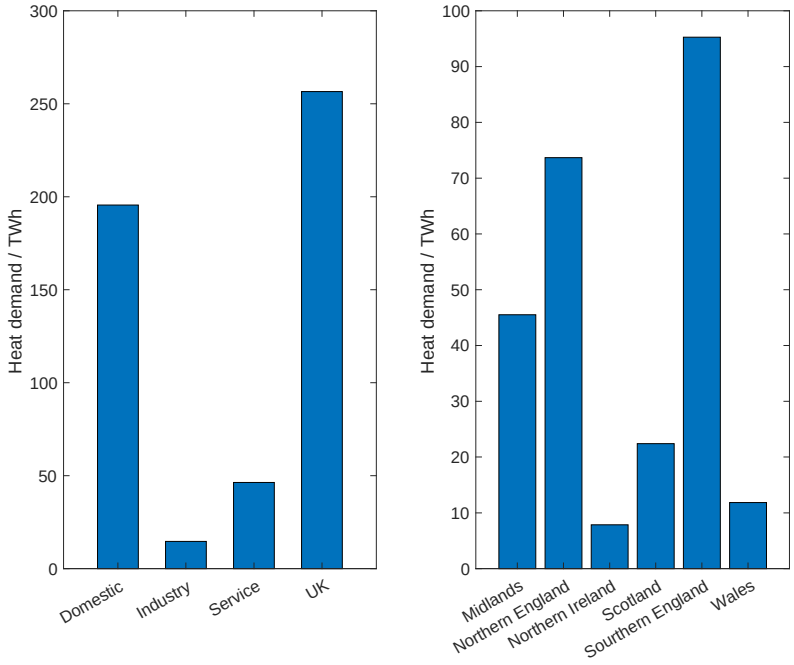

Figure 4-11 Heat demand of different sectors and regions of the high scenario in 2050

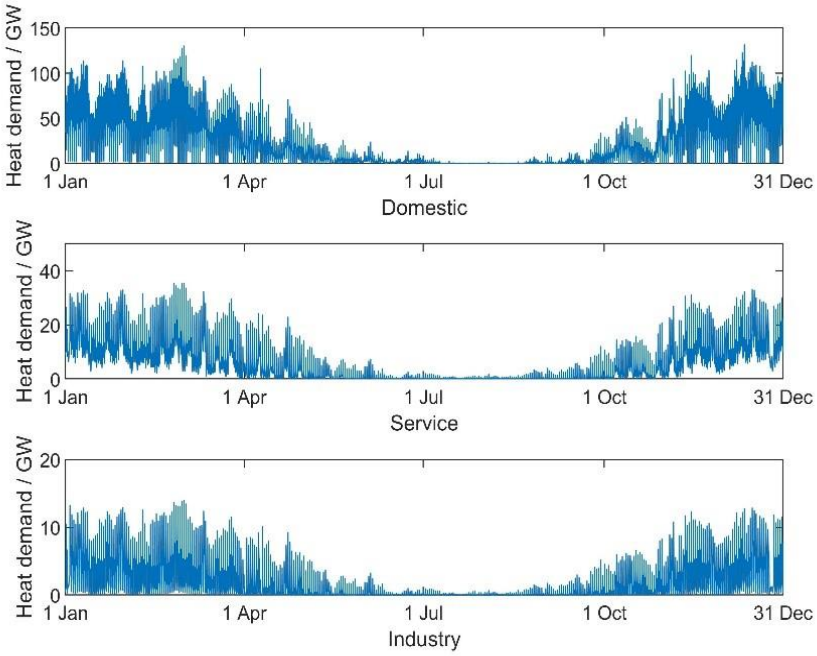

Figure 4-12 Heat demand of Domestic, Service and Industry of high scenario in 2050

4.5 Conclusion

This work has discussed the impacts of electrifying heat on the grid through a high-resolution forecasting model for heating demand at a nationwide level which allows for hourly demand analysis up to 2050. Hourly heat demand profiles of eight types of buildings from domestic, service and industry for the six regions in the UK were developed by building simulation. While the decarbonization of heat will certainly require significant network reinforcement, it may be the case that global warming will offer some small mitigation to this peak power increase. Without global warming, the hourly peak demand could reach 201.9 GW, whereas with severe global warming, it might only be 180.9 GW. However, the potential range of electricity demand in 2050 could be between 135.8 GW and 146.7 GW and it shows that the electrification of heat will require a significant increase in power generation capacity for the UK electricity network, of which the domestic sector will contribute 76.2%.

Heating demand is heavily concentrated in the winter with a direct correlation to the population density of each region, making network reinforcement requirements inconsistent across both geography and seasonally. Even in the worst scenarios of global warming, the highest hourly demand for domestic heating is 132 GW while demand can decrease to 2 GW during the same day. Energy storage, whether thermal or electrical, has shown to be a potential solution to this. For peak shaving caused by the electrification of domestic heating, the required heat storage is between 282 GWh and 344.7 GWh. The required hourly peak power demand could be reduced by 30-40% through coordinated heat storage operations.

Chapter 4 has detailed the application of building simulation techniques for predicting heating demand, highlighting the method's comprehensive but time-intensive nature. Transitioning into Chapter 5, the focus shifts to employing Artificial Neural Networks (ANN) as a predictive tool. Building simulations, while thorough, are constrained by their substantial computational requirements. The adoption of ANN is motivated by the potential to integrate the detailed dynamics captured through building simulations into a more streamlined, scalable predictive model. Training an ANN with data from building simulations facilitates the maintenance of accuracy while markedly decreasing the time required for predictions. This methodological shift enhances the feasibility of implementing real-time heating demand forecasting across various building scenarios.

Chapter 5

Artificial Neural Network for Space Heating Demand

5.1 Introduction

This research aims to introduce a novel framework for the efficient acquisition of high-resolution national-level data. The proposed approach replaces the traditional physical model with an ANN-based model, which is ignored in the field of high-resolution modelling at a national level in UK.

Based on the literature review presented, the following key issues are summarised for ML applications in heat demand prediction.

i. For heating demand prediction, ML is mainly applied to individual buildings or small-scale building complexes.

ii. Most research has focused on improving ML algorithms and applying different ML algorithms, but there is a lack of assessments of future scenarios like 2050.

iii. The lack of architectural and meteorological data is also an important reason for the low application of ML for large-scale, high-precision heat demand forecasting.

In this framework, information pertaining to buildings is omitted, while weather and timing data are retained as the main inputs. The lack of high-resolution heating demand data in the UK is a prominent issue, as it is challenging to directly monitor and is typically recorded on a yearly or monthly basis. To address this limitation, this study relies on a validated simulation model to provide data. The simulation model acts as a source of data, while the ANN model simplifies the construction of the simulation model. Furthermore, this chapter suggests a combination of sensitivity analysis and correlation analysis for selecting relevant features, thereby reducing the required types of meteorological data. This feature selection technique enhances the efficiency of the model. To validate the practical application of this framework, the model will be employed to predict the domestic heating demand in Scotland in the year 2050. The contribution of this model are as follows:

i. The proposed model provides a fast response compared to the physical model, while maintaining the same high resolution at a national level.

ii. It offers a prediction model solely based on weather data for building space heating, thereby eliminating the need for building-specific information.

iii. The improved model successfully reduces the number of inputs required, while still ensuring accuracy. This enhancement greatly enhances the practical applicability of the model.

In this chapter, BP is selected to do the prediction of heating demand. Compared to other ANNs, BP neural networks offer unique advantages. They feature a mature, stable algorithm with extensive support and experience due to early development and widespread use. BP is highly flexible, adaptable to various tasks and data scales, and performs well with small-scale datasets, achieving high accuracy where deeper

models may struggle. It is computationally efficient, suitable for environments with limited resources, and has a robust mathematical foundation, making it straightforward to understand and implement.

5.2 Basic of ANN

ANN is proposed based on the structure of the human brain. It is a simplified model of the biological neural network, which has the ability to store empirical knowledge and process-related problems [172]. The basic elements of an ANN are neurons, which are connected in parallel to form each layer of the ANN. The simplest ANN is called perceptron, which has only one layer with one neuron. Each input of the perceptron has a corresponding weight, while the neuron can be considered as a mapping function. A single neuron is connected to thousands of other neurons. The information from the environment or other neurons is transmitted through numerous dendritic links. It is mentionable that a neural network is considered as a black box due to the unviewable internal working. It is difficult to investigate the relevance between the addressed problem and its internal structure. The ANN should be trained with a large amount of data before using it to solve the corresponding problems [173]. Because of its massively parallel distributed structure and its powerful learning and generalisation capabilities, ANN can solve many complex problems.

5.3 Basic of feature selection

The selection of model inputs is essential to the result. The selection of inputs is known as FS in ML, which is the process of selecting the most relevant features for use in model construction. Features are divided into three categories: those that are useful for the learning task and can enhance the effectiveness of the learning algorithm are called relevant features; features that do not help the algorithm in any way and do not bring any improvement to the effectiveness of the algorithm are called irrelevant features;

features that do not bring new information to the algorithm, or whose information can be inferred from other features, are called redundant features [174]. Removing irrelevant and redundant features reduces the difficulty of the learning task, simplifies the model and makes it easier to understand. Fewer inputs also save on storage and computational overheads. The additional features, while better fitting the training data, may also increase the variance. Typically, the training sample of a model increases significantly with the number of features. Therefore, FS reduces the risk of overfitting and improves generalization ability. The three types of feature selection methods are filter, wrapper and embedded [92]. The filter applies feature selection before training the network, so the process of feature selection is independent of the learning process. It is similar to applying a filter to the features and then using a subset of the features to train the network. It does not rely on any ML methods and does not require cross-validation, making it computationally more efficient. However, the characteristics of ML algorithms are not considered. Wrapper combines FS with ML algorithms. The usage of ML algorithms to evaluate the effectiveness of feature subsets allows the detection of interactions between two or more features. In general, different combinations of subsets are generated. These combinations are compared, and the selection of subsets can be considered as an optimization problem. However, this method requires training a model for each subset of features, which is computationally intensive. It is likely to be overfitting if the training sample is not sufficient, and the computational complexity is too high when the number of feature variables is large. Embedded in the selection of those features that are important for the training of the model in the process of determining the model, which has the advantage of being combined with an ML algorithm, as well as the computational efficiency of the filter method. However, this method does not eliminate noisy or irrelevant features and therefore sacrifices model performance [92], [174] [175], [176].

5.3.1 Sensitivity analysis

Sensitivity analysis is the study of the importance of different inputs to a model and measures the effect of changes in the inputs on the output. Typical sensitivity analysis is divided into local and global sensitivity analyses. The one-way method is a type of local sensitivity analysis where one parameter is changed at a time and the change in output is observed to determine the effect of the input on the output. Although local sensitivity analysis does not consider the interactions between inputs, it is a simple and intuitive way of explaining the effects of inputs. Hence, the local sensitivity analysis method is a common approach in engineering research.

Global sensitivity analysis has the ability to show the influence between inputs and it can be applied to non-linear models. However, global sensitivity analysis is computationally intensive and is highly dependent on the assumed probability distribution of the input parameters or their range of variation [176]. At the same time, global sensitivity analysis does not have a uniform definition of sensitivity coefficients, so different methods often lead to different sensitivity rankings.

5.3.2 Correlation analysis

Correlation analysis is the analysis of two or more variables that are correlated to measure how closely the variables are related to each other. There needs to be a certain association or probability between the variables for correlation analysis to be carried out. Correlation analysis in statistics usually refers to the degree to which a pair of variables are linearly correlated. A well-known correlation analysis method is the Pearson Correlation Coefficient, which is defined as the quotient of the covariance and standard deviation between two variables, with a value between -1 and 1. If the coefficient is positive, the two variables are positively correlated, i.e., the larger the value of one variable, the larger the value of the

other variable. If the coefficient is negative, the two variables are negatively correlated, i.e., the larger the value of one variable, the smaller the value of the other variable. The larger the absolute value of the coefficient, the stronger the correlation, but it should be noted that there is no causality between them. If the coefficient is zero, it indicates that the two variables are not linearly related. The Pearson Correlation Coefficient is a linear correlation analysis method. In addition to this, linear regression is a very powerful tool in terms of studying the relationships between variables, but the complexity of engineering problems makes it difficult to describe the variable relationships with a straight line. Polynomial regression can handle nonlinear problems, and it occupies an important place in regression analysis because any function can be approximated by polynomials in segments. The great advantage of polynomial regression is that it can approach the objective by adding higher terms of inputs until the results are satisfactory. Therefore, polynomial regression can always be used to analyse the usual practical problems, regardless of the relationship between the dependent variable and other independent variables [152], [177].

5.4 Training data for ANN

Scotland, as a complex region where energy policy is governed by both the Scottish and UK governments, is often neglected in research. In the case study, we took the Scottish domestic sector as an example to analyse its heating demands. There are many monitoring stations in Scotland, and it is impossible to obtain data from all of them. The meteorological data of Glasgow has been chosen to model Scotland 's climate because Glasgow is one of the most densely populated areas in Scotland, and secondly the meteorological data for Glasgow are the most comprehensive we have access to. Figure 5-1 shows some of the meteorological data used by the model.

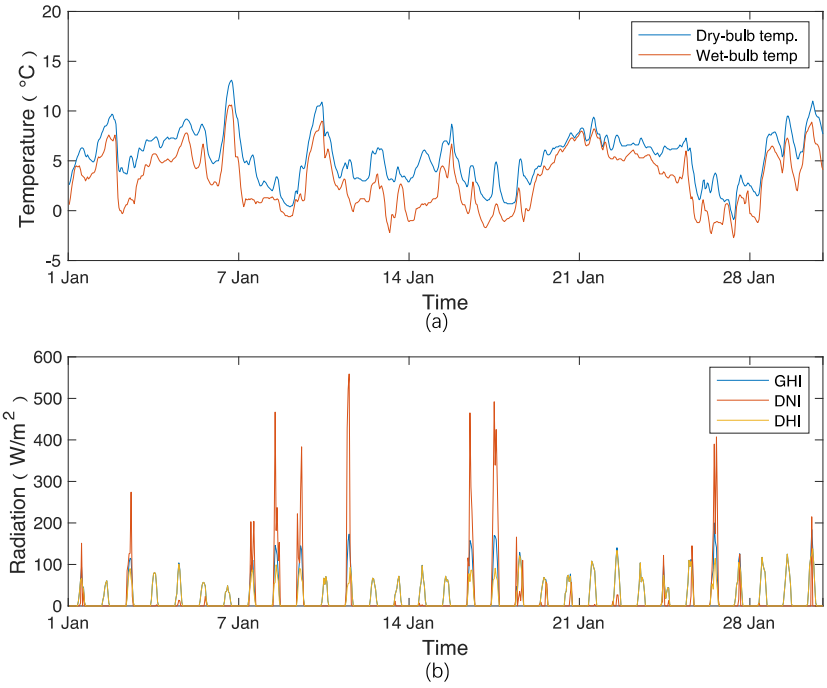

Figure 5-1 Examples of meteorological data used by the model: (a) temperature and (b) radiation.

The simulation results (monthly demand) from DesignBuiler were used as the training data in this work. In total, the domestic buildings in Scotland are divided into twelve types and the stock is estimated for each type of building to produce a specific heating demand profile. The DB model produces 12 heating demand profiles. The Scottish domestic heating profile is the sum of these profiles, which are used as the training data for the ANN model. The training data on heating demand is taken from the building simulation model of Scottish domestic buildings for the period between January to November 2020. The trained model was used to predict the heating demand in December 2020 to validate the ANN model.

5.5 Model evaluation

As previously stated, the absence of monitors for heating demand has resulted in a scarcity of actual heating data. In an expansive region like Scotland, obtaining hourly heating data is not as readily available as data for electricity demand. The evaluation of the model involves two crucial elements to verify the

reliability of the model. Firstly, a comparison is made between the annual heating demand obtained from the DB and the official data obtained from the government. Secondly, a comparison of the hourly heating data in this chapter with the data obtained from the building simulation is conducted.

5.5.1 Comparison DB data with Government Data.

The BEIS provides energy consumption in the UK, including subnational total final energy consumption in 2020. the domestic energy consumption in Scotland in 2020 is 3750 ktoe (thousand tonnes of oil equivalent)[178]. Scottish Energy Statistics Hub provides the percentage of the end use of household energy consumption, with space heating accounting for 76% [179]. Based on the percentage and efficiency of the four main types of heating in the UK (Gas boiler, Resistive heating, Oil-fired boiler, and Solid-fuel boiler), the average energy efficiency of all heating methods is estimated as 84%. According to official statistics, domestic space heating in Scotland in 2020 is estimated at 2,394 ktoe, converting energy units from thousand tonnes of oil equivalent to Terawatt hour is 27.84 TWh. The total domestic heating demand in 2020 from the DB model is 27.59TWh. It can be demonstrated that the results of the DB model are highly reliable.

5.5.2 Comparison prediction results with DB Data

In accordance with the guidelines set forth by the ASHRAE, the performance evaluation of an ANN model is conducted through the computation of the NMBE and the CV-RMSE. NMBE is the mean of the prediction errors divided by the mean of the actual values. It gives the total difference between the predicted and actual values of the model. CV-RMSE is the root mean square error divided by the mean of the actual values. This metric shows the ability of the model to predict the overall shape of the load reflected in the data. Their acceptable ranges for building energy prediction are indicated in Table 1. This

study commences by contrasting the training performance and the test performance of a basic ANN model, depicted in Figure 5-1, to assess its performance. Subsequently, the basic model is compared with an improved model, with the objective of determining the efficacy of the proposed method in enhancing the performance of the ANN model.

Table 5-1 Acceptable range of building energy prediction

Data resolution	Acceptable range (%)	
	NMBE	CV-RMSE
Monthly	±5	15
Daily	±7.5	22.5
Hourly	±10	30

5.6 Results and analysis

5.6.1 Training and testing performance of 2020

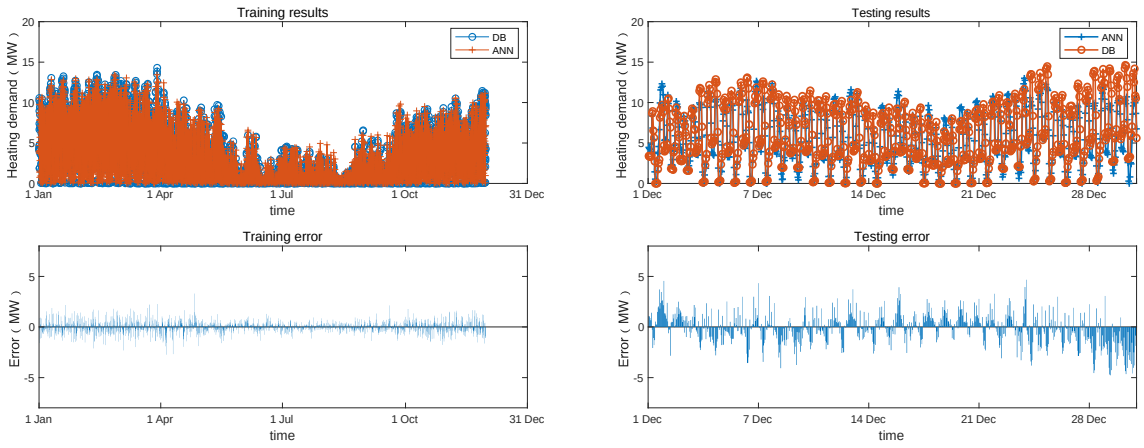

(a) (b)

Figure 5-2 The comparison of predicted results and DB results

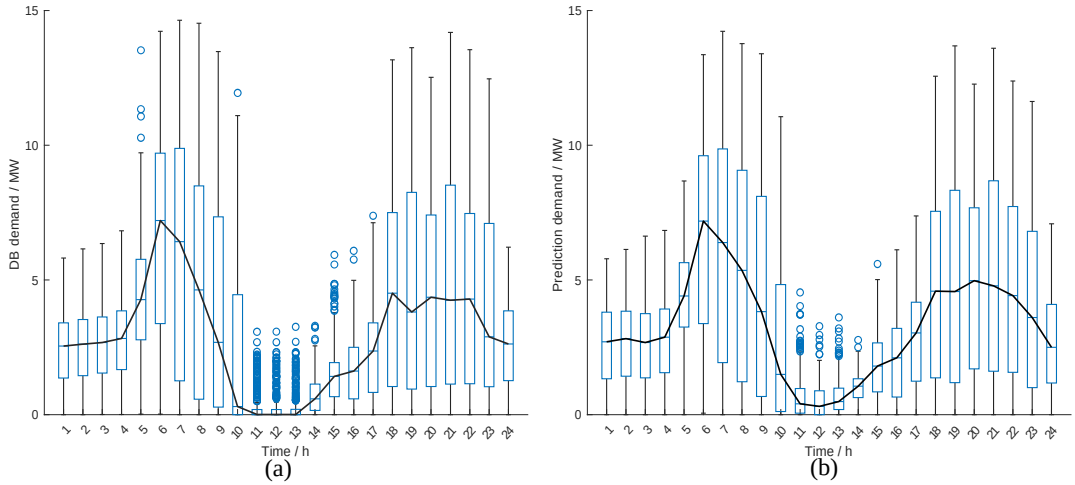

Figure 5-3 Boxplot of (a) DB results and (b) prediction results of ANN

Figure 5-2 shows a comparison of the predicted results of ANN and the DB results. Figure 5-2(a) shows the training results, where the training data is from January to December 2020. Figure 5(b) shows the test results of the model, using data from December 2020. The error percentage is not used to show the difference as there are periods where the heating demand is zero or almost zero. When expressing the predicted difference as a percentage of error, the prediction error needs to be divided by the heating demand, resulting in infinite errors in some cases. To enhance the clarity of analysis, Figure 5-3 presents a comparison of the box plots for the DB and ANN models. This comparison allows for a more comprehensive examination of the results. The findings indicate that the discrepancy between ANN and DB primarily occurs during periods of low heating demand, specifically from 11 a.m. to 3 p.m. Notably, the black curves representing the median values in both box plots exhibit a similar overall trend. This investigation provides valuable insights into the performance and behaviour of the two models. The NMBE value of training data is 2.1% and the CV-RMSE value is 23.1%. The NMBE value of testing data is 2.2% and the CV-RMSE value is 26.6%. The acceptable value of NMBE and CV-RMSE is 10% and 30%. Table 5-2 gives the comparison of CVRMSE and NMBE for the training and test results, both of

which are within the accepted limits. The maximum error in the training results is 3.75 MW, the minimum error is 0 MW, and the average error is 0.432 MW. The graph also shows that large errors occur mainly when high heating demand. The maximum error in the test results is 4.67MW, the minimum error is 0.02MW and the average error is 1.22MW. Even though the model achieves good results during training, it still had large errors when it is used to test new data, indicating the weak generalisation ability of the network. The most basic reason for the weak generalisation capability is the lack of training data in the case of complex models. An important reason for weak generalisation is excessive sample noise, i.e. the network disrupts the system by treating noise as an important feature. Therefore, it is important to remove the inputs that are not causally related or that interfere more than they contribute from the ANN network. On the other hand, it is also possible to add inputs where features have a significant impact on the results.

Table 5-2 Comparison of training and testing performance of ANN based on 2020 Scottish domestic heating demand.

	Acceptable value	Training	Testing
NMBE	10%	2.1%	2.2%
CV-RMSE	30%	23.1%	26.6%

5.6.2 Results of sensitivity analysis and correlation analysis

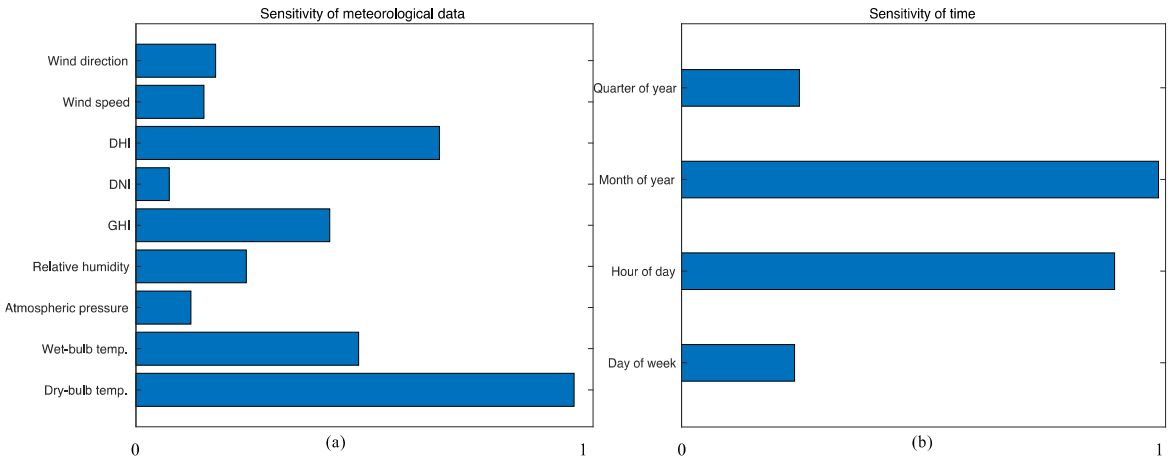

Figure 5-4 Sensitivity analysis of meteorological data and time (normalised results)

Figure 5-4 (a) shows the sensitivity analysis of the meteorological data. The result shows that the dry-bulb temperature has the highest sensitivity, followed by the Diffuse Horizontal Irradiance (DHI). Wet-bulb temperature and Global Horizontal Irradiance (GHI) also have large effects on the results. Direct Normal Irradiance (DNI) and atmospheric pressure have the lowest impact on the predicted results. Neither wind speed nor wind direction has a high sensitivity. It can be concluded that temperature and radiation are the two most important factors influencing heating demand, while wind and atmospheric pressure have a small effect on heating demand, and they can be neglected in the ANN model in order to reduce interference. Figure 5-4(b) shows the sensitivity analysis of temporal data, and the results show a quarter of the year and day of the week can be ignored. As the temperature is the most important physical parameter, it is important to improve the impact of temperature on the network. The temperature input to the model is the temperature point at the current time, but the change in heating demand is not sudden but has a process. Since the heating demand changes with the temperature, the temperature profile is also important. After removing some meteorological data, the temperature profile for the following 24 hours is used as input to the ANN.

The correlation analysis is done to analyse the relationship between the meteorological inputs and to identify features of the inputs. For example, if an input can be fitted by several other inputs, then removing one or two of the duplicate inputs can be effective in reducing the interference, especially if this input has a low sensitivity. In this model, time does not have physical significance and therefore the correlation analysis does not consider temporal inputs. Taking the example of dry bulb temperature and DHI being selected as dependent variables for correlation analysis, with other meteorological data as independent variables, Table-3 is the results of the correlation analysis. A higher R^2 value means a higher correlation. The highest correlation with the dry bulb temperature is the wet bulb temperature and the highest correlation with the DHI is the GHI. It is not reasonable to remove the wet bulb temperature and GHI as they also have a high sensitivity. Also, the results in Table 5-3 only show the correlation of two parameters, in real engineering problems more parameters are often included in complex relationships.

Table 5-3 R^2 value of correlation analysis

	Dry-bulb temp.	DHI
Wind direction	0.01	0.03
Wind speed	0.02	0.01
DHI	0.29	1
DNI	0.08	0.14
GHI	0.3	0.79
Relative humidity	0.16	0.25
Atmospheric pressure	0.07	0.02
Wet-bulb temp.	0.75	0.07
Dry-bulb temp.	1	0.3

The correlations were further analysed with the dry bulb temperature as the dependent variable, the wet bulb temperature as one independent variable, and the input in the model introduced as another independent variable. Using the same polynomial regression approach, the R^2 value increases significantly with the introduction of humidity as the third independent variable. The same calculations were applied to the DHI and GHI, with a significant increase in R^2 value with the introduction of DNI. Figure 5-5(a) is a polynomial regression fit curve for dry bulb temperature, wet bulb temperature, and humidity with an R^2 value of 0.926. Figure 5-5(b) is a polynomial regression fit curve for DHI, GHI and DNI with an R-value of 0.985. The results indicate that there is some relationship between the three meteorological data, which allows one item to be removed, reducing duplicate meteorological information while retaining all features. Combined with the sensitivity analysis results, the removal of DNI and humidity is reasonable.

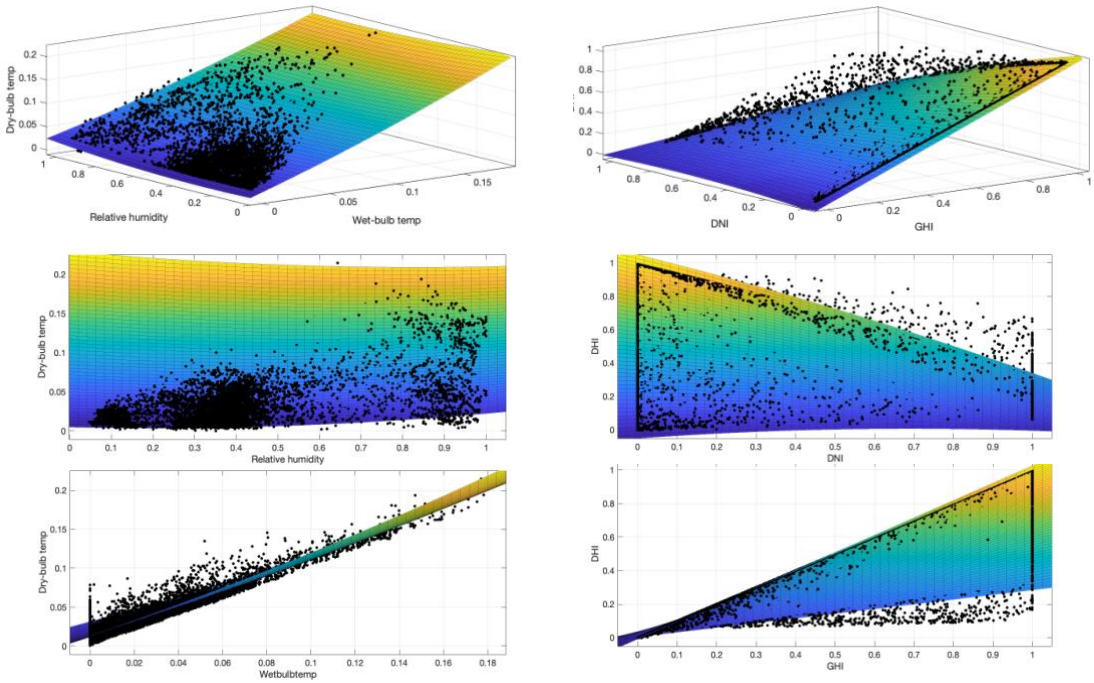

(a) (b)

Figure 5-5 Polynomial regression fit curve for three inputs

(a)Dry-bulb temperature, relative humidity wet-bulb temperature; (b)DHI, DNI, GH

5.6.3 Results of improved ANN network

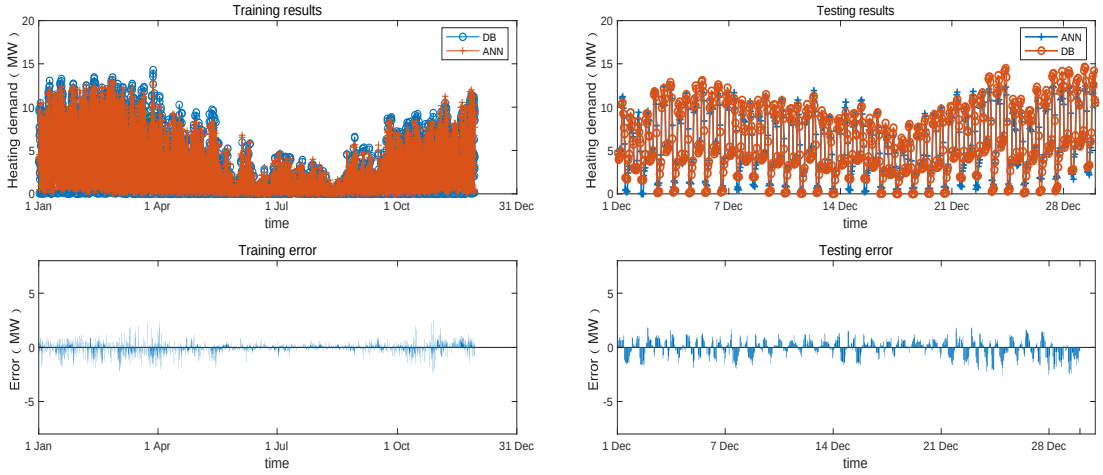

(a) (b)

Figure 5-6 Training and testing results of improved ANN model

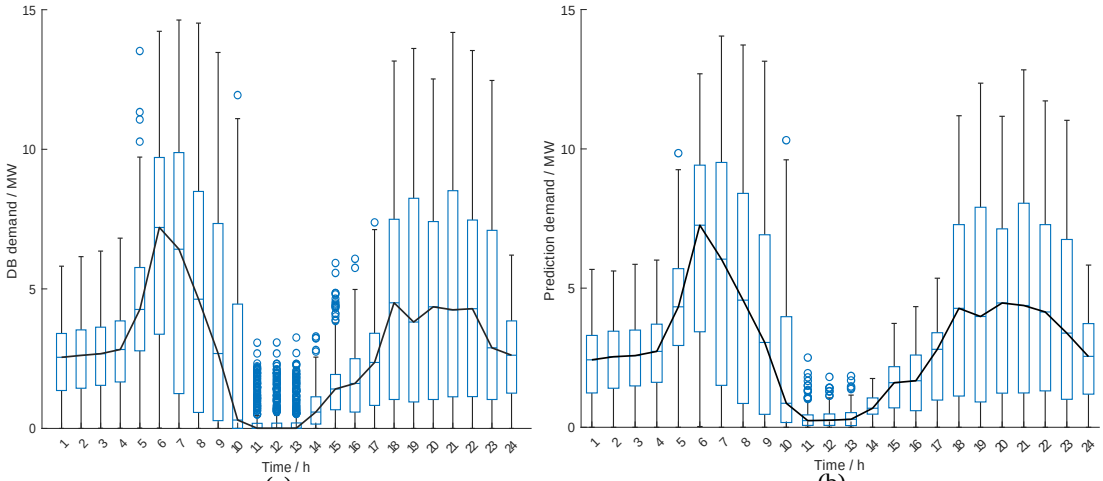

(a) (b)

Figure 5-7 Boxplot of (a) DB results and (b) prediction results of improved ANN

As previously mentioned, sensitivity and correlation analyses were conducted to refine the input dataset. Inputs with minimal impact on outcomes were removed, along with redundant variables that could be derived from other data. This selective approach optimises the predictive model's focus and efficiency. An improved ANN model includes a dry-bulb temperature 24h profile, wet-bulb temperature, DHI, GHI, month and hour. Figure 5-6 shows the results of the modified ANN training and testing. The

maximum error in the training of the modified ANN model is 3.17 MW, the minimum error is 0 MW, and the average error is 0.37 MW. The maximum error in the test data is 1.85 MW, the minimum error is 0.01 MW, and the average error is 0.71 MW. While the error reduction for training is minimal, the error reduction for testing is significant. The box plots in Figures 5-7 shows that the improved ANN is yielding results that are much more consistent with DB. The prediction results from 11:00 a.m. to 3:00 p.m. have decreased to a much closer proximity with the results of DB, and the trend of the median curve is now much more aligned. Comparing Tables 5-1 and 5-4, it can be found that although both training and testing performance have improved, the testing performance has improved significantly. The NMBE of testing results was improved from 2.1% to 1.2% and the CVRMSE was reduced from 26.6% to 14.6%, while the trained NMBE improved from 2.2% to 1.3% and the CVRMSE was reduced from 23.1% to 18.5%. The results show that removing and selecting appropriate inputs of ANN models when predicting building heating demand of a large-scale can effectively improve the generalisation ability of the model.

Table 5-4 Performance of improved ANN model

	Acceptable value	Training	Testing
NMBE	10%	1.3%	1.2%
CV-RMSE	30%	18.5%	14.6%

The initial ANN weights were assigned randomly by the code, which can lead to large differences in results. The models were therefore trained 100 times to compare the distributions of the NMBE and CVRMSE data sets. Figure 5-8(a) compares the NMBE values for the basic and improved ANN. The values of NMBE are distributed in the range of -0.4 to 0.8 before the improvement and approximately -0.1 to 0.2 after the improvement. Figure 5-8(b) shows the CVRMSE of the ANNs. The values of

CVRMSE for the basic ANN are distributed between 0.1 and 0.7. The CVRMSE of the improved ANN is distributed between 0.15 and 0.35, but mainly in the range of 0.15 to 0.25. The performance of improved ANN is much better than basic ANN and the values for both NMBE and CVRMSE are within reasonable limits.

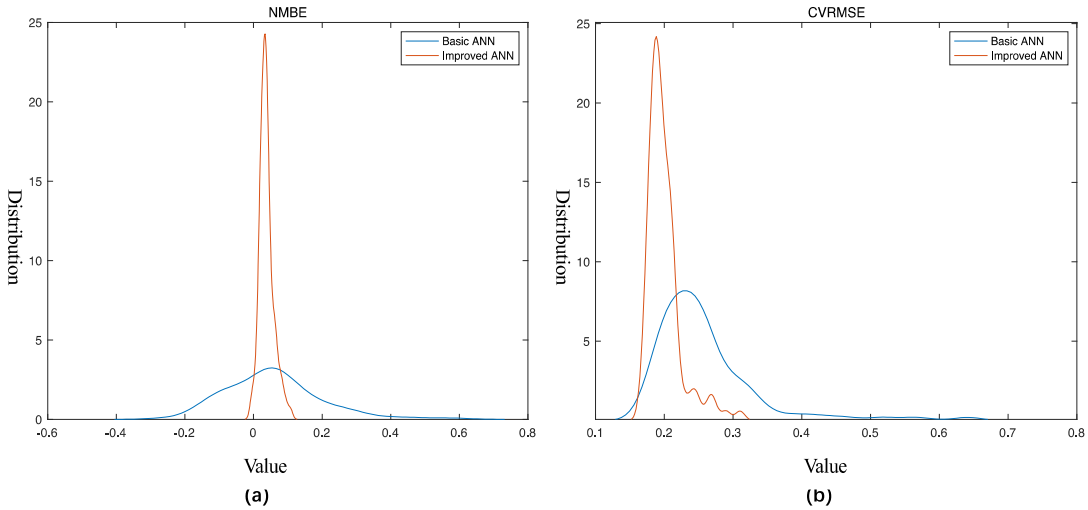

Figure 5-8 The distribution of (a) NMBE and (b) CVRMSE vale of basic ANN and improved ANN

5.6.4 Prediction of 2050

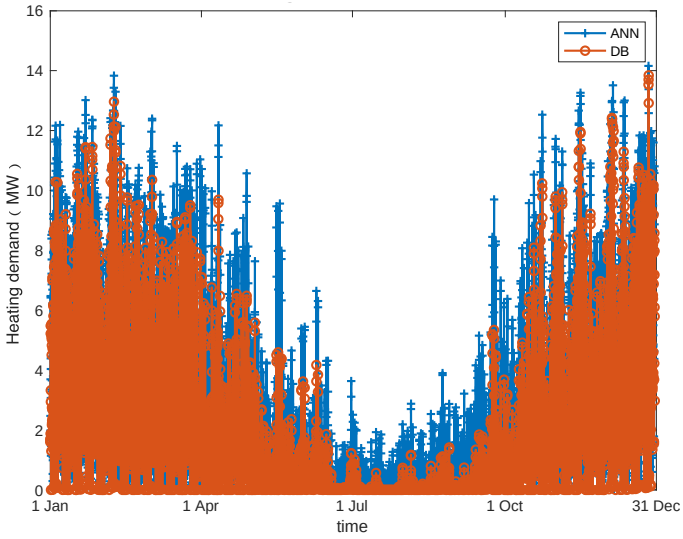

Figure 5-9 Prediction results with improved ANN model of 2050

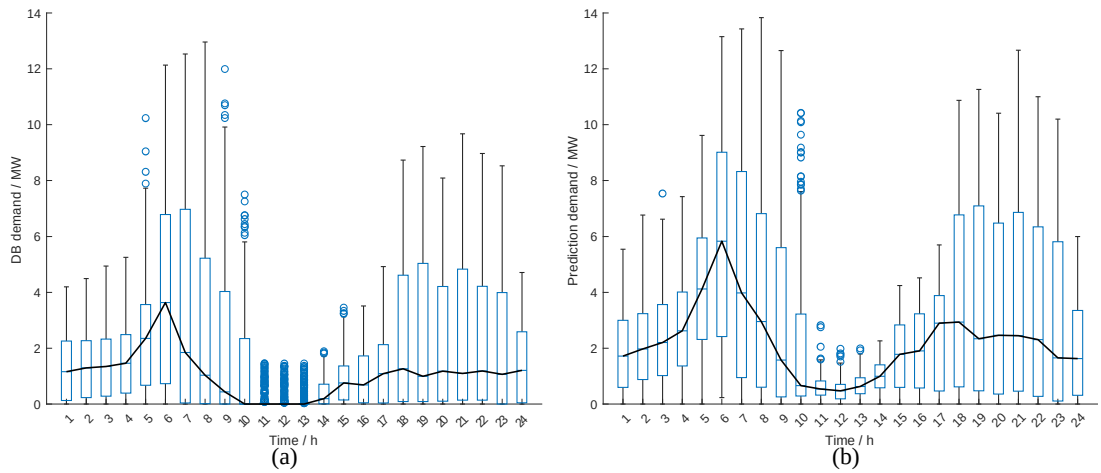

Figure 5-10 Boxplot of (a) DB results and (b) prediction results of improved ANN

Generally, the training data is at least ten times larger than the predicted data to give a reasonably accurate result. Due to the shortage of meteorological data, hourly heating demand for ten years cannot be calculated through the building simulation model. Hence, the heating demand data (from DB model) and meteorological data from January to November 2020 were used as training data when predicting the heating demand in 2050. Figure 5-9 shows the results of the predictions for 2050. The figure shows that the prediction errors between ANN model and DB model are mainly concentrated in the summer months, with the smallest forecast errors in the winter months. It can be seen from Figure 5-10's box plot that the results of ANN are generally greater than those of DB. This is attributed to the fact that the training data for the model is from 2020 and is too limited. With the heat demand usually higher in 2020 than in 2050, the estimations for 2050 will be on the high side. The errors of prediction increase as the year progresses, peaking in July and then gradually decreasing. January and February show moderate variability in prediction accuracy with CVRMSE at 25.01% and 29.74%, respectively, and minimal bias, with NMBE at 8.28% and 1.16%. This suggests that the model is fairly accurate during these colder months. Towards the end of the year, November and December also exhibit moderate variability (CVRMSE at 33.53% and

35.31%) with slight biases (-1.05% and 1.89% NMBE), indicating that the model slightly underestimates in November and overestimates in December. Overall, the forecasts for January, February and March are all within the error range, and the forecast errors for November and December are also close to the error allowance. There are three reasons for the large errors in summer and the small errors in winter. The first is that the 2010 and 2020 data are insufficient to forecast heating demand for the whole of 2050. The second is that both 2010 and 2020 temperatures are lower than 2050 temperatures due to global warming, so the predictions are more accurate in the lower temperature bands. The third is that the error in the calculation is increased by the low heating demand in summer as well as the fact that the heating demand is often zero for the period.

5.7 Conclusion

In this study, an ANN was used to predict the domestic heating demand in Scotland based on meteorological data. The results show that ANN is a useful tool for predicting heating demand, with a reasonable level of accuracy. The model achieved good results during training, with an NMBE value of 2.1% and a CV-RMSE value of 23.1% for the training data, and an NMBE value of 2.2% and a CV-RMSE value of 26.6% for the testing data, which were within the acceptable limits of 10% and 30%, respectively. Sensitivity and correlation analysis were conducted to identify the most important meteorological inputs, with temperature and radiation being identified as the two most important factors affecting heating demand.

The performance of the improved ANN improves in both NMBE and CV-RMSE by removing the inputs that have the least impact on the ANN prediction. The improved ANN demonstrates better

performance than its predecessor, as evidenced by a shift in NMBE values from -0.4 to 0.8 before the improvement to approximately -0.1 to 0.2 after the enhancement. Additionally, the CVRMSE values for the improved ANN range from 0.15 to 0.35, with the majority between 0.15 and 0.25, while the basic ANN had values between 0.1 and 0.7. The improved ANN model predicts heating demand for 2050 using data from 2010 and 2020. The results show that the errors in the predictions increase as the year progresses, peaking in July and gradually decreasing. The model's limitations include insufficient data for heating demand in summer and the low heating demand during this period, which leads to a higher error in the calculation. Overall, the improved ANN model can be used to predict heating demand in winter, but additional data is needed to support the prediction of heating demand in summer. Furthermore, this study does not delve into the exploration of machine learning algorithms. Instead, it emphasises the application of machine learning and the significance of discussing the performance of various algorithms in terms of prediction.

The preceding chapters have extensively analysed the ramifications of transitioning to electrified heating systems on power grid dynamics. This inquiry revealed significant implications for energy demand and grid stability. However, as global temperatures continue to rise, the demand for cooling systems is becoming increasingly critical, paralleling the need for heating in colder seasons. Extreme heat conditions impose substantial stress on power grids, mirroring the challenges observed with heating. The forthcoming chapters will extend this discussion by applying a similar methodological framework to explore the future impact of increased cooling demand on power infrastructure. This analysis aims to provide a comprehensive understanding of how seasonal shifts in temperature affect energy systems, highlighting the dual challenges of heating and cooling in maintaining grid reliability.

Chapter 6

Building Simulation for Space Cooling Demand

6.1 Introduction

The development of a high-precision model applicable to the whole city has been achieved in this chapter by merging a physical model and aneconomic data-based model, utilising building simulation and collecting building inventory information. London, for instance, has been used as a reference point, with building simulation employed to derive typical domestic cooling profiles. Information on the overall housing in London is provided by economic data such as stock, dwelling size, age, etc. The cooling profiles obtained from this model, which are of high resolution can be used not only for dynamic analyses but also for future scenarios of cooling demand. The study's innovations are as follows:

i. A solution for the prediction of high-resolution urban cooling demand is provided by the combination of physical andeconomic data-based modelling.

ii. The impact of cooling on the power grid is analysed in a more comprehensive way by the study, bridging the research gap in this area in the UK.

iii. Support for future investment and planning of different cooling scenarios is provided by the study.

In order to effectively analyse the impact of cooling demand, it is imperative to obtain a high-resolution cooling profile. Various building energy simulation methods exist to facilitate this process. The modelling for cooling demand is introduced in chapter 3. The proposed building simulation model has been validated successfully using diverse data from the literature and government report. It is important to emphasise that the utilization of data from official sources is crucial to further substantiate the reliability and robustness of the model in this chapter.

This chapter presents a systematic approach comprising three key stages to thoroughly investigate cooling demand and its implications on energy consumption and conservation within the engineering domain. The first stage is the generation of cooling data through the utilization of a building simulation model. This step is crucial for obtaining accurate and relevant data that can be further analysed in subsequent stages. Following the data generation, the second stage focuses on validating the reliability of the obtained results with authoritative data provided by government agencies. This step ensures the credibility and robustness of the generated results. Finally, the third stage delves into the analysis and prediction of cooling demand and its potential impact on energy consumption patterns. By employing this rigorous approach, the study aims to offer a comprehensive understanding of cooling demand, ultimately paving the way for the optimization of energy consumption and the promotion of sustainable practices in the engineering field.

6.2 case study: London

6.2.1 Classification of domestic buildings in London

In the UK, the BEIS categorises energy end consumption into four primary sectors. These sectors encompass domestic, industry, services, and transport [154]. This classification system provides a comprehensive framework for understanding and analysing energy consumption patterns across various aspects of society.

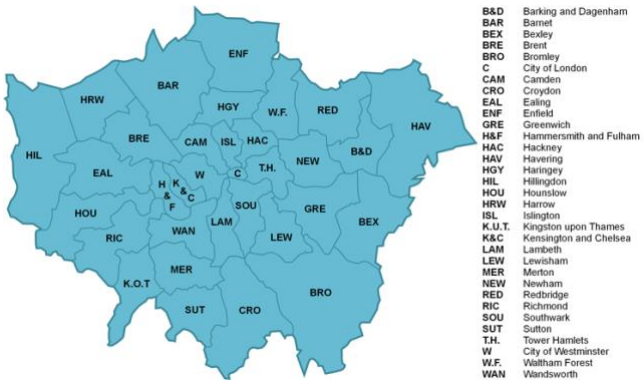

Figure 6-1 London Borough Map[180]

In this chapter, the focus has been specifically placed on the space cooling demand of domestic buildings in London, primarily because unlike commercial and public buildings, many domestic structures historically lack integrated cooling systems. This omission is significant because it highlights a unique vulnerability in residential areas as temperatures rise due to climate change. Commercial and public buildings typically already have robust cooling systems designed to handle variable loads, which means their cooling demands, although indeed increasing with rising temperatures, are usually managed with existing infrastructure adjustments and upgrades. However, the increasing temperature will certainly elevate the cooling demand across all types of buildings, suggesting that future studies should extend the analysis to include these sectors. Acknowledging this limitation, it is intended that future research will include the cooling demands of commercial and public

buildings to provide a comprehensive view of urban cooling needs in the face of warming climates. Based on the building surveys in each country, domestic buildings were categorised into four categories, detached, semi-detached, terraced and flat. In this study, London is divided into 33 regions based on boroughs, as shown in Figure 6-1. In contrast to commercial buildings, where data are sparse or unclear, the information on domestic buildings in London is considerably more comprehensive. The London Government has undertaken a comprehensive survey of the city's housing stock, categorising them into detached, semi-detached, terraced, purpose-built flats, flats in a converted/shared house, flats in a commercial building or other converted non-residential and caravan / other mobile or temporary structure [181].

The building stock and age across various regions, focusing on the impact of insulation levels on energy demand profiles. Three insulation levels can be distinguished for each building morphology, resulting in three unique demand profiles for each morphology. This approach generates 12 different hourly cooling demand profiles, derived from 12 distinct building models in each region. Data from 33 distinct regions were analysed to obtain a comprehensive understanding of the city's cooling requirements. This involved the aggregation of 396 individual cooling profiles, which provided valuable insight into the overall cooling demand across London.

6.2.2 Stock of buildings in London

The data on the domestic buildings provided is broken down by each borough in London. For the purposes of this study, caravans or any other mobile or temporary structures are not included in the model. Furthermore, the three different types of flats will be collectively referred to as 'Flat'. As depicted in Figure 6-2, the stock of detached, semi-detached, terraced, and flats in each borough is

provided by the London govnment. This classification aligns with the categorization used by the national government in its housing survey.

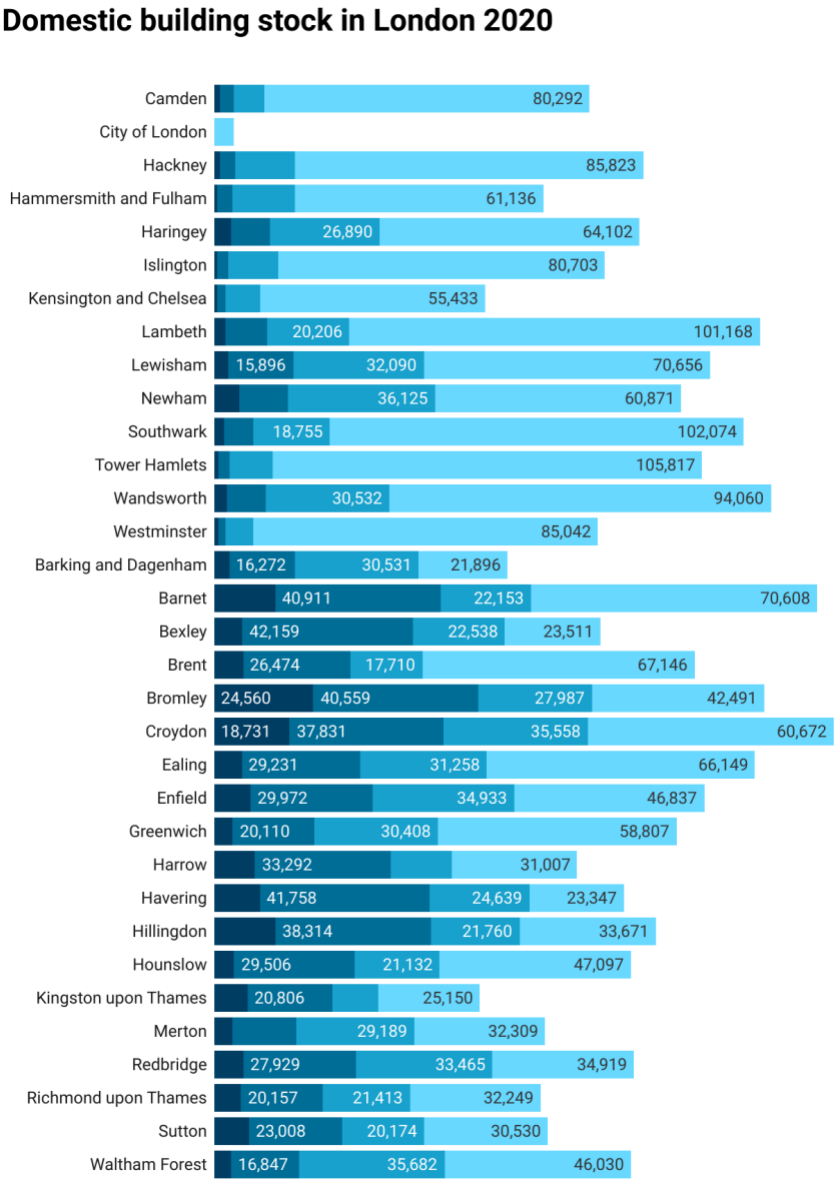

Figure 6-2 London domestic building stock[181]

In addition to the type of housing, each borough provides thorough statistics on the age of domestic buildings, with the oldest dating back to pre-1900. In this chapter, the age of buildings is re-divided according to the classification criteria [52], and buildings of different ages are divided into three categories as shown in Figure 6-3, pre-1919, 1919-1964, and 1964-present. Each age category

represents a different building construction, influencing the parameter settings of the building simulation.

While the UK government has only provided official forecasts for the stock of domestic buildings in 2050, there are no available projections for the evolution of London's building stock. Consequently, the 2050 cooling demand predictions in this study do not account for potential increases in building stock or additional insulation measures. The results presented in this chapter will be based exclusively on climate change, suggesting that actual values could potentially be higher.

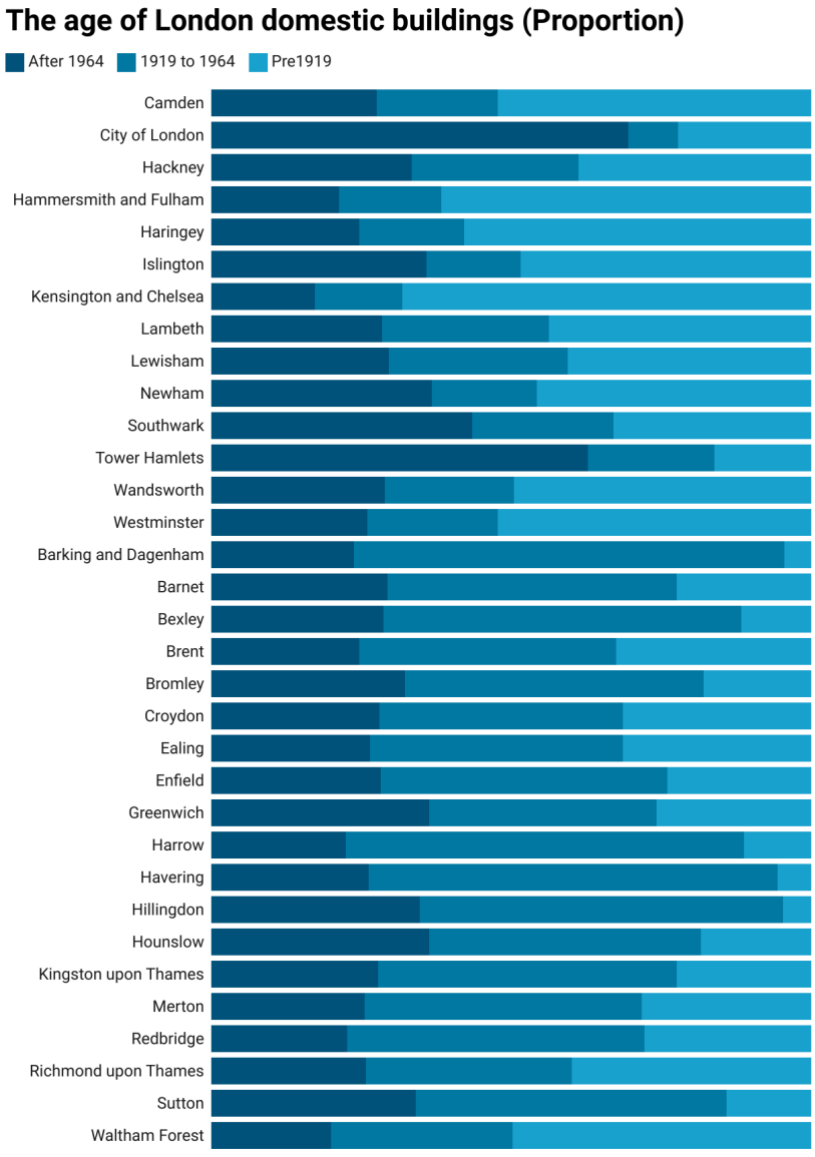

Figure 6-3 The age of London domestic building[181]

6.2.3 Meteorological data

The meteorological file serves as a crucial input for building simulations, as it establishes the climatic conditions of the simulated building's location. These conditions largely influence the heating or cooling demand within the building. The meteorological files utilised in this study are endorsed for UK government compliance calculations. For 2020, actual historical data was incorporated to more accurately represent the authentic cooling demand.

For the projections into 2050, the TMY weather file provided by the CIBSE was used for the analysis. Some of the weather data used in the model is given in Figure 6-4. It is noteworthy to mention that July is typically regarded as the peak month for cooling demand. Both July temperatures and GHI are projected to be higher in 2050 compared to 2020.

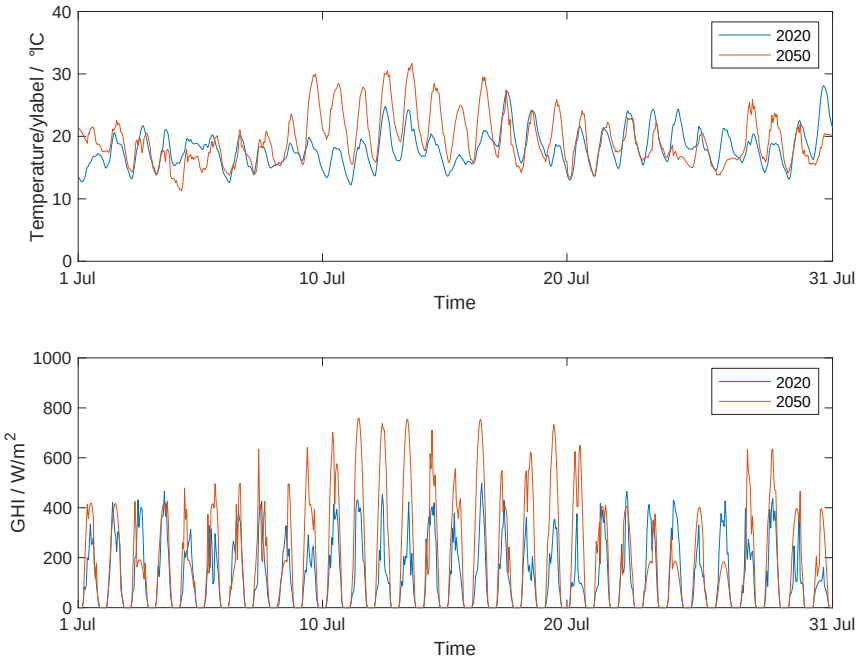

Figure 6-4 Comparison of partial meteorological data for July 2020 and July 2050

6.2.4 Building simulation of cooling

The cooling demand within a building is not only influenced by the structure itself but also by the internal heat gain. The detailed parameters such as radiation from appliances and luminaires, as well as personnel activity, could not be precisely set due to the absence of comprehensive data and monitoring. Furthermore, a comprehensive HVAC system inclusive of equipment and piping can be designed in the model, though this study primarily utilises a simplified HVAC model. The cooling setpoint was established at 24°C, a threshold above which the building's cooling system would be activated.

In this chapter, it is presumed that all buildings in London possess efficient ventilation systems. Thus, both natural and mechanical ventilation are inherently available in the model. However, it is worth noting that this may not all buildings have efficient ventilation systems. The architectural design of a building may inherently restrict ventilation. Moreover, safety reasons in various areas further curtail the availability of natural ventilation. This is often achieved by implementing measures such as keeping the windows closed. These factors are not addressed in this study. Consequently, the results derived from this study can be viewed as the minimum cooling demand in London under the given weather conditions.

6.3 Model comparison

As previously stated, the model discussed in this chapter has undergone validation checks for accuracy in past research. To further enhance the dependability of this model, the model will be validated again when applied to cooling forecasts. Data pertaining to cooling in the UK, particularly domestic data, is notably limited. The lack of domestic cooling demand data in the government's public

archives adds complexity to the model's validation process. Unlike the validation method for heat demand, which compares overall annual demand against the government's publicly available energy consumption data for space heating, the approach in this chapter contrasts the average peak month cooling demand per square metre of the building. This alternate validation and cross-validation methodology augments the model's reliability.

The London Government has mandated a suggested cooling demand benchmark, providing benchmarks for two distinct calculation methods [182]. The first method is based on the Standard Assessment Procedure (SAP), a UK government-proposed standardised calculation of residential cooling demand across the UK. While this calculation provides a fair reference, it is static, primarily focusing on temperature effects while excluding other factors. Despite this, it is widely regarded as a reliable and accurate standard. The second benchmark improves upon the limitations of the SAP and is specifically tailored for the London area. This benchmark considers the building's dynamic balance and the cooling demand in various scenarios, which is the new proposed benchmark (PB) in the report.

Table 6-1 Average (for June, July and August) cooling demand per square meter in different buildings. (The notation "kWh/m/m²" represents the kilowatt-hours consumed per square meter per month.)

kWh/m/m^2	After 1964	1919 to 1964	Pre1919	Average
Detached	1.23	0.73	0.66	0.88
Semi-Detached	1.22	0.78	0.73	0.91
Terraced	1.20	0.82	0.75	0.93
Flat	1.48	1.36	1.11	1.32

Table 6-1 presents the mean cooling demand for each type of building, per square meter, over the summer months (June, July, and August) according to the model utilised in this study. It indicates that

detached buildings require the least cooling, while flats necessitate the most. A correlation is observed between building density and cooling demand, with less dense buildings having lower cooling requirements. Furthermore, older buildings tend to have lower cooling demands than newer ones due to the superior insulation performance of modern structures. An examination of the mean values for the four building types reveals that the figures for the three types are similar, with flats being slightly higher.

Table 6-2 provides the acceptable cooling demand range for flats and duplexes as per the SAP and BP standards. These standards categorise buildings into two classes: good and poor. The "good" category refers to the cooling demand of buildings under optimal conditions, while "poor" represents the cooling demand under extreme conditions. Since the classification of buildings in this study differs from these standards, detached, semi-detached, and terraced houses are categorised as duplexes. A comparison of Tables 6-1 and 6-2 reveals that the average values for all building types align with these standards, with slight deviations for post-1964 detached, semi-detached, and terraced houses, and pre-1919 flats. These variations primarily stem from differences in construction methods and materials used in this study compared to those in the government report. The structures highlighted in the governmental report were specifically selected, characterised by their fixed structures and representative of quintessential London residences. Contrarily, the buildings examined in this study are more encompassing, aligning with and reflecting the broader spectrum of London's architectural landscape. Hence, these discrepancies fall within acceptable margins.

Table 6-2 Suggested average cooling demand per square meter from SAP and PB

kWh/m/m^2	SAP good	SAP poor	PB good	PB poor
Duplex	0.57	0.94	0.45	1.10
Flat	1.29	1.51	1.27	2.33

6.4 Results and Discussions

The findings of this research are organised into three primary sections. The initial section provides an intuitive understanding of the cooling demand in London for the years 2020 and 2050. It offers a comparative study of the geographic variations in annual cooling demand across London's 33 boroughs and employs daily demand curves to analyse the temporal spread of the demand throughout the year. The subsequent section delves into the implications on electricity demand if the cooling demand is entirely satisfied in 2020, and it further explores the practicability of addressing this cooling electricity demand via energy storage solutions. The final section scrutinises the cooling demand under varying scenarios, in the framework of a net-zero emissions scenario in 2050. It also considers the necessary installed capacity and annual plant usage to fulfil this demand.

6.4.1 Cooling Demand in 2020 and 2050

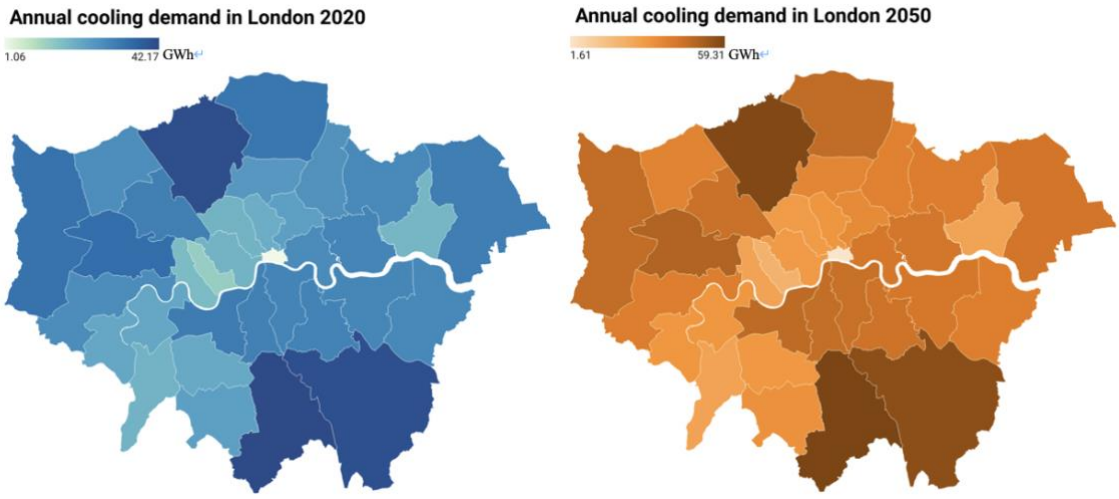

Figure 6-5 Annual cooling demand for domestic by London boroughs in (a) 2020; (b)2050

The data presented in Figure 6-5 provides a comprehensive view of the predicted annual cooling demand of the model across the 33 London boroughs for the years 2020 and 2050. The cooling demand,

measured in Gigawatt hours (GWh), is projected to increase in all boroughs by 2050, with an overall estimated growth of approximately 45% for London. The borough of Croydon presents the highest cooling demand for both years, with a demand of 42.17 GWh in 2020, expected to rise to 59.31 GWh in 2050, marking an increase of 40.6%. This is primarily due to the high domestic building stock in Croydon, the highest among the London boroughs. Conversely, the City of London exhibits the lowest cooling demand, with 1.06 GWh in 2020, projected to increase to 1.61 GWh in 2050, an increase of 51.9%. This significant increase is attributed entirely to climate change, as the study does not consider factors such as expansion in building stock or changes in building insulation.

In 2020, the cooling demand of Inner London is 310.18 GWh and is projected to increase to 468.37 GWh by 2050. On the other hand, Outer London, which is significantly larger in area, has a higher cooling demand of 548.63 GWh in 2020, which is expected to rise to 776.58 GWh by 2050. The larger cooling demand in Outer London is primarily due to its greater area, which spans 1253 square kilometres, compared to Inner London's 318.6 square kilometres. This means that Outer London has more buildings that need to be cooled, thus requiring more energy. The number of inhabitants in Inner London is recorded to be approximately 3.4 million. In contrast, Outer London boasts a larger population, with an estimated count of around 5.4 million. Interestingly, despite Inner London's higher population density compared to Outer London, its per capita cooling demand is lower. This implies that residents of Outer London experience a higher degree of comfort during the summer months compared to those residing in Inner London. This difference is attributed to the variance in dwelling types in these areas, which will be explored in further detail in the subsequent sections.

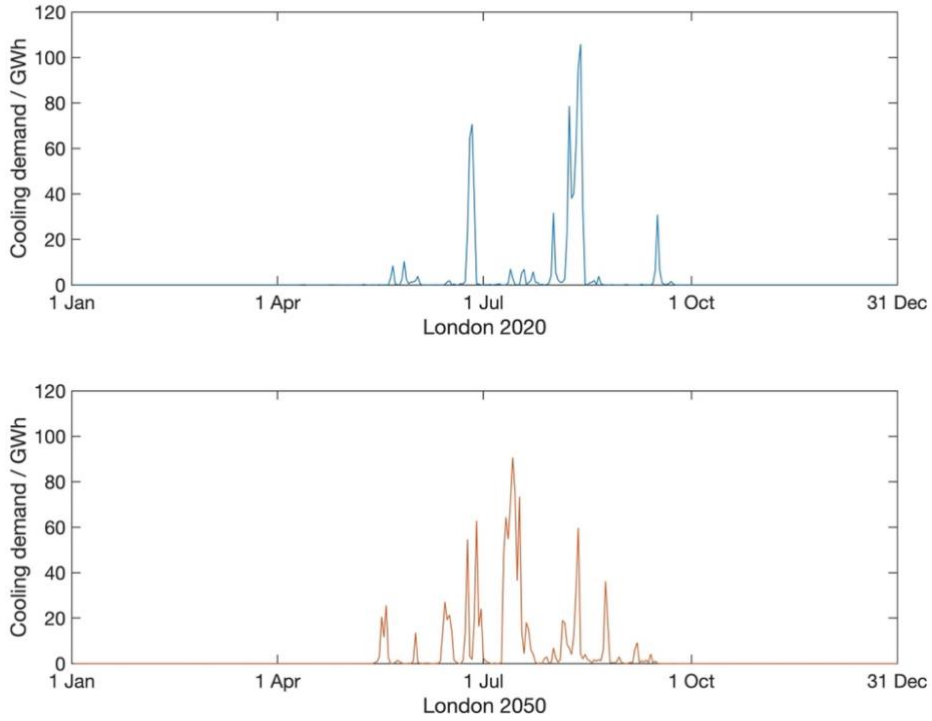

Figure 6-6 Comparison of daily cooling demand in London in 2020 and 2050

As depicted in Figure 6-6, the daily cooling demands for London for the years 2020 and 2050 are illustrated. The cooling season in London initiates in May and concludes by October, a duration notably shorter than the heating period. The annual cooling demand for 2020 was recorded as 858.81 GWh, with the maximum daily cooling demand peaking at 105.7 GWh. This peak day accounts for 12.3% of the annual cooling demand, a remarkably high proportion, indicating a concentrated pressure on the grid on this particular day. In the year 2020, the climatic conditions in London during the month of July were notably milder compared to the preceding month of June and the following month of August. The average temperature recorded in July closely mirrored that of May. Moreover, the absence of any extreme weather patterns resulted in the non-occurrence of a peak in cooling during this month. The cooling demand in 2020 was predominantly concentrated in the months of June and August, correlating with numerous instances of extreme heat events. The cooling demand curve for 2050 aligns more closely with the typical cooling demand scenario. As temperatures escalate throughout the year, the

cooling demand follows a similar upward trend, reaching its zenith in July, after which the demand gradually diminishes as temperatures recede.

Comparing the cooling demand in 2020 and 2050, it is evident that although the total cooling demand in 2050 exceeds that of 2020, the peak demand is smaller in 2050. Despite a higher peak in 2020, the number of days with a cooling demand exceeding 20 GWh is significantly higher in 2050. This can be attributed to the extreme heat experienced in the summer of 2020, while the TMY file for 2050 is used for comparison. The TMY file is derived from the monthly averages of the preceding 10 or 30 years, selected from the corresponding data for each month of a year that closely matches the 10 or 30-year average. The Met Office relies on TMY data and global warming to predict the weather in 2050, implying that the 2050 weather file incorporates global warming effects but neglects extreme weather conditions. The model considers the effects of global warming but not the extreme weather events. Therefore, if the frequent occurrence of extreme weather events is factored in, the pressure on future cooling demand could potentially exceed the projections made in this study.

6.4.2 Impact of cooling demand on electricity supply

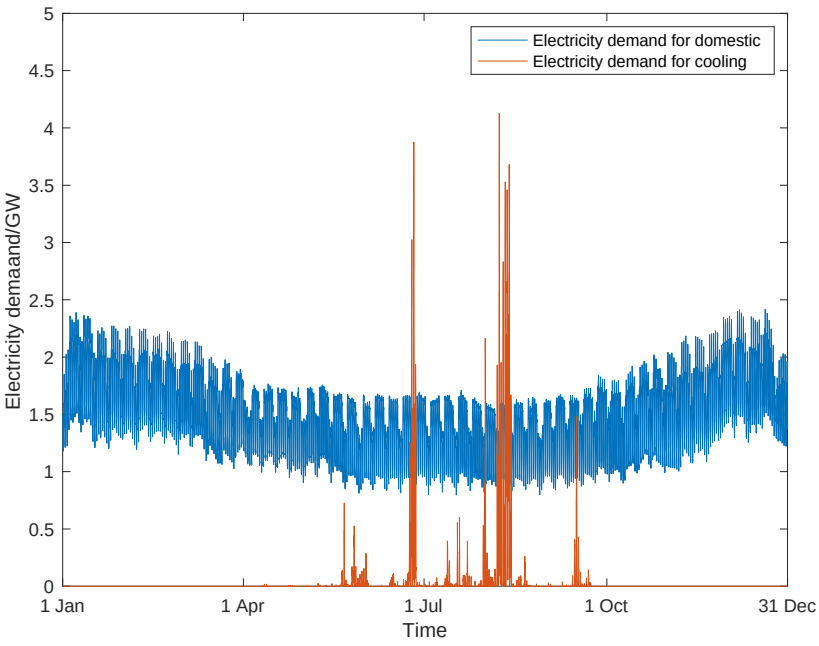

Figure 6-7 Comparison of domestic electricity demand and cooling electricity demand in London 2020 (CoP=3)

While comprehensive yearly data on London's electricity use across various sectors are accessible, the city lacks detailed hourly data. Given that London's population comprises 13% of the entire UK populace, it is reasonable to infer that its electricity consumption contributes significantly to the overall UK electricity demand. Therefore, the annual electricity demand in London is broken down approximately into hourly demand based on the available hourly electricity demand in the UK. Although this methodology may not be entirely precise, it provides a useful estimate of London's hourly electricity usage, which is expected to reflect the city's electricity profile in 2020.

London's total domestic electricity consumption for 2020 was 13113.9 GWh, and the hourly demand following decomposition is depicted in Figure 6-7. The distribution of electricity demand appears to be consistent throughout the year, albeit slightly elevated during winter compared to summer.

During winter, London's electricity demand can surge to a peak of 2.5GW, while summer peaks generally remain below 2GW.

The topic of cooling methods and the suitability of different types of cooling equipment for various buildings is expansive and beyond the scope of this section. However, it is worth noting that the CoP of different cooling equipment can vary significantly. For the purposes of this study, we have assumed an average CoP of 3 for such cooling equipment [183], [184], [185]. Figure 67 also depicts the hourly electricity demand in London in 2020 for cooling purposes. Interestingly, the peak electricity demand for cooling soars to 4.12GW, more than double the domestic electricity demand at the same time. London's summer domestic electricity demand hovers around 1.4GW, with the electricity demand for cooling exceeding 1.4GW for 66 hours dispersed over 18 days. For instance, in 2020, to meet all cooling needs, the London region would have required an additional 4GW of installed generation capacity to avoid power shortages during peak cooling periods.

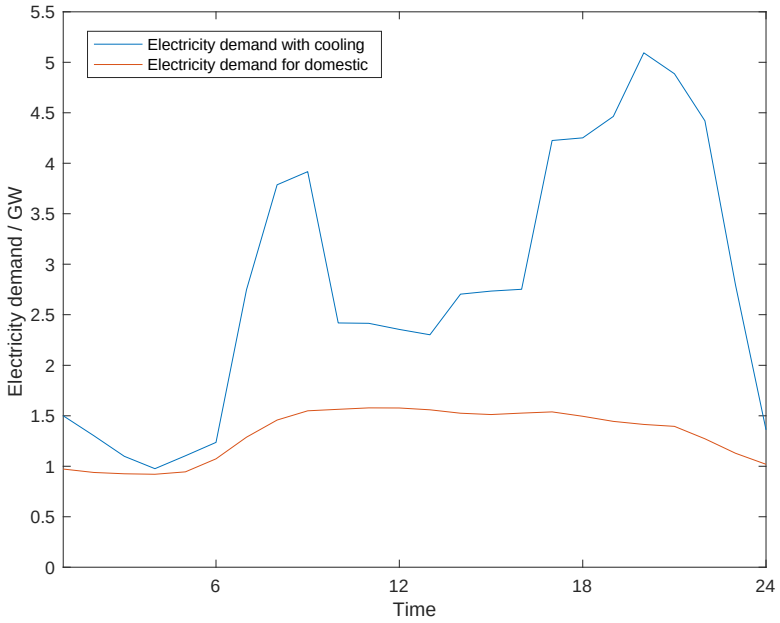

(a)

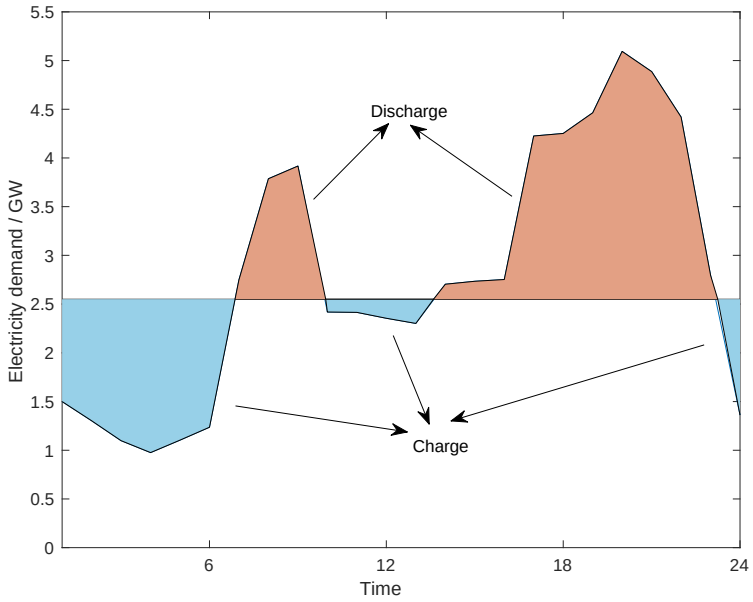

(b)

Figure 6-8(a) Electricity profile of peak day in 2020; (b) Storage demand for peak day in 2020

Figure 6-8 examines the day of maximum cooling demand in London. In Figure 5-9(a), a comparison is made between the domestic electricity demand of London and the total electricity demand with cooling. The electricity demand throughout this day, when no cooling needs are addressed, maintains a nearly steady pattern and stays below 1.5GW. The demand gradually escalates from 6 a.m. until approximately 9 a.m., maintaining stability thereafter without any significant peaks. However, once the cooling demand is factored in, the electricity usage curve exhibits two distinct peaks - one in the morning from 7-10 am and another in the evening from 6-10 pm. This pattern is typical for domestic buildings, where cooling demand typically arises during periods of human activity, i.e., mornings and evenings. The morning peak reaches up to 4GW and the evening peak is up to 5GW.

Addressing this segment of the electricity demand could involve grid upgrades or the implementation of an energy storage system. The latter is a potential solution to the challenges posed by the high variability of cooling energy demand. Figure 6-8(b) explores the potential of using energy storage, such as batteries, to manage peak electricity consumption. Energy storage can be initiated during off-peak periods, storing surplus energy, possibly from renewable sources. Then releasing the stored energy during peak periods can help alleviate the impact on power generation and enhance the utilization of renewable energy sources. The figure suggests that to halve the peak and maintain it near 2.51GW, an energy storage capacity of approximately 26.8GWh is required. This translates to a per-household storage requirement of about 18.8 kWh. Given that 26.8GWh of energy storage corresponds to the day of maximum cooling demand, it indicates that 26.8GWh of energy storage could entirely address the peak power demand caused by cooling needs in 2020. According to Figure 6, even though the total cooling demand in 2050 is expected to be higher than in 2020, the peak demand is projected to be about 14% lower. Moreover, with the anticipated widespread adoption of renewable energy by

2050, the corresponding energy storage systems will also have evolved significantly. Therefore, the application of energy storage to regulate the surge in demand induced by cooling is not just a practical solution, but also a sustainable alternative.

Beyond the realm of batteries, an array of diverse energy storage methods exists, each characterised by distinct dimensions and uses. The focus of this chapter predominantly lies on the capacity of these energy storage systems in regulating the surge in electricity demand instigated by cooling requirements, thereby refraining from an in-depth analysis of the technical intricacies of such systems.

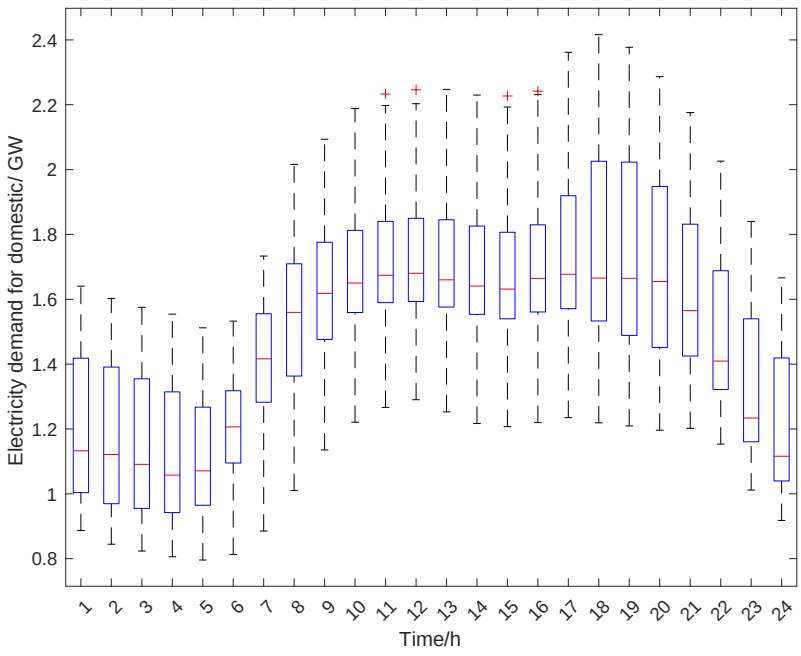

(a)

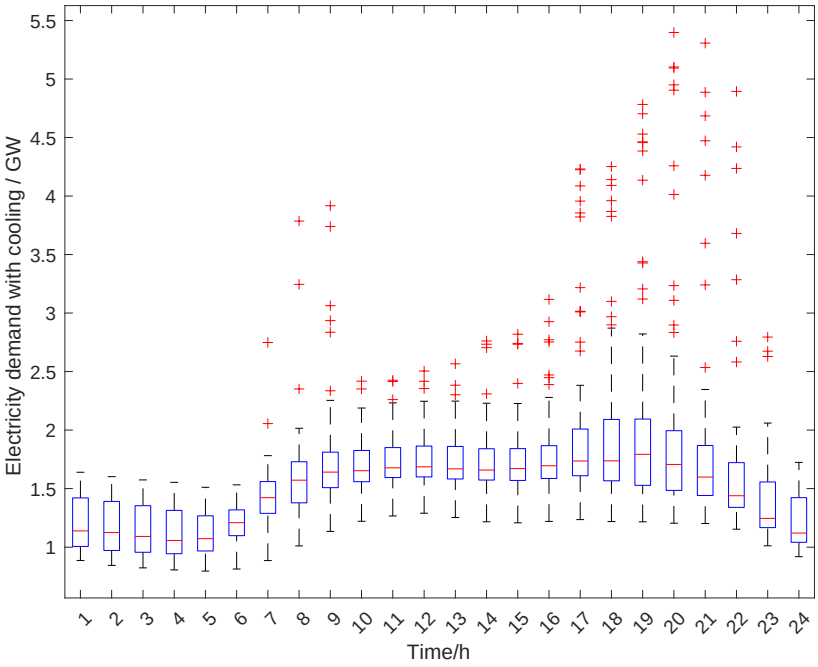

(b)

Figure 6-9 (a) Boxplot of the electricity demand in 2020; (b) Boxplot of total electricity demand with cooling demand in 2020

In the analysis of the electricity profile of a day in a year, Figure 6-9 presents a boxplot that illustrates the domestic electricity consumption patterns throughout various hours in the year 2020 in London. Each hourly data point is represented by 365 individual measurements, each corresponding to a different day of the year, and their distribution within a single hour is visualised in the boxplot. The boxplot's structure is as follows: the 'red line' within the box signifies the median (Q2), the lower boundary of the box indicates the first quartile (Q1), and the upper boundary represents the third quartile (Q3). The boxplot's 'whiskers' are denoted by '-' symbols, with the formula for the upper whisker being $q3 + w \times (q3 - q1)$ and the lower whisker being $q1 - w \times (q3 - q1)$. These whiskers roughly encapsulate the maximum and minimum values. In instances where the values within the data set surpass the boundaries set by the upper and lower whiskers, they are denoted by red '+' symbols, which are identified as outliers.

The boxplot illustrated in Figure 6-9 (a) delineates the pattern of electricity demand for domestic buildings in London throughout the year 2020. The demand profile generally corresponds to conventional working hours, registering its nadir at 5 am each day. As the day progresses, electricity consumption escalates steadily, stabilising around 11 am. Post 4 pm, the consumption trajectory continues to climb, culminating in a daily apex around 7 pm. This escalation is primarily attributable to amplified demand for lighting and increased utilization of other electrical home appliances.

In contrast, Figure 6-9 (b) portrays the boxplot of the aggregate electricity demand, inclusive of cooling. Both graphs display a similar 24-hour electricity consumption pattern, peaking at 7 pm and bottoming out at 5 am. A notable distinction between Figure 6-9(a) a and Figure 6-9(b) is the significant number of '+' symbols observed beyond the cap in Figure 9(b). The outliers in Figure 9(b) predominantly transpire between the hours of 5-7 am and 5-10 pm, corresponding to periods of heightened residential activity. This signifies that the amalgamated demand for electricity and cooling remains largely unvarying throughout the year. However, the emergence of a substantial number of outliers indicates that on specific days, the electricity demand considerably surpasses the typical range for that time slot, potentially doubling in some instances. It not only impacts London's total electricity demand during the summer but also influences the demand profile's shape, resulting in a steep peak. While this does not affect London's electricity demand for the majority of the year, it imposes a significant strain on the grid for brief period.

6.4.3 Comparison of different cooling scenarios in 2050

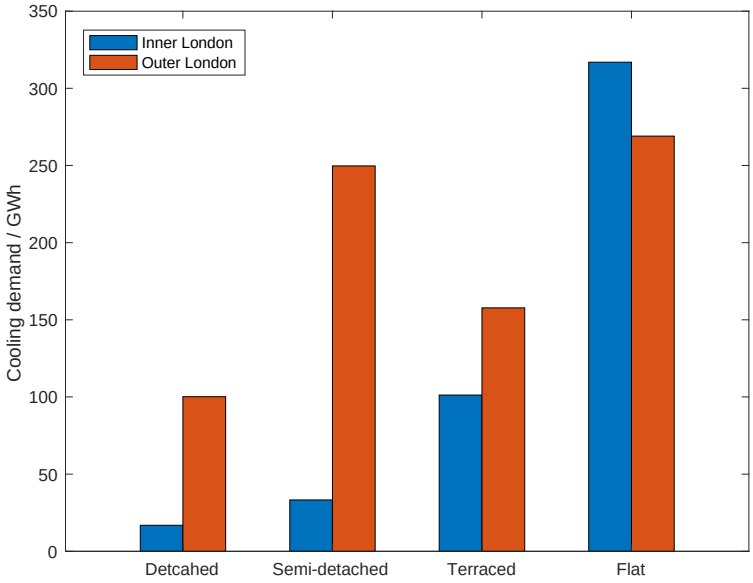

Figure 6-10 Annual cooling demand of different domestic buildings in London in 2050

As illustrated in Figure 6-10, the cooling demand for various types of residences in Inner and Outer London for the year 2050 varies significantly. In Inner London, the highest demand for cooling is seen in flats, requiring 350GWh, followed by terraced houses with a demand of 110GWh. Semi-detached and detached houses show a lower demand for cooling, requiring 40GWh and 15GWh, respectively. The peak demands for these four types of buildings are represented in Table 6-3, showing values of 0.14GW, 0.31GW, 1.02GWh, and 3.45GW, respectively. This higher demand in Inner London can be attributed to the higher number of commercial buildings present. The prevalence of commercial buildings in Inner London also leads to a lesser number of detached dwellings compared to flats. In Outer London, flats continue to demonstrate the highest cooling demand at 280GWh, peaking at 2.88GW. Semi-detached houses follow closely with a cooling demand of 250GWh, similar to that of flats, peaking at 2.3GW. The cooling demand for terraced and detached houses in Outer London is recorded at 150GWh and 100GWh, with peak demands of 1.66GW and 0.85GW respectively. Even

though flats in Outer London continue to have the highest cooling demand, their contribution to the total regional demand has decreased.

Table 6-3 Peak demand for different domestic buildings in London

Peak demand / GW	Detached	Semi-detached	Terraced	Flat
Inner London	0.14	0.31	1.02	3.45
Outer London	0.85	2.30	1.66	2.88

Upon comparing Inner and Outer London, it is observed that, except for flats, the cooling demand for the other three types of buildings in Inner London is significantly less than in Outer London. Flats in Inner London, however, show a marginally higher cooling demand than those in Outer London. It's important to note that Outer London's larger geographical area allows for more detached homes, while Inner London's smaller area and higher population density result in a predominance of flats. The per capita cooling demand in Inner London is elevated owing to the dense aggregation of flats, which inherently support a larger population and thus amplify the total cooling needs. Therefore, in Inner London, it is imperative to not only manage the electrical demand for cooling efficiently but also to prioritise the comfort of future residential occupants.

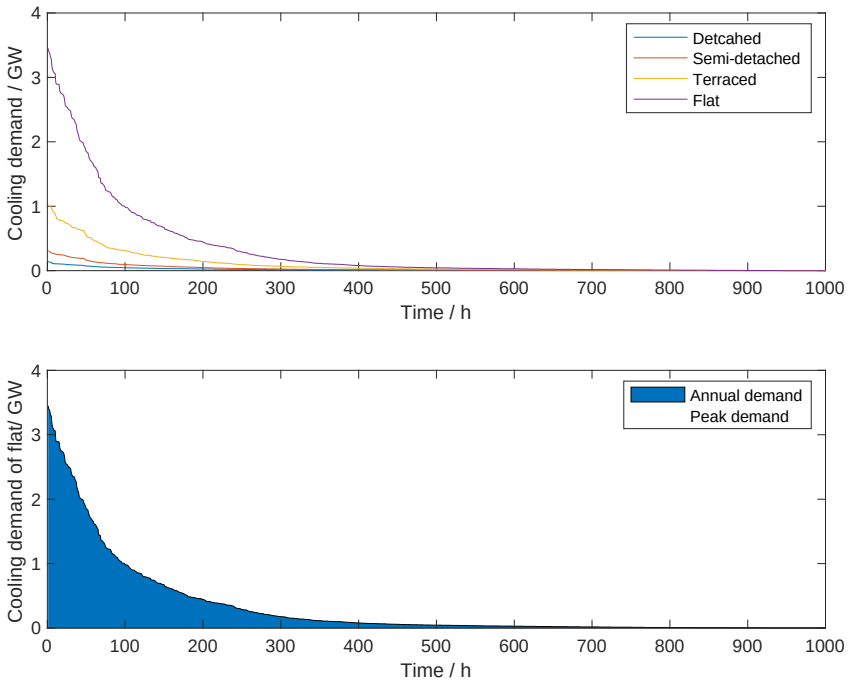

Figure 6-11 (a) Duration curve of cooling demand for domestic buildings in inner London in 2050; (b) Duration curve of cooling demand for Flat in inner London in 2050.

For a more comprehensive understanding of the cooling demand characteristics in London by 2050, Inner London was used as a case study. Figure 6-11(a) presents a duration curve for four representative buildings. The x-axis of the diagram represents time in hours, while the y-axis denotes the cooling demand of the four buildings in 2050, ordered from the highest to the lowest value. The maximum x-axis coordinate in the figure is capped at 1000, significantly less than the annual total of 8760 hours. This adjustment is due to the reduced duration of cooling demand, which allows for a clearer representation of the data in the figure. It's noteworthy that the curves for these four buildings in Inner London exhibit a steep incline when plotted against a full 8760-hour year. This suggests a substantial fluctuation in load across different periods, indicating that the cooling equipment's output

varies dramatically throughout the year. For instance, it's entirely inactive during winter, while operating at full capacity in summer. Hence, the duration curve can be instrumental in examining the correlation between cooling demand and capacity utilization, providing a foundation for planning the cooling plant's installed capacity. Figure 6-11(b) is the duration curve of flats in Inner London, comparing the annual cooling demand with the total energy that can be supplied by full load operation. The blue segment of the figure represents the annual cooling demand, while the blank space beneath the dotted line signifies the wasted output of the unit at full load. The figure suggests that if cooling equipment is installed to cater to peak demand, the equipment utilization rate is remarkably low.

Table 6-4 delineates the necessary installed capacity to cater to varying peak scenarios in London by 2050, including the annual cooling demand fulfilled and the equipment utilization rate. When the entire peak demand is satisfied, the cooling equipment's installed capacity is 12.52GW, which addresses the annual cooling demand. However, the equipment's usage rate is a mere 1.13%. If the peak demand is only 80% satisfied, the installed capacity can be decreased to 10.02 GW. This capacity meets 1231 GWh of the annual cooling demand, approximately 98.88% of the total yearly demand. Consequently, the cooling equipment's usage rate increases from 1.13% to 1.4%. When only 50% of the peak demand is satisfied, the installed capacity demand is approximately 6.26 GW. This satisfies 1099 GWh of the yearly refrigeration demand, which constitutes 88.27% of the total annual cooling demand. The equipment's usage rate then rises from 1.4% to 2%.

These comparisons illustrate that the majority of the annual cooling demand can be met without necessarily meeting the year's cooling peaks, indicating that weather extremes are relatively rare and can be disregarded when considering cooling equipment installation. This approach could potentially

lead to cost reduction and increased equipment utilisation. However, regardless of how much the installed capacity is reduced, the cooling equipment's usage rate remains significantly low. Therefore, exploring ways to improve equipment usage rates is a topic worthy of further discussion. For instance, the employment of reversible heat pumps, which provide cooling in summer and heating in winter, could be considered.

Table 6-4 Cooling demand and utilization of facilities under different peak conditions

Peak demand / GW	Capacity / GW	Annual demand / GWh	Utilization
100%	12.52	1245	1.13%
80%	10.02	1231	1.40%
50%	6.26	1099	2.0%

Table 6-5 provides a succinct discussion of the potential installed capacity of various equipment and the achievable cooling peaks to meet different levels of annual heat demand. The focus is on three prevalent types of active cooling equipment: reversible heat pumps, chillers, and traditional AC units (air conditioner units for cooling only). The choice of these cooling apparatuses was guided by proven technological reliability, effective active cooling, and commonplace usage in residential settings.

Reversible Heat Pumps are notable for their dual functionality, providing both heating and cooling solutions. They align well with net-zero objectives, making them ideal for detached homes that have sufficient space for installation. Their efficiency is augmented by the ability to reverse the refrigeration cycle, thus offering year-round climate control. Chillers are utilised predominantly in larger residential complexes and commercial buildings; chillers excel in their cooling capacity and operational efficiency.

They work on the principle of vapor compression or absorption to remove heat from the indoor environment, making them particularly effective in settings that demand significant cooling over large areas. Traditional AC Units are tailored specifically for cooling and are typically used when other types of cooling systems are impractical. Their straightforward, cooling-only function makes them suitable for quick retrofit options in existing buildings where space or architectural constraints prevent the installation of more complex systems. Currently, there are no specific Building Regulations in the UK for home air conditioning systems. Residents in restricted or protected areas should follow the standard rules that apply to any home improvement work. AC units are suggested for scenarios where reversible heat pumps and chillers may not be suitable. Based on the proportions of the pre 1919 domestic buildings and the official publication from UK Government in 2020 ‘A guide to air conditioning inspections in buildings’, it is postulated that 80% of detached and semi-detached homes can accommodate reversible heat pumps and 80% of flats and terraces can install AC units. The remaining 20% are AC units, assuming the CoP of the cooling equipment is 3 [181], [185]. Table 5-6 outlines the installed capacity requirements for each cooling equipment type under different scenarios.

Assuming 100% of the annual cooling demand is satisfied, the peak cooling is likewise fulfilled. Under this condition, the installed capacity of the reversible heat pump, chiller, and AC units is approximately 2.88 GW, 7.18 GW, and 2.52 GW respectively. If 80% of the annual cooling demand is met, the installed capacity of the reversible heat pump, chiller, and AC units is 2.09 GW, 5.2 GW, and 1.83 GW respectively. This provides a maximum power output of 9.07GW, which is 72.44% of the peak. If only half of the annual cooling demand is met, the installed capacity of all three cooling equipment types is nearly halved compared to a scenario where 80% of the annual demand is met.

However, this only satisfies 34.43% of the peak demand, indicating insufficient cooling for the majority of hot summer days.

Table 6-5 offers an estimated installed capacity for different scenarios. However, if an optimal installed capacity is sought, factors such as equipment costs, operational costs, equipment utilization, and environmental comfort must also be considered. This introduces a complex optimization problem worthy of further research, which is beyond the scope of this chapter.

Table 6-5 Peak demand and installed capacity of cooling equipment for different cooling demand scenarios

Annual demand / GWh	Peak demand / GW	Reversible HP / GW	Chiller / GW	AC units / GW
100%	12.52	2.88	7.18	2.52
80%	9.07	2.09	5.2	1.83
50%	4.31	1.01	2.41	0.89

6.5 Conclusion

In this chapter, a bottom-up approach is used to build a model of cooling demand through building simulation, which can be used to obtain the hourly cooling demand on a city scale. London is used as a representative example, with the city being segmented into 33 zones based on its administrative layout. Each zone's domestic buildings are further categorised into 12 types, allowing for an in-depth analysis of the cooling demand either regionally or in totality. This model serves to fill the gaps in the UK's incomplete cooling data, particularly in the domestic sector which has been largely overlooked in UK policy.

The findings indicate a projected 45% increase in cooling demand for London from 2020 to 2050, attributed to expected temperature rises. However, the 2050 weather file used in the study does not account for extreme weather conditions, unlike the 2020 data, brings some limitations to the research in the thesis. Considering only the impacts of climate extremes in 2020, the peak electricity used for cooling would double the residential electricity usage if the cooling demands are fully met. Although such variations would minimally affect the annual electricity consumption, they could potentially lead to instability during the summer and add pressure on the power grid operations.

The study's conclusions emphasise the integration of energy storage systems as a strategy to manage the anticipated increase in summer cooling demand and to improve the efficiency of renewable energy use. The analysis of cooling demand duration curves, particularly for flats in Inner London, reveals significant variances in equipment output throughout the year, thereby highlighting the necessity of accurately aligning the cooling plant's installed capacity with the varying demand. Although the research indicates that a substantial portion of the annual cooling demand can be met without fully catering to peak demand scenarios, the persistently low utilization rates of cooling equipment point towards a need for optimization. The deployment of reversible heat pumps, offering dual functionality for heating and cooling, presents a promising solution to enhance the usage rate of installed capacities. This integrated approach not only promises cost savings but also aligns with the objective of maximising energy efficiency and operational effectiveness of cooling installations.

Chapter 7

Artificial Neural Network for Space Cooling Demand

7.1 Introduction

Initially, a BP neural network was used to predict heating demand with good performance. However, when it was applied to cooling demand prediction, the accuracy was found to be insufficient due to limited data. In the UK, cooling demand is primarily concentrated in July, August, and September, resulting in a scarcity of data for accurate predictions. To address this issue, various models were explored, including CNN, LSTM, GRU, and CRNN. The goal is to compare these methods to identify the most suitable model for predicting cooling demand.

Similar to Chapter 5, this chapter primarily focuses on utilising neural networks for predicting cooling demand. While Chapter 5 emphasised improving the performance of established network structures, common techniques such as adjusting learning rates, hidden layers, and activation functions, though not discussed in detail, are employed. Chapter 5 primarily strengthened network performance

through feature selection. In reality, there are many types of neural networks, and choosing the right network architecture is crucial. In this chapter, the fundamental and widely used BP neural network continues to be applied. Additionally, different neural network architectures are explored for predicting cooling demand. What sets this chapter apart from the deep perspective of Chapter 5 is its broader exploration of neural network applications within the context of this model.

7.2 Feature Comparison of CNN, RNN, and CRNN

CNNs are adept at processing data with spatial structures, such as images, using their distinctive architecture. Central to CNNs are convolutional layers, where specialised filters efficiently extract spatial features like edges and textures from input data. These layers are adept at capturing increasingly complex features as the network deepens. Pooling layers complement these by reducing the spatial dimensions of the data, thereby lowering computational requirements and enhancing the network's robustness to variations in the input. A defining characteristic of CNNs is their use of parameter sharing, which allows the network to apply the same filter across the entire input, significantly reducing memory usage. Local connectivity ensures that each neuron processes data from a small, localised region of the input, enabling the network to detect local patterns effectively. The architecture typically concludes with fully connected layers, which synthesise the learned spatial features into a form suitable for specific tasks like classification or regression. This combination of feature extraction, local processing, and parameter efficiency makes CNNs particularly powerful for tasks involving spatial data interpretation.

RNNs are distinguished by their unique ability to maintain an internal or hidden state, which captures and carries information across different time steps in a sequence. This feature is central to their capability in processing sequential data, such as time series or language sequences, accommodating various lengths

of input. A defining characteristic of RNNs is parameter sharing across the sequence, where the same weights and biases are applied to each time step, enhancing efficiency and reducing the model's complexity. Additionally, RNNs have feedback loops, allowing outputs from previous time steps to be used as inputs to the network. This feedback mechanism enables RNNs to handle complex, time-dependent tasks, as the output at each step is influenced by both the current and previous inputs, making them particularly effective in tasks requiring an understanding of temporal dynamics.

CRNN combines CNN and RNN. This integration allows CRNN to seamlessly integrate spatial and temporal information, making it suitable for tasks where both types of dependencies are essential. It achieves this by utilising convolutional layers to extract spatial features and recurrent layers like LSTM or GRU to process sequential data. Weight sharing across time steps improves parameter efficiency. CRNN finds applications in various domains, including text processing, speech recognition, and time-series analysis. Its deep learning capabilities enable automatic parameter optimization during training, resulting in reliable performance, particularly in tasks involving temporal data.

7.3 Case Study

7.3.1 Parameter setup of networks

The Figure 7-1 shows the flowchart of the BP model used in this chapter, and Table 7-1 shows the key data settings of the network. It takes input data consisting of 7 features and undergoes a sequence of transformations to achieve this prediction. The process begins with the input data, which is fed into the network. The data is first processed through a fully connected layer (fc_1) comprising 100 neurons. Each neuron performs a linear transformation on the input features, enabling the network to extract relevant information. Following fc_1, a ReLU activation function (relu_1) is applied. This activation function

introduces non-linearity to the model, allowing it to capture complex patterns and relationships within the data. Subsequently, the output from relu_1 is directed to another fully connected layer (fc_2) with 100 neurons. This layer performs a second linear transformation, further refining the representation of the input data. After fc_2, another ReLU activation function (relu_2) is employed, enhancing the network's ability to model intricate data patterns and relationships. The final stage of the network involves a fully connected layer (fc_3) consisting of a single neuron. This layer performs the last linear transformation to produce the ultimate prediction, which is the regression output. To evaluate the accuracy of its predictions, the network employs the mean squared error (MSE) loss calculation. This involves comparing the network's output (the predicted value) with the ground truth data, known as the "response." The MSE loss quantifies the dissimilarity between predictions and actual values, guiding the network's training process.

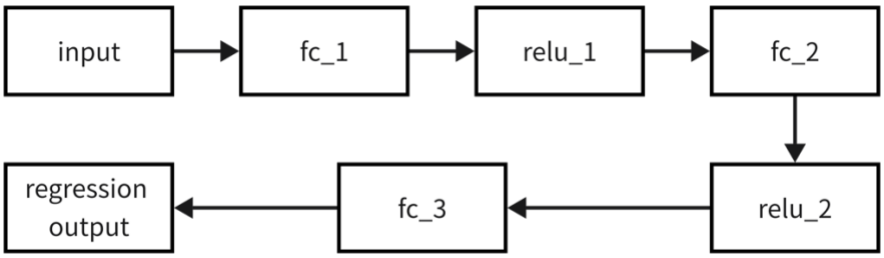

Figure 7-1 The flowchart of the BP model

Table 7-1 The key data settings of the BP model

Name	Network Setting
input	7 features
fc_1	100 fully connected layer
relu_1	ReLU
fc_2	100 fully connected layer
relu_2	ReLU
fc_3	1 fully connected layer
regression output	mean-squared-error with response 'Response'

The Figure 7-2 shows the flowchart of the CNN model used in this chapter, and Table 7-2 shows the key data settings of the network. The network starts by receiving a sequence input with 7 dimensions. It then applies a 1D convolution operation, known as "conv1d," using 16 filters of size 3x7. This operation is applied with a stride of 1 and 'same' padding. The purpose of this convolution is to extract spatial features from the input sequence. Following the convolution, batch normalization is applied to the 16 channels generated by the convolutional layer. Batch normalization helps stabilise and accelerate the training process by normalising the data within each mini batch. After batch normalization, a ReLU activation function, denoted as "relu_1," is applied elementwise. ReLU introduces non-linearity to the model, allowing it to capture complex patterns in the data. Subsequently, the network performs 1D max pooling with a pool size of 2, a stride of 1, and 'same' padding. Max pooling reduces the spatial dimensions of the data while retaining the most important information. The output from the max pooling layer is then connected to a fully connected layer, "fc_1," which consists of 100 neurons. Each neuron performs a linear transformation on the data. After "fc_1," another ReLU activation function, "relu_2," is applied. This additional non-linearity enhances the network's ability to model intricate data patterns. Finally, the network connects the output from "relu_2" to a last fully connected layer, "fc_2," with a single neuron. This layer is responsible for producing the final regression prediction.

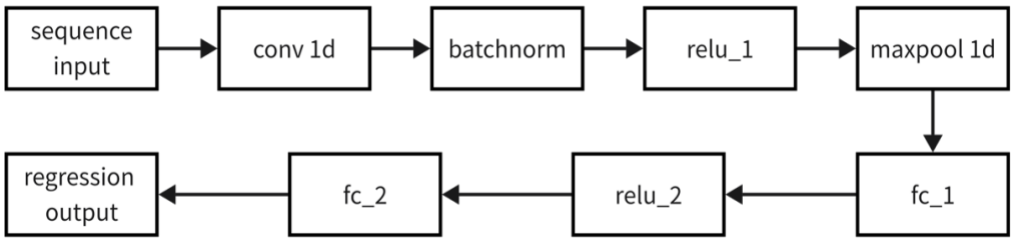

Figure 7-2 The flowchart of the CNN model

Table 7-2 The key data settings of CNN model

Name	Network Setting
Sequence input	Sequence input with 7 dimensions
conv1d	16 3×7 convolutions with stride 1 and padding 'same'
batch norm	Batch normalization with 16 channels
relu_1	ReLU
Maxpool 1d	Max pooling with pool size 2, stride 1, and padding 'same'
fc_1	100 fully connected layer
relu_2	ReLU
fc_2	1 fully connected layer
regression output	Mean-squared-error with response 'Response'

The Figure 7-3 shows the flowchart of the LSTM model used in this chapter, and Table 7-3 shows the key data settings of the network. The network begins by receiving a sequence input with 7 dimensions. It employs an LSTM layer with 100 hidden units. LSTM is a type of RNN known for its ability to capture dependencies in sequential data. It maintains an internal state that can capture information from previous time steps, making it well-suited for sequential data analysis. Following the LSTM layer, the network connects to a fully connected layer denoted as "fc" with a single neuron. This layer performs the final linear transformation.

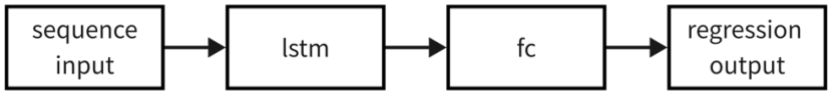

Figure 7-3 The flowchart of the LSTM model

Table 7-3 The key data settings of LSTM model

Name	Network setting
sequence input	Sequence input with 7 dimensions
lstm	LSTM with 100 hidden units
fc	1 fully connected layer
regression output	mean-squared-error with response 'Response'

The Figure 7-4 shows the flowchart of the LSTM model used in this chapter, and Table 7-4 shows the key data settings of the network. The network begins by accepting a sequence input with 7 dimensions. It employs a GRU layer featuring 100 hidden units. GRU is a variant of RNNs known for its efficiency in capturing sequential dependencies. Unlike traditional LSTM, GRU uses fewer gating mechanisms, making it computationally more efficient. Next, the network connects to a fully connected layer labeled "fc" with a single neuron. This layer performs the final linear transformation.

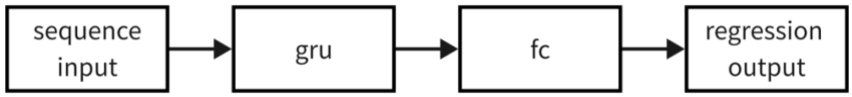

Figure 7-4 The flowchart of the GRU model

Table 7-4 The key data settings of GRU model

Name	Network setting
sequence input	Sequence input with 7 dimensions
gru	GRU with 100 hidden units
fc	1 fully connected layer
regression output	mean-squared-error with response 'Response'

The Figure 7-5 shows the flowchart of the CRNN model used in this chapter, and Table 7-5 shows the key data settings of the network. The network begins by taking a sequence input with 7 dimensions.

It starts with a 1D convolutional layer ("conv1d") that applies 8 convolutional filters of size 2x7 with a stride of 1 and 'same' padding. This layer helps extract relevant features from the input sequence. Following the convolutional layer, batch normalization is applied to the output, maintaining data consistency and aiding in training. This step involves 8 channels. The ReLU activation function is then applied elementwise to introduce non-linearity into the model. Next, the network incorporates an LSTM (layer with 100 hidden units. LSTM is well-suited for modelling sequential data, and it can capture long-term dependencies effectively. A fully connected layer ("fc") with a single neuron follows the LSTM layer. This layer performs the final linear transformation.

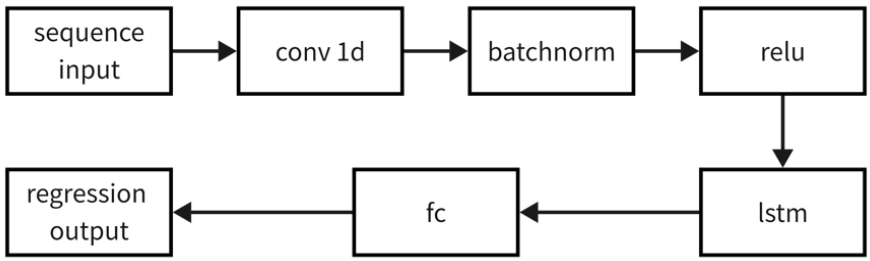

Figure 7-5 The flowchart of the CRNN model

Table 7-5 The key data settings of CRNN model

Name	Network setting
sequence input	Sequence input with 7 dimensions
conv1d	8 2×7 convolutions with stride 1 and padding 'same'
batch norm	Batch normalization with 8 channels
relu	ReLU
lstm	LSTM with 100 hidden units
fc	1 fully connected layer
regression output	mean-squared-error with response 'Response'

7.3.2 Training data

London, as a southern city with a pronounced urban heat island effect, has consistently experienced high cooling demand during scorching summer seasons. In this case study, we selected the London metropolitan region to analyse its cooling demands. The meteorological data used for this study is from historical records in 2020, and the cooling demand data specifically covers the hottest months of June, July, August, and September.

7.4 Results and Discussion

7.4.1 Training and testing performance of BP

The data spans in Figure-7-6 from June to September and focuses on evaluating the accuracy of BP against a standard set by building simulation results (DB). The figures illustrate cooling demand predictions, where DB's outcomes serve as a benchmark to assess the effectiveness of the BP model. The evaluation metrics show that during the testing phase, the BP model achieved a RMSE of 0.49, a MAE of 0.21, and a MAPE of 67.53%. In contrast, during the training phase, the BP model recorded an RMSE of 0.61, an MAE of 0.24, and a MAPE of 29.72%.

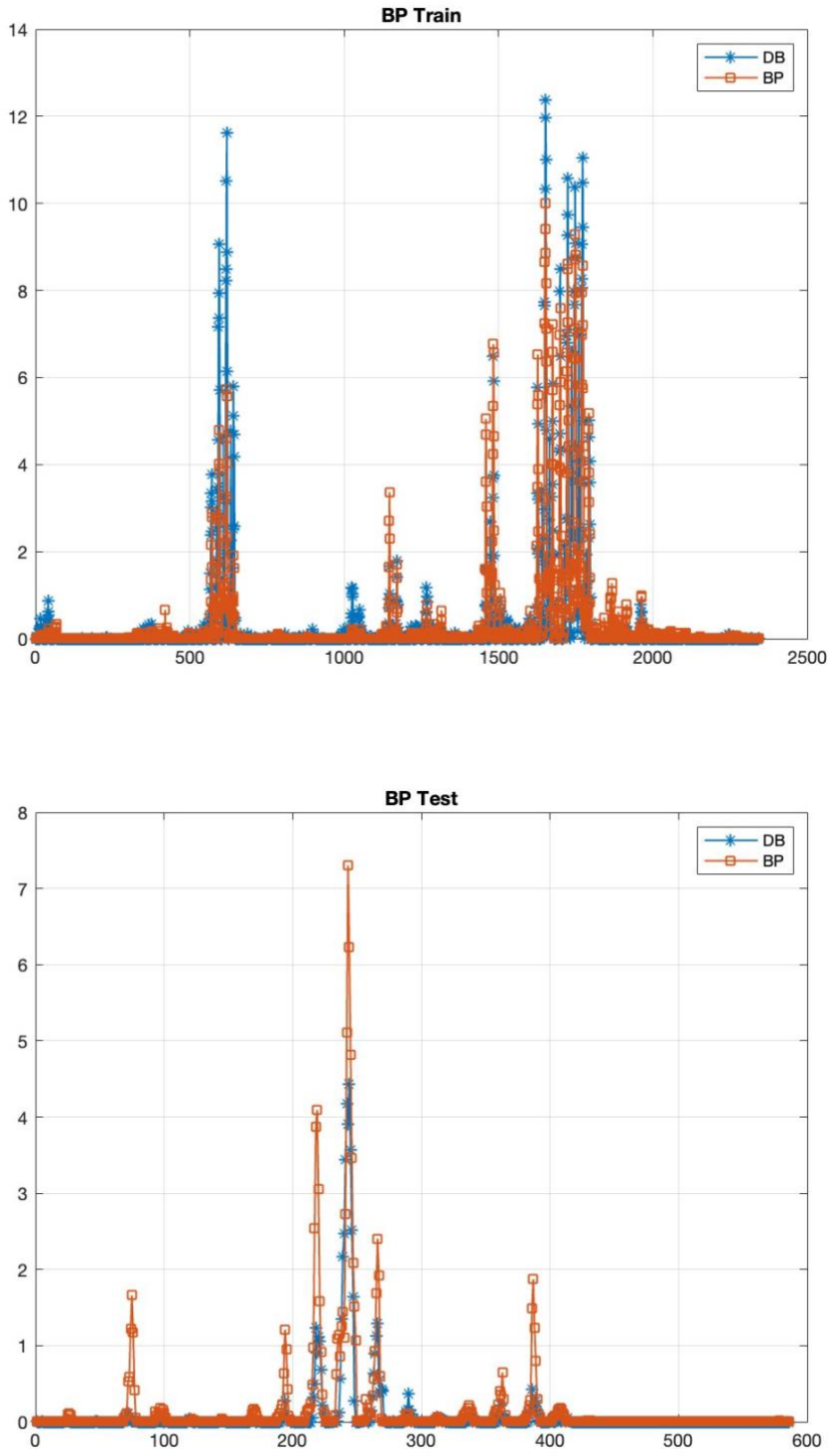

Figure 7-6 Training and testing results of BP

Throughout the training phase, which includes the majority of the data, the BP model displays significant variance and a wider distribution of prediction values compared to the more consistent DB results. This suggests that while BP can capture complex patterns in cooling demand, it might be prone

to overfitting or overly sensitive to the training data's specific characteristics. Such tendencies could lead to less reliable predictions when faced with new or varying conditions, as evidenced in the later portion of the data used for testing.

During this final 20% of the data used for testing, the predictions from BP continue to show greater variability and several outliers compared to DB. These outliers are critical as they indicate instances where BP significantly deviates from the expected values set by DB, highlighting days with unusual cooling demands that the neural network failed to predict accurately. The presence of these discrepancies suggests that the BP model, despite its ability to model complex dependencies, struggles with stability and accuracy when applied beyond its training set.

This analysis underscores the need for further tuning of the BP model to enhance its generalization capabilities and reduce sensitivity to non-essential fluctuations. Strategies might include refining the training algorithm, incorporating regularization techniques to prevent overfitting, or using a more representative dataset that includes a wider range of cooling demand scenarios. Such improvements could help align BP's predictions more closely with the reliable benchmarks provided by DB, ensuring that the neural network model is both accurate and practical for real-world applications. In this section, different neural networks are primarily compared, with no further discussion on methods to enhance neural network performance. The analysis focuses on exploring the performance differences among various neural network models on similar datasets, along with their respective advantages and limitations in practical applications.

7.4.2 Training and testing performance of CNN

Performance for the CNN model in Figure 7-7 during both the training and testing phases show a notable improvement in prediction accuracy compared to earlier results from other models. During training, the CNN model achieved a RMSE of 0.54, a MAE of 0.15, and a Mean Absolute Percentage Error (MAPE) of 30.72%. These metrics indicate a relatively high level of prediction accuracy during the model's training phase, suggesting effective learning from the dataset.

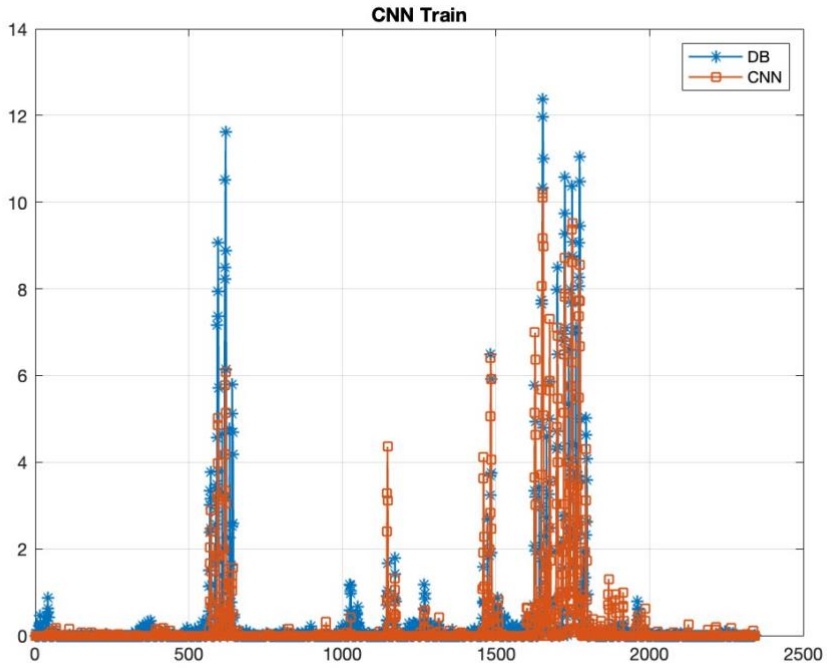

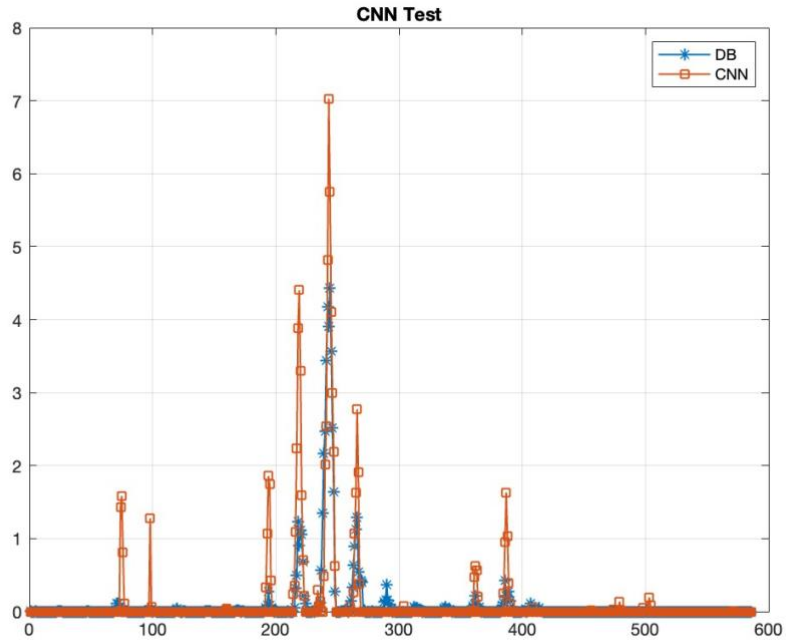

Figure 7-7 Training and testing results of CNN

In the testing phase, the CNN model demonstrates enhanced performance with an RMSE of 0.34, an MAE of 0.08, and a MAPE of 46.55%. The reduction in RMSE and MAE in the testing phase compared to the training phase suggests that the model generalises well to new data, maintaining a high degree of accuracy in its predictions. However, the increase in MAPE indicates a higher relative error in terms of percentage, which may point to specific instances where the model's predictions deviate significantly from actual values, particularly in cases of lower absolute values where percentage errors can be misleadingly high.

The CNN model shows lower values of RMSE and MAE in both training and testing phases compared to the BP model. This indicates that the CNN model generally produces predictions that are closer to the actual values, with less deviation and error. The lower RMSE in the testing phase for the CNN model particularly underscores its superior ability to generalise to new data, which is crucial for practical deployment.

While the CNN model exhibits lower numerical errors in terms of RMSE and MAE, its MAPE is higher in the testing phase compared to the training phase. This contrasts with the BP model, where the MAPE is significantly higher in both phases, reaching an exceptionally high level in the testing phase (67.5306%). The higher MAPE for the CNN model in testing might suggest specific instances where percentage errors are amplified, likely in cases of very low or near-zero demands.

7.4.3 Training and testing performance of LSTM

The LSTM in Figure 7-8 neural network model exhibits notable performance improvements in its testing phase with a reduction in RMSE from 0.62 to 0.31 and MAE from 0.24 to 0.14, highlighting its effective generalization capabilities. Although the MAPE increases slightly from 27.22% to 29.71%, this suggests that the model, while generally accurate, may experience proportional errors especially in scenarios of low demand.

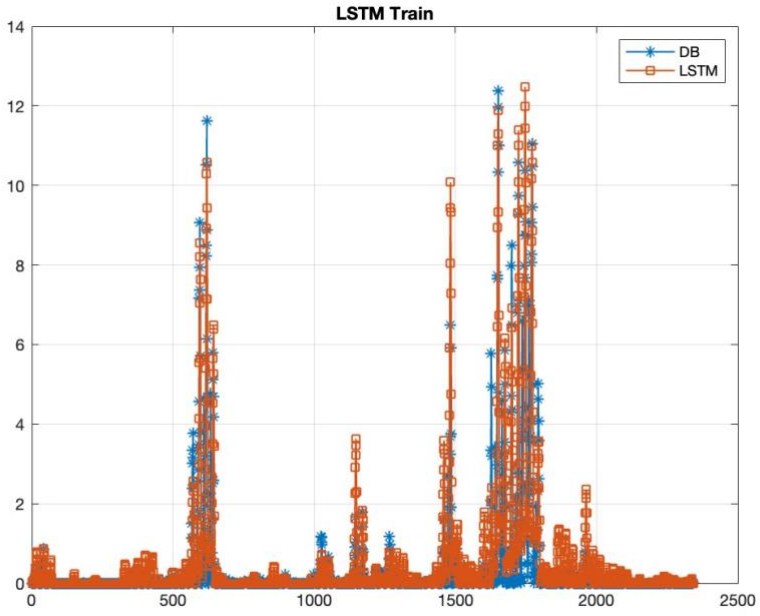

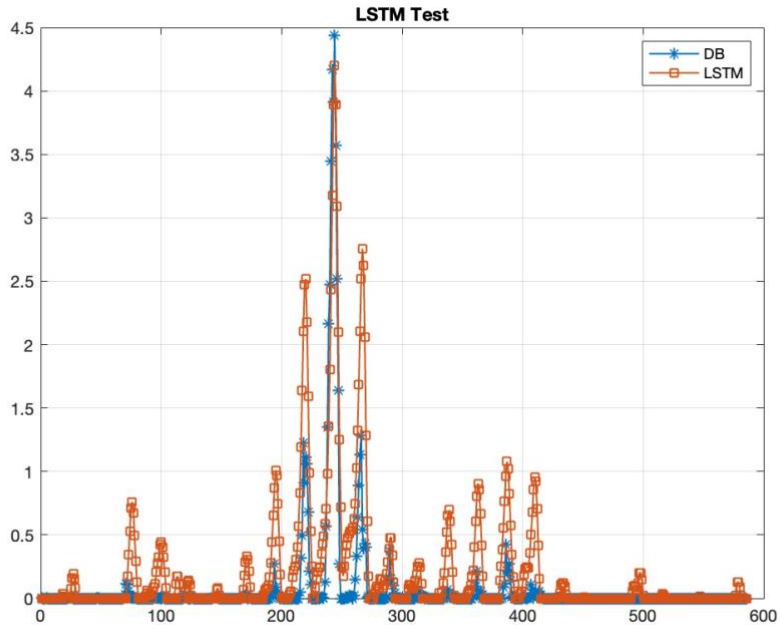

Figure 7-8 Training and testing results of LSTM

When compared to the BP and CNN models, the LSTM model stands out particularly for its ability to lower RMSE and MAE significantly in the testing phase, indicating a strong predictive accuracy. The BP model, with higher RMSE and MAE across both phases and a very high MAPE of 67.5306% during testing, shows less accuracy and consistency. The CNN model, although achieving the lowest RMSE and MAE during testing, exhibits a higher MAPE of 46.5526%, indicating it may also struggle with proportional errors under varied test conditions.

Overall, the LSTM model proves to be the most robust in handling predictive tasks for cooling demand, combining accuracy with relatively consistent error percentages. This makes it particularly suitable for applications were understanding temporal dynamics and maintaining prediction accuracy over time are crucial. However, the choice among LSTM, BP, and CNN should be guided by specific application needs, considering both absolute error margins and the importance of relative error consistency.

7.4.4 Training and testing performance of GRU

In the training phase as shown in Figure 7-9, the GRU model displays moderate errors with RMSE at 0.45 and MAE at 0.17. The relatively lower MAPE of 20.38% suggests the model's predictions are closely aligned with actual data values proportionally. Moving to the testing phase, there is a significant improvement in RMSE (0.23) and MAE (0.12), indicating the model's robust ability to generalise well to new, unseen data. However, the increase in MAPE to 28.06% signals that while the model is precise in error magnitude, it may experience issues with proportional errors under certain conditions, possibly linked to variations in demand that aren't as well-represented in the training data.

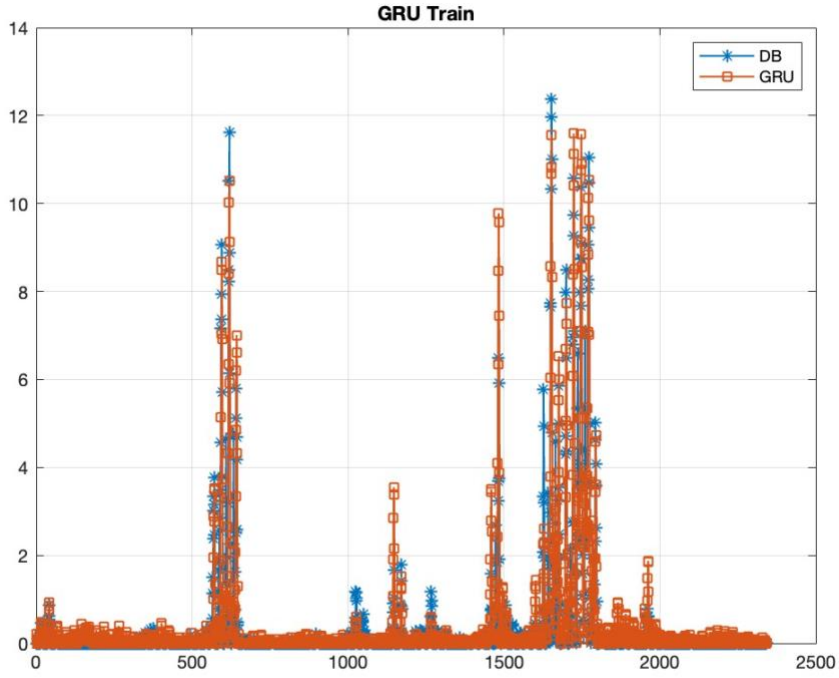

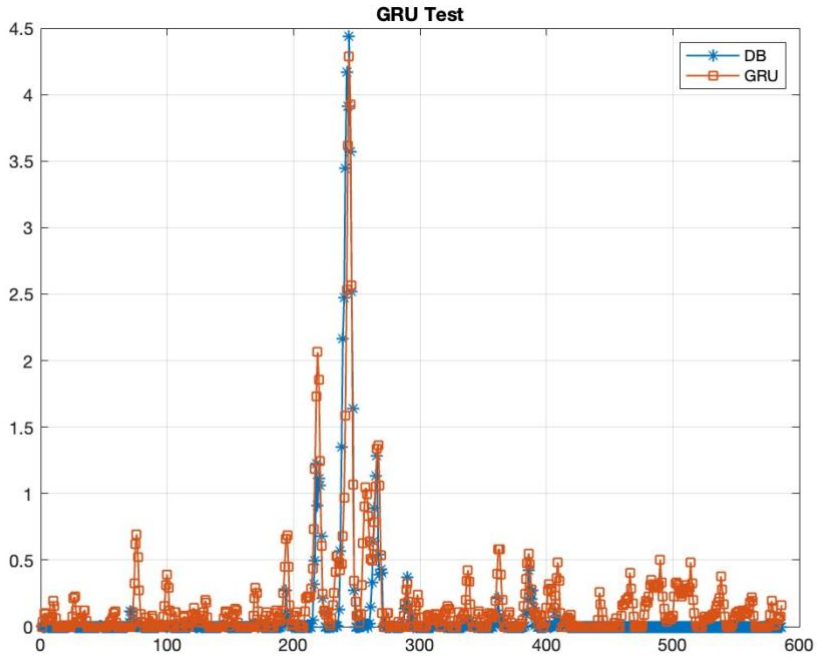

Figure 7-9 Training and testing results of GRU

Compared to the LSTM model which showed an RMSE of 0.31 and MAE of 0.14 in its testing phase, the GRU model performs better in both these metrics. This points to GRU's potentially higher efficiency in modelling sequences and making predictions. Both models, however, show an increase in MAPE in the testing phase, a common trait indicating that proportional errors increase when applied to new data. This could be attributed to the models capturing complex dependencies which may not always scale linearly with actual values, especially in varied operational scenarios.

The GRU model demonstrates a strong capability in accurately forecasting cooling demands, with superior generalization indicated by its testing phase metrics. Its performance, especially in comparison with LSTM and other models, suggests it could be more effective in applications requiring high precision and reliability. Future improvements might focus on reducing the variability in MAPE to enhance the

model’s consistency across different demand levels and operational conditions. This evaluation showcases GRU as a compelling choice for time-series prediction tasks where detailed temporal dynamics are crucial.

7.4.5 Training and testing performance of CRNN

In the training phase as shown in Figure 7-10, the CRNN model already demonstrates strong predictive accuracy, but its performance becomes more evident in the testing phase. The significant reduction in RMSE and MAE from training to testing underscores its effective generalization to new, unseen data. This transition suggests that the CRNN model not only learns the general trends and anomalies within the training data but also applies these learnings effectively to different datasets. However, the increase in MAPE in the testing phase indicates that while the model predicts more accurate values, it still faces challenges with proportional errors which could escalate in scenarios with extremely low or high demands. GRU Model exhibited a testing phase RMSE of 0.23504 and MAE of 0.11904, which are marginally higher than those of the CRNN. Although GRU is effective for sequential data, it may lack the spatial feature extraction capabilities that CRNN's convolutional components provide. LSTM Model showed a testing phase RMSE of 0.31432 and MAE of 0.14094, considerably higher than the CRNN's metrics, possibly due to LSTM's primary focus on long-term dependencies without the enhanced spatial analysis offered by convolutional layers.

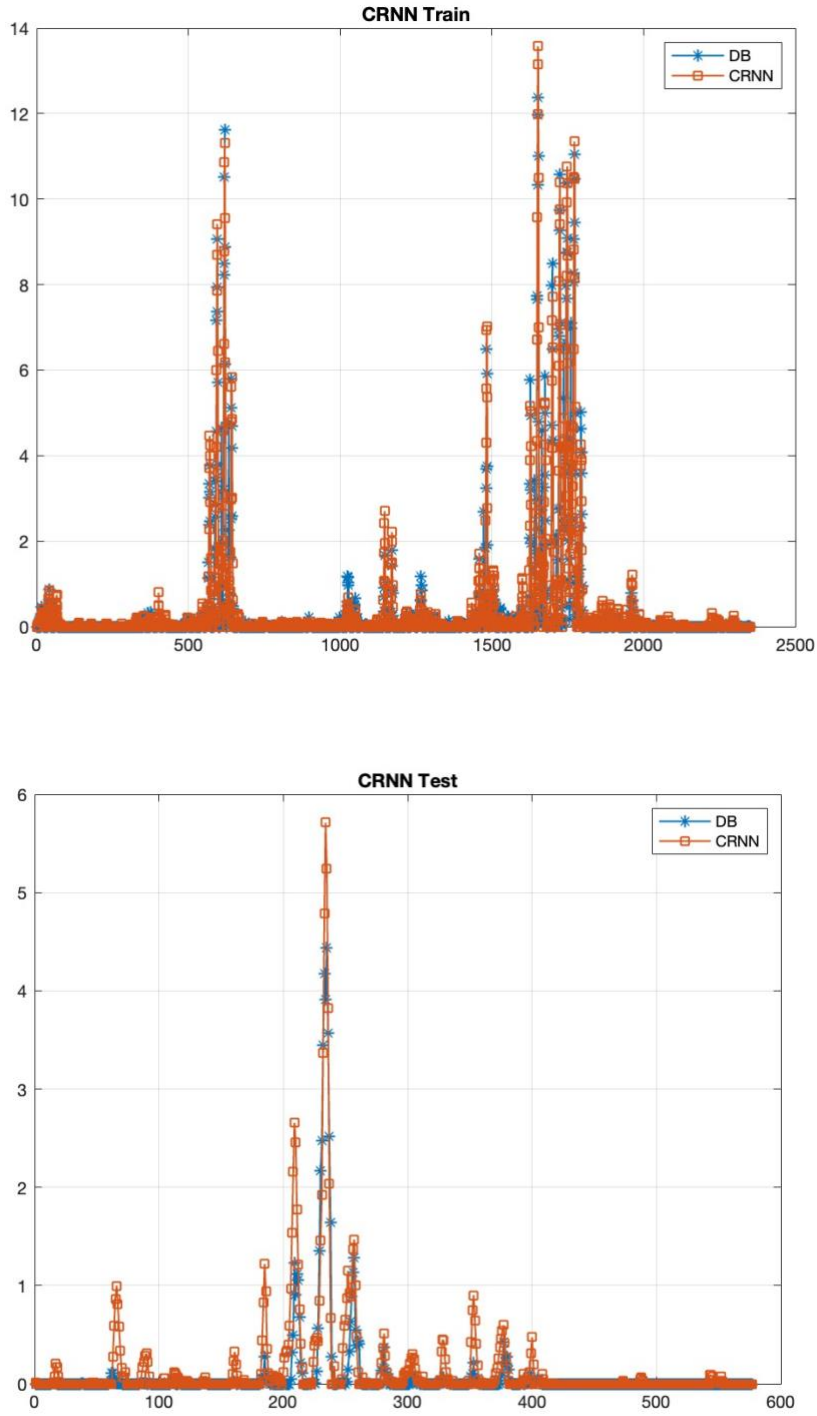

Figure 7-10 Training and testing results of CRNN

The CRNN model's performance can largely be attributed to its dual-layer architecture, which processes data through multiple dimensions—recognising both temporal sequences and spatial patterns. This multidimensional analysis is crucial in environments where inputs are not only sequential but also

interdependent based on spatial characteristics. Additionally, CRNN can efficiently manage the vanishing gradient problem, common in standard RNNs, through its integrated convolutional structures, leading to more stable and robust learning over long sequences. Overall, the CRNN's ability to capture and integrate complex patterns and dependencies in the data makes it highly effective for predicting cooling demands. Its performance across both training and testing phases suggests it could be particularly beneficial in practical applications requiring high precision and adaptability.

7.4.6 Training performance

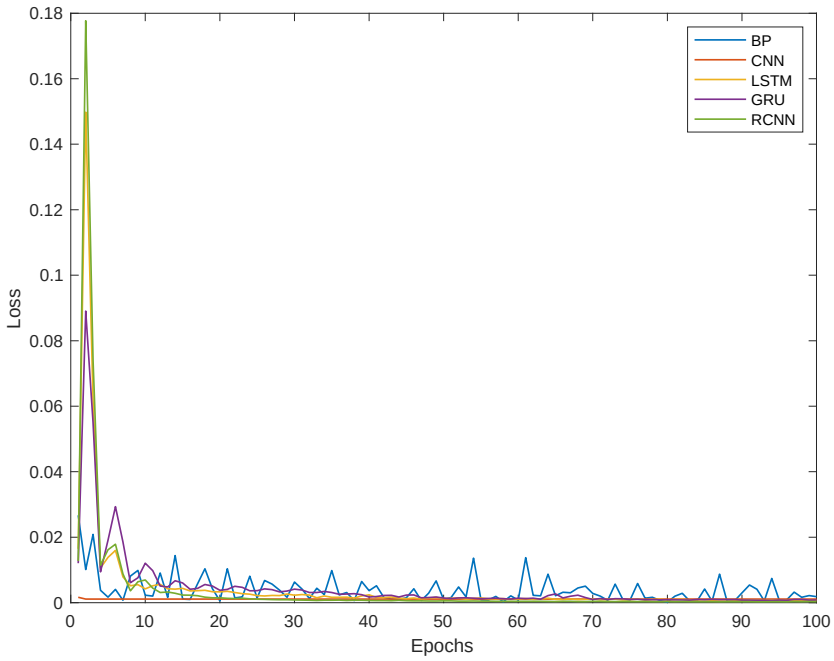

Figure 7-11 The comparison of the loss values across iterations

Figure 7-11 is the comparison of the loss values across iterations for the five neural networks. The BP network's loss decreases sharply at the beginning and then stabilises with some variability. The CNN network's loss also decreases sharply and then shows a stable trend with very slight fluctuations. The LSTM network's loss follows a similar sharp decrease and stabilises, but with fewer fluctuations than the BP. The GRU networks, which is another type of RNNs, show similar patterns with a quick decrease

followed by stability. The GRU has a bit more fluctuation than LSTM. The CRNN shows a rapid decrease as well and its loss settle slightly higher than CNN but with more fluctuations.

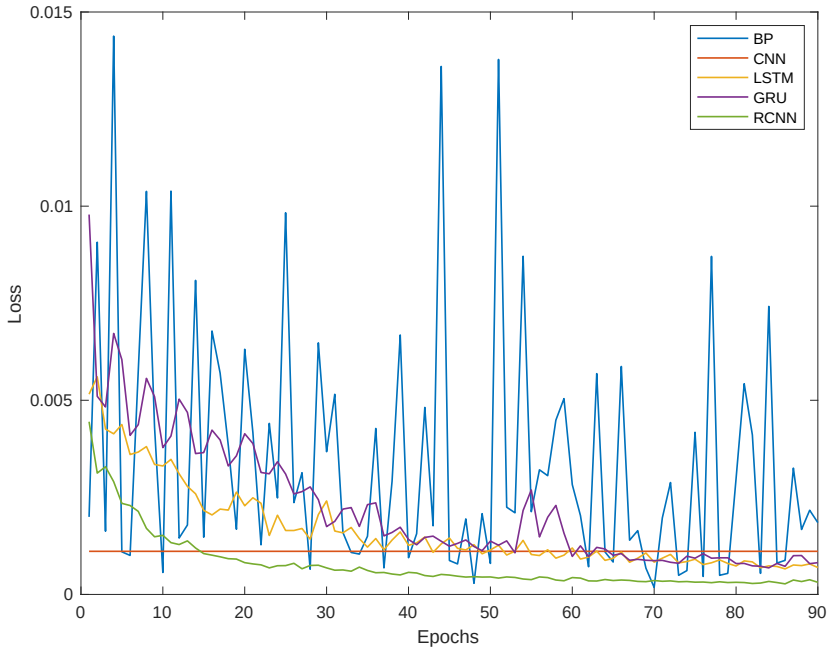

Figure 7-12 The comparison of the loss values after 10^{th} iterations

The initial data encompassing ten iterations reveal considerable volatility in the loss values, rendering an early analysis less definitive. Consequently, Figure 7-12 provides a more telling visualization of the loss trajectories post the initial ten iterations. This figure elucidates that, with progressive training epochs, there is a consistent decrement in the loss for all networks under scrutiny, with the exception of the BP. Notably, as the loss for the competing architectures converges to approximately 0.001 and demonstrates signs of stabilization, the BP network's loss persists at an elevated level of 0.008—indicative of a magnitude eightfold greater than its counterparts. This pronounced variance may suggest the BP network's challenges in achieving stabilization, potentially due to an architecture that lacks the complexity requisite for the task. The elevated and erratic loss metrics observed for the BP network could imply a

deficiency in effectively discerning the underlying patterns within the dataset, in stark contrast to the other examined architectures.

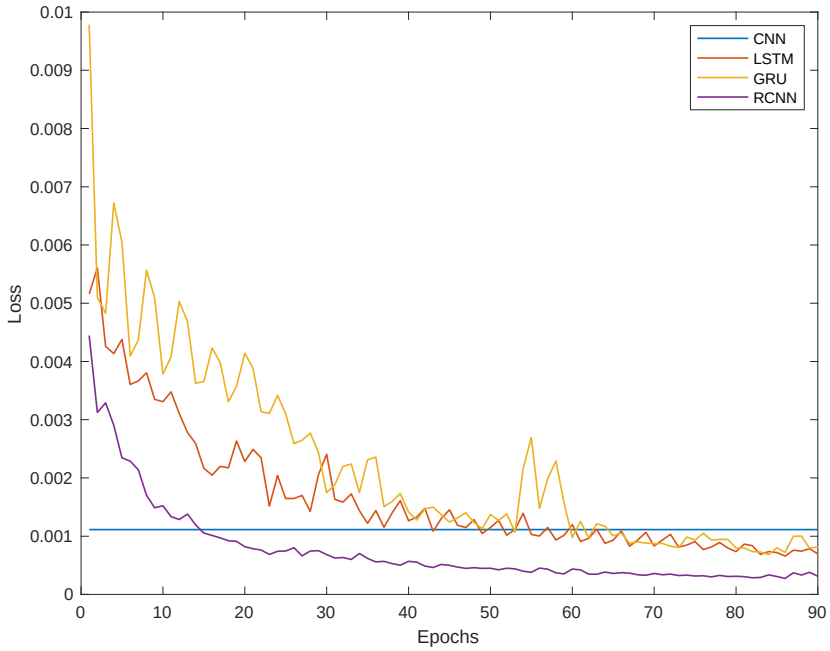

Figure 7-13 The comparison of the loss values for CNN, LSTM, GRU and CRNN after 10^{th} iterations

Upon the exclusion of the Backpropagation network from the analysis, Figure 7-13 elucidates the loss metrics of the remaining architectures. The CNN, in particular, exhibits a markedly distinct behaviour from its counterparts. It is noteworthy that the CNN's loss stabilises at a value of approximately 0.0011, manifesting negligible variation over successive epochs. This consistent performance by the CNN, evidenced by its sustained low loss, accentuates its capacity for effective feature extraction from the training data. The network's rapid convergence to and stabilization at this loss value suggests that it has efficiently assimilated the primary patterns within the dataset. Moreover, the plateau observed in the CNN's loss trajectory indicates that the network may have reached an optimization threshold. Beyond this juncture, additional training epochs appear to confer no substantial improvement in predictive

performance, implying that the model has potentially exploited the training data to its fullest extent. The cessation of loss reduction at this level also intimates the onset of a saturation point, signalling that the model's learning capacity, with respect to the current data distribution, has been maximised.

The LSTM exhibits a decreasing trend in loss, albeit with greater variability than the CNN. The initial sharp decline indicates a robust learning capacity, while the subsequent variability could be reflective of the network attempting to model the temporal dynamics within the data, which can be inherently more complex than spatial patterns. The GRU follow a similar pattern to LSTMs, with a notable initial decrease in loss, followed by fluctuations. The CRNN displays a loss reduction from approximately 0.0044 at the outset of training to 0.00031 by the final epoch. This significant decrease in loss is indicative of the CRNN's ability to refine its model parameters effectively over time. The steady downward trajectory, starting at a higher loss and converging to a markedly lower value, suggests that the CRNN is successfully learning and capturing the underlying patterns within the dataset with increasing accuracy. The absence of pronounced spikes or erratic behaviour in the loss curve implies a stable learning process without the setbacks that might be caused by overfitting, underfitting, or difficulties in navigating the optimization landscape.

Table 7-6 Training performance of different networks

	BP	CNN	LSTM	GRU	CRNN
RMSE	0.60	0.52	0.43	0.43	0.26
MAE	0.19	0.15	0.15	0.15	0.13
MAPE	29.9%	29.2%	19.0%	19.4%	11.0%

Table 7-7 Training time of different networks

Time	BP	CNN	LSTM	GRU	CRNN
max	5.78	1.90	23.08	16.14	9.93
min	5.49	0.95	9.35	9.19	9.03
average	5.08	0.78	8.86	7.56	8.79

The BP model shown in Table 7-6 and Table 7-7, while showing the highest error rates with an RMSE of 0.60, MAE of 0.19, and MAPE of 29.9%, also demonstrates a comparatively moderate demand on computational resources. The average training time for BP is recorded at 5.08 minutes, with a minimum and maximum range of 5.49 to 5.78 minutes, respectively. This relatively consistent training duration could indicate a computational simplicity that aligns with the traditional structure of BP networks.

In contrast, the CNN not only achieves improved accuracy metrics (RMSE of 0.52, MAE of 0.15, MAPE of 29.2%) but also boasts the most expedient training times, averaging at 0.78 minutes. This efficiency, spanning from a minimum of 0.95 to a maximum of 1.90 minutes, underscores the CNN's optimization for both performance and speed, likely a result of the shared-weight architecture inherent to convolutional layers.

The LSTM and the GRU network, designed for their temporal processing capabilities, naturally incur longer training times due to their complex architectures. The LSTM averages at 8.86 minutes, ranging from 9.35 to 23.08 minutes, and the GRU averages at 7.56 minutes, with a span from 9.19 to 16.14 minutes. Despite the increased time investment, both networks exhibit enhanced accuracy (RMSE and MAE of 0.43 for both, with MAPEs of 19.0% and 19.4% for LSTM and GRU, respectively), reflecting the trade-off between temporal sophistication and computational load.

The CRNN, which integrates the spatial acuity of CNNs with the sequential depth of RNNs, manages to strike a balance in its training time. With an average of 8.79 minutes and a range between 9.03 to 9.93 minutes, the CRNN's training duration is comparable to the LSTM and GRU. This is particularly notable given the CRNN's superior accuracy statistics (RMSE of 0.26, MAE of 0.13, MAPE of 11.0%), suggesting an efficient utilization of training time relative to the predictive benefits gained.

7.4.7 Testing performance

Training performance refers to how well a model performs on the dataset it was trained on. Evaluating training performance helps understand the progress and pace of the model's learning, as well as identify any potential issues with underfitting. Testing performance, on the other hand, pertains to how the model performs on a dataset it has not seen during training. This test dataset is used to assess the model’s generalization capabilities after the training has concluded. Testing performance is often measured by metrics such as accuracy, which provide a comprehensive reflection of the model’s behaviour on unknown data. It is the ultimate measure of a model’s quality because it indicates the model’s effectiveness in real-world applications. Therefore, in this section the main focus is on the test performance of the different models.

The initialization of networks weights with random values from a defined distribution is a standard practice that can lead to variability in model performance due to the stochastic nature of the training process. To account for this and gain a more reliable assessment of the models' performance, a kernel density estimation (KDE) approach was employed. KDE is a method for estimating the probability density function of a dataset. It smooths out the data distribution and provides a continuous curve that gives a

visual sense of the density of different outcomes. Unlike a histogram, KDE produces a smooth estimate without relying on predefined bins, thus offering a more refined view of the data's underlying structure.

By training the models 100 times and applying KDE to the resulting RMSE, MAE and MAPE values, we can observe a smoothed probability distribution of model outcomes. This method provides a comprehensive view of variability and the robustness of the models' performance, minimising the influence of initial weight randomness.

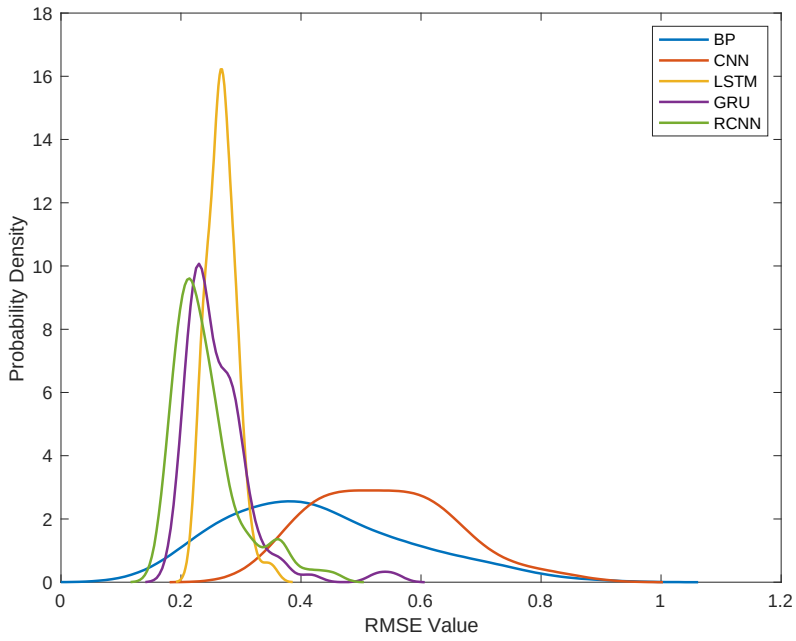

Figure 7-14 The distribution of RMSE value of different networks

Figure 7-14 shows the distribution of RMSE value of different networks. The BP network shows a broad distribution of RMSE values with a peak around 0.4 indicating the most common error rate. The width of the BP's distribution suggests variability in its performance, which could be due to the simplistic nature of the model or its sensitivity to the initialization of weights. The CNN has a narrower peak than BP, which indicates a more consistent RMSE across different runs. However, its peak is also positioned towards the higher end of the RMSE scale, which suggests that the CNN generally has a higher error rate.

This indicates a high probability of extreme values appearing in the prediction of the CNN, which shows a poor generalization ability of the CNN compared to the training performance. The LSTM and GRU distributions have similar shapes and peaks, with the GRU showing a slightly broader distribution than LSTM. The probability density of LSTM reaches up to 16 and GRU reaches up to only 10. This means that while both models are capturing temporal dependencies effectively, GRU might have more variability in its performance. The CRNN distribution is the narrowest and is skewed towards the lowest RMSE values, while the most common RMSE values is around 0.2. This indicates that the CRNN not only tends to have a lower error rate on average but also that its performance is more consistent across different training runs compared to other models.

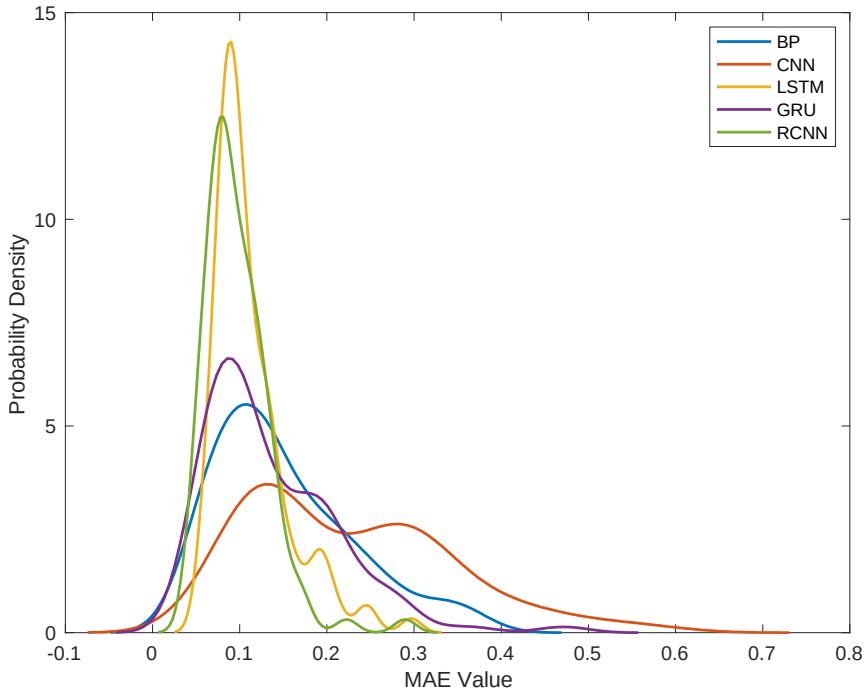

Figure 7-15 The distribution of MAE value of different networks

Figure 7-15 shows the distribution of MAE value of different networks. The MAE is a measure that provides the average magnitude of errors in a set of predictions, without considering their direction. In

contrast to RMSE which focuses on outliers MAE focuses more on the overall model error. BP and CNN show the widest peaks among the models, indicating higher average MAE and greater variabilities in the model's predictions. The most common BP value is around 0.1 and has narrower width compare with CNN. This suggests that CNN model is the least accurate and most inconsistent in terms of error magnitude. BP and GRU show similar distributions with their peaks slightly higher and narrower than that of the CNN, indicating a small increase in average MAE and variability. In line with the distribution of the RMSE, the distribution of the MAE is also very narrow, with a peak up to around 14 near MAE value 0.1. CRNN stands out with a high peak, which is also the most narrowly distributed around a small MAE value. A moderate spread in the MAE values would indicate that while the CRNN model may not have the lowest possible error on every single instance in the test set, it does not exhibit extreme variations in accuracy, which is a positive sign of its ability to generalise across different samples of data. This suggests that the CRNN's predictions are relatively stable across various cases within the test set, striking a balance between being too rigid and too erratic in its error rates on new data.

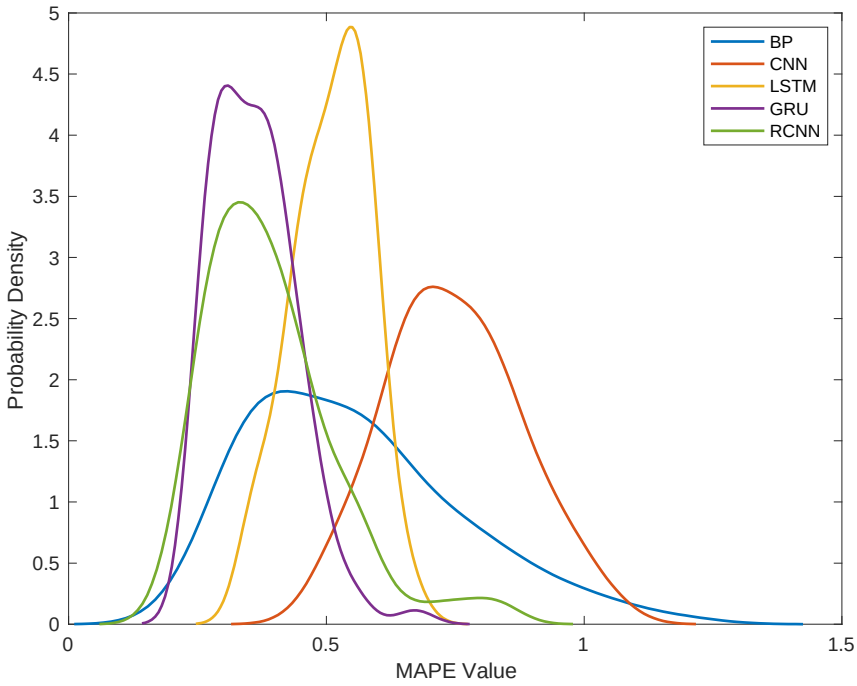

Figure 7-16 The distribution of MAPE value of different networks

Figure 7-16 shows the distribution of MAPE value of different networks. The BP network has a peak that is neither particularly high nor low, which suggests a moderate density of MAPE values. The peak's position indicates that BP's predictions are not the most accurate among the compared models, with a wider spread suggesting variability in its performance. The CNN has a lower and wider peak than the BP, indicating that while its most common MAPE values are not the lowest, its errors are more evenly distributed across a range of values. The LSTM's peak is similar in height to the CNN's but is shifted towards the left, which suggests a higher concentration of lower MAPE values and, thus, better performance in terms of prediction accuracy. The GRU shows a peak that is quite tall and located further to the left compared to the CNN and LSTM, indicating a high density of lower MAPE values, which suggests good predictive accuracy with a higher probability of achieving low error rates. The CRNN has a prominent peak, which is not the tallest but is positioned the furthest to the left among all the models.

This suggests that the CRNN frequently achieves lower MAPE values than the other models, indicating it has the highest prediction accuracy on average.

7.5 Conclusion

Chapter 7 extends the analysis of neural network applications for predicting cooling demand, building upon the groundwork laid in Chapter 4. While the prior chapter enhanced network performance through feature selection and optimization techniques, the current chapter expands the scope to a wider array of neural network architectures. These include the fundamental BP neural network and more sophisticated structures such as CNNs, LSTMs, GRUs, and CRNNs.

Networks were benchmarked based on their loss values over training iterations. The BP network, while initially decreasing sharply, showed fluctuating stability thereafter. CNN's loss also dropped swiftly and maintained low variability, indicating steady feature extraction. LSTM and GRU saw similar initial declines with subsequent stability, though GRU had slightly more fluctuation, reflective of the intricacies involved in modeling temporal sequences. CRNN stood out by achieving a significant reduction in loss, suggesting a strong capability in integrating spatial and temporal data patterns. Testing performance was assessed through the distribution of RMSE, MAE, and MAPE values. KDE was used to provide a visual representation of the models' predictive accuracy. The distributions indicated the variability and robustness of each model's performance, with the CRNN model showing the narrowest distribution and lowest error rates, suggesting its high stability and accuracy in predictions. However, the CNN that performed well in training instead lacked the ability to generalise.

The chapter's rigorous evaluation sought to identify the neural network architecture that most effectively predicts cooling demand. The goal was to find a model with an optimal balance between

complexity and predictive accuracy, capable of discerning data patterns and generalising to unseen data. The results from this analysis contribute valuable insights into the application of neural network models in the realm of urban climate control and energy management systems.

Chapter 8
Conclusion and Future work

8.1 Conclusion

A deep investigation into the UK's energy situation and policies reveals three key issues that could significantly impact the country's future energy use. First, the study identifies the challenges associated with decarbonising heating, a critical aspect of the UK's broader strategy for reducing carbon emissions. Second, it highlights the often-overlooked issue of increasing overheating in buildings, an emerging concern in the context of global warming. Finally, the research points out a gap in the current landscape of energy modeling – the lack of large-scale, high- resolution energy demand models. These issues, if not addressed, could have far-reaching implications for the UK's future energy decarbonization efforts, economic stability, and security.

Building on this foundation, the thesis goes on to present a comprehensive narrative that intertwines these critical issues with practical aspects of energy demand forecasting. It illustrates the shift from traditional to advanced modeling techniques, highlighting the critical role these models play in informing sustainable energy policies and infrastructure development. The findings offer significant insights for

policymakers, energy distributors, and the broader field of energy management. This thesis presented an in-depth investigation into the modeling of space heating and cooling demand in the UK, leveraging both traditional building simulation methods and advanced machine learning techniques.

Chapter 4 focuses on building simulation for space heating demand in the UK. It highlights the creation of a high-resolution model that predicts heat demand up to 2050, considering both domestic and non-domestic sectors. The chapter validates this model against historical data and explores the impact of electrification of heat on the UK's electricity network, emphasising the importance for policy makers and energy distributors. The study uses a bottom-up model, validated against historic predictions, to produce forecasts and discusses the resilience needed for the UK's electricity network considering the electrification of heat. The results demonstrate the significant effect of heat demand on power generation capacity, suggesting that wide installation of heat storage could reduce the required investment in new power generation. In chapter 5, the application of ANNs is explored for predicting space heating demand, marking a shift from traditional physical models to data-driven approaches. The research introduces a novel ANN-based framework for high-resolution, national-level data acquisition. It utilises sensitivity and correlation analysis for feature selection to enhance efficiency and employs meteorological data as the primary input. The key contributions include an ANN model based solely on weather data and a significant reduction in input variables without compromising accuracy. The model is validated against the heating demand in Scotland for 2050, highlighting its utility despite some limitations in predicting summer demand. The chapter concludes by underscoring the potential of ANNs in accurately forecasting heating demand and the importance of choosing relevant features for model.

Chapter 6 of the thesis presents a detailed investigation of cooling demand in London, employing a high-precision model that merges physical and economic approaches using building simulation. This model allows for dynamic analysis and future scenario planning for cooling demand, addressing a significant research gap in the UK. It offers a novel solution for urban cooling demand prediction, a more comprehensive analysis of the impact on the power grid and supports future investment planning. The methodology includes generating high-resolution cooling profiles, validation with government data, and analysing the impact on energy consumption. Key findings include a projected 45% increase in London's cooling demand from 2020 to 2050 due to rising temperatures, and the necessity of energy storage systems to manage increased summer demand efficiently. The research emphasises the need for optimising the capacity of cooling plants and equipment to align with varying demand, suggesting reversible heat pumps as a dual-function solution for enhanced efficiency. Chapter 7 explores neural network applications for predicting cooling demand, building on the feature selection and optimization techniques introduced in Chapter 5. It examines various neural network architectures, including BPNN, CNN, RNN, LSTM, GRUs, and CRNN. The chapter evaluates these models based on their loss values over training iterations and generalization capabilities in testing performance, using metrics like RMSE, MAE, and MAPE. KDE visualises model accuracy. CRNN emerges as the leading architecture, showing the narrowest distribution and lowest error rates, indicating high stability and accuracy in predictions.

The contributions of this thesis are multifaceted and significant in advancing the field of energy demand forecasting.

The research presents state-of-the-art predictive models that substantially enhance the forecasting of heating and cooling demands. This innovative model transforms national-scale heating demand forecasting with its ability to deliver hourly predictions. Capturing the complex rhythms of heat demand

with remarkable precision, the model is instrumental in devising targeted energy distribution strategies and managing peak loads adeptly. Its insightful analysis is particularly beneficial for the shift towards eco-friendly heating solutions, offering strategic guidance to ensure energy conservation and reduce environmental impact. The model for assessing urban cooling demand is exceptional in its granularity and breadth. It synthesises a wide array of data, from the architectural features of buildings to economic considerations, delivering an all-encompassing view of metropolitan cooling requirements. In an era marked by amplified urban heat islands and escalating global temperatures, this model's precise predictions are invaluable. It empowers urban developers and decision-makers to formulate measures that alleviate pressure on power systems during peak usage and guides the creation of buildings and city designs that inherently minimise the need for cooling.

The thesis also breaks new ground with the pioneering application of ANNs in energy demand forecasting. Employing ANNs in forecasting represents a quantum leap in energy prediction methodologies. These networks adeptly handle extensive and intricate data, extracting patterns and delivering precise forecasts of future heating and cooling needs. The model's versatility across different environmental and geographical contexts enhances its value, making it a potent tool in the global landscape of energy management. The model's reliance on meteorological data as a primary input significantly refines the forecasting process, bypassing the complexities of collecting extensive building data. This approach amplifies the model's reach and practicality, allowing for broader application.

Furthermore, the thesis underscores the enhancement of grid stability through sustainable energy solutions. The studies shine a spotlight on the pivotal function of energy storage systems in synchronising energy supply with the oscillating demands. These systems are vital for grid equilibrium, especially as

we face more frequent and severe peak demand instances due to climate change. They enable a harmonious integration of renewable energy, storing surplus power during low-demand periods for use during high-demand times, thus bolstering the reliability and sustainability of the energy supply. The scenario planning included in the heat demand analysis is an essential instrument for fortifying energy infrastructure against future uncertainties. It contemplates various prospective situations, from extreme weather conditions to the transition to complete electrification. This forward-looking approach equips energy systems to stay resilient and adaptable, ready for the array of challenges that the future may hold.

8.2 Future work

Future research could aim to diversify the types of building models used in simulations. While the current thesis uses 24 building models incorporating different insulation levels (U-values), there's scope to include a wider range of building ages, architectural styles, construction materials, and usage patterns to better reflect the diversity of the building stock. Expanding the models to account for regional variability within the country, such as differences in climate, local building regulations, and cultural practices in energy use, could provide more tailored and accurate predictions for specific areas.

Building upon the existing use of neural networks, future research could venture into the wider domain of machine learning techniques to enhance energy demand forecasting models. While neural networks have proven effective, there are other machine learning methodologies like decision trees, SVM, and ensemble methods like RF and GB machines that could be tested for their efficacy in energy demand forecasting. Combining various machine learning methods could lead to hybrid models that harness the strengths of each approach. For example, ensemble models can be used to reduce the variance and bias of predictions, potentially leading to more robust forecasting. Different machine learning models might

benefit from or necessitate different feature engineering techniques. Exploring various feature selection methods could reveal the most impactful variables and reduce model complexity without sacrificing accuracy.

The exploration of heat pumps, energy storage, and cooling equipment represents a solid foundation for understanding the dynamics of energy systems. To take this further, future work could focus on optimising models to maximise the efficiency and efficacy of these systems. Introducing dynamic variables into the models could provide a more responsive and accurate reflection of energy systems. This could involve real-time pricing, weather fluctuations, or user demand changes to optimise energy usage. By considering multiple energy sources and their interactions, future research can create optimization models that determine the best mix of energy generation and storage options for different scenarios. Incorporating demand-side management strategies into the optimization model could reduce peak loads and flatten demand curves, leading to more stable and efficient energy systems. Future work could involve creating models that optimise the scheduling of renewable energy sources, aligning energy supply with predictable patterns of heating and cooling demand. Including economic variables like cost of electricity, tariffs, and incentives in the model could optimise not just energy usage, but also the financial aspects of energy consumption and production. Integrating life-cycle cost analysis into optimization models could ensure that the long-term costs and benefits of different energy systems are considered, leading to more sustainable decision-making.

Reference

[1] WMO, “WORLD METEOROLOGICAL ORGANIZATION: Global Annual to Decadal Climate Update.”

[2] A. Kazmierczak, R. Lowe, K. R. van Daalen, K. Johnson, S. Dasgupta, and E. Robinson, “Climate change as a threat to health and well-being in Europe: focus on heat and infectious diseases,” 2022.

[3] WMO, “EUROPEAN STATE OF THE CLIMATE SUMMARY 2022,” 2022.

[4] P. Agreement, “Paris agreement,” in report of the conference of the parties to the United Nations framework convention on climate change (21st session, 2015: Paris). Retrived December, HeinOnline, 2015, p. 2017.

[5] H. C. De Coninck, IPCC special report on carbon dioxide capture and storage. Cambridge: Cambridge University Press, 2005.

[6] C. Le Quéré et al., “Global carbon budget 2018,” Earth System Science Data Discussions, vol. 2018, pp. 1–3, 2018.

[7] G. Energy, “Global Energy & CO2 Status Report,” International Energy Agency: Paris, France, 2019.

[8] M. Pathak, R. Slade, R. Pichs-Madruga, D. Ürge-Vorsatz, R. Shukla, and J. Skea, “Climate Change 2022 Mitigation of Climate Change: Technical Summary,” 2022.

[9] M. Lennan and E. Morgera, “The Glasgow Climate Conference (COP26),” The International Journal of Marine and Coastal Law, vol. 37, no. 1, pp. 137–151, 2022.

[10] P. Walker, R. Mason, and D. Carrington, “Theresa May commits to net zero UK carbon emissions by 2050,” The Guardian, vol. 11, no. 6, p. 19, 2019.

[11] Tamsin Edwards, Nicole Watson, and Nuala Burnett, “The UK’s Plans and Progress to Reach Net Zero by 2050,” London, Jun. 2023.

[12] “Transforming heating-Overview of current evidence,” Department for business, energy & industrial strategy, 2018. [Online]. Available: https://assets.publishing.service.gov.uk/government/uploads/system/uploads/attachment_data/file/766109/decarbonising-heating.pdf

[13] E. and I. S. Secretary of State for Business, “HM Government – Heat and Buildings Strategy,” London, 2021.

[14] M. González-Torres, L. Pérez-Lombard, J. F. Coronel, I. R. Maestre, and D. Yan, “A review on buildings energy information: Trends, end-uses, fuels and drivers,” Energy Reports, vol. 8, pp. 626–637, 2022, doi: https://doi.org/10.1016/j.egyr.2021.11.280.

[15] S. Cran-McGreehin, “Heating buildings-Reducing energy demand and greenhouse gas emissions,” Energy Research Partnership, London, 2016. [Online]. Available: https://erpuk.org/wp-content/uploads/2017/01/ERP-Heating-Buildings-report-Oct-2016.pdf

[16] E. and I. S. C. Business, “Decarbonising heat in homes Seventh Report of Session 2021-22 Report, together with formal minutes relating to the report,” London, 2022. [Online]. Available: www.parliament.uk.

[17] Committee on Climate Change, “Annex 2. Heat in UK buildings today,” London, 2017. [Online]. Available: http://bpie.eu/publication/europes-buildings-under-the-microscope/

[18] J. Rosenow et al., “The pathway to net zero heating in the UK A UKERC policy brief Key findings”, doi: 10.5286/ukerc.edc.000941.

[19] W. Smith, N. Pidgeon, C. Demski, and S. Becker, “Mapping the Landscape of Public Attitudes Towards Low-Carbon Heating Technologies,” 2024, doi: 10.5286/UKERC.EDC.000969.

[20] Lord Deben, “The Sixth Carbon Budget,” London, 2020. [Online]. Available: www.theccc.org.uk/publications

[21] R. Gupta, M. Gregg, and K. Williams, “Cooling the UK housing stock post-2050s,” Building Services Engineering Research and Technology, vol. 36, no. 2, pp. 196–220, Mar. 2015, doi: 10.1177/0143624414566242.

[22] M. Kendon, M. McCarthy, S. Jevrejeva, A. Matthews, T. Sparks, and J. Garforth, “ State of the UK Climate 2020 ,” International Journal of Climatology, vol. 41, no. S2, pp. 1–76, Jul. 2021, doi: 10.1002/joc.7285.

[23] F. Khosravi, R. Lowes, and C. E. Ugalde-Loo, “Cooling is hotting up in the UK,” Energy Policy, vol. 174, Mar. 2023, doi: 10.1016/j.enpol.2023.113456.

[24] “Sustainable cooling,” London, Apr. 2021. Accessed: Apr. 03, 2023. [Online]. Available: https://researchbriefings.files.parliament.uk/documents/POST-PN-0642/POST-PN-0642.pdf

[25] “Sustainable cooling,” London, Apr. 2021. Accessed: Apr. 03, 2023. [Online]. Available: https://researchbriefings.files.parliament.uk/documents/POST-PN-0642/POST-PN-0642.pdf

[26] “Risks to health, wellbeing and productivity from overheating in buildings,” London, Jul. 2022. Accessed: Apr. 03, 2023. [Online]. Available: https://www.theccc.org.uk/wp-

content/uploads/2022/07/Risks-to-health-wellbeing-and-productivity-from-overheating-in-buildings.pdf

[27] F. Khosravi, R. Lowes, and C. E. Ugalde-Loo, “Cooling is hotting up in the UK,” Energy Policy, vol. 174, Mar. 2023, doi: 10.1016/j.enpol.2023.113456.

[28] M. Chaudry, M. Abeysekera, S. H. R. Hosseini, N. Jenkins, and J. Wu, “Uncertainties in decarbonising heat in the UK,” Energy Policy, vol. 87, pp. 623–640, 2015.

[29] E. & I. S. Department for Business, Ed., “Apply for the Boiler Upgrade Scheme,” 2021, London. [Online]. Available: https://www.gov.uk/apply-boiler-upgrade-scheme

[30] Kevin Harris, “Energy Trends December 2023,” London, 2023.

[31] P. Bolton, “Energy imports and exports,” 2018. [Online]. Available: www.parliament.uk/commons-library|intranet.parliament.uk/commons-library|papers@parliament.uk|@commonslibrary

[32] BEIS, “UK ENERGY IN BRIEF 2021.” [Online]. Available: www.gov.uk/government/statistics/uk-energy-in-brief-2021

[33] Kevin Harris, “Digest of UK Energy Statistics Annual data for UK, 2021.”

[34] BEIS, “Energy Consumption in the UK (ECUK) 1970 to 2021,” 2021.

[35] Secretary of State for Energy and Climate Change, “Electricity Market Reform: policy overview,” 2012.

[36] BEIS, “Five Year Review of the Energy Act 2013,” 2022.

[37] Ofgem, “Upgrading Our Energy System Smart Systems and Flexibility Plan,” 2017. [Online]. Available: https://www.gov.uk/government/consultations/call-for-evidence-a-smart-flexible-energy-system;

[38] BEIS, “The Clean Growth Strategy Leading the way to a low carbon future,” 2017. [Online]. Available: www.nationalarchives.

[39] BEIS, “Energy White Paper,” 2019.

[40] S. Hinson, “Energy policy: an overview.” [Online]. Available: www.parliament.uk/commons-library|intranet.parliament.uk/commons-library|papers@parliament.uk|@commonslibrary

[41] D. Helm, “Cost of Energy Review,” 2017.

[42] H. Government, “The Ten Point Plan for a Green Industrial Revolution,” 2020.

[43] HM Treasury, “Net Zero Review: Interim report,” 2020.

[44] HM Government, “Powering up Britain,” London, 2023.

[45] Adcock and Alex, “Energy Company Obligation (ECO).” [Online]. Available: www.parliament.uk/commons-library|intranet.parliament.uk/commons-library|papers@parliament.uk|@commonslibrary

[46] BEIS, “Sustainable Warmth Competition Guidance for Local Authorities,” 2021.

[47] “Home Upgrade Grant: Phase 2 Guidance for local authorities,” 2022.

[48] BEIS, “The Boiler Upgrade Scheme Switch to low carbon heating.” [Online]. Available: www.gov.uk/find-energy-certificate

[49] Paul Wakeley, “Electricity Ten Year Statement,” 2023.

[50] T. Cholewa et al., “On the short term forecasting of heat power for heating of building,” J Clean Prod, vol. 307, p. 127232, 2021.

[51] P. Hietaharju, M. Ruusunen, and K. Leiviskä, “Enabling demand side management: Heat demand forecasting at city level,” Materials, vol. 12, no. 2, p. 202, 2019.

[52] S. Clegg and P. Mancarella, “Integrated electricity-heat-gas modelling and assessment, with applications to the Great Britain system. Part I: High-resolution spatial and temporal heat demand modelling,” Energy, vol. 184, pp. 180–190, 2019.

[53] A. Mavrogianni, M. Davies, M. Kolokotroni, and I. Hamilton, “A GIS-based bottom-up space heating demand model of the London domestic stock,” in Proceddings 11th International IBPSA Conference, Building Simulation, 2009.

[54] C. Sinclair, G. Unkaya, and T. Jennings, “Mapping of district heating feasibility studies in Scotland,” 2020.

[55] J. S. Michael Brown Dina Darshini Valts Grintals Andrew Turton, “Electrification of Heat and the Impact on the Scottish Electricity System,” Delta Energy & Environment Ltd, 2016.

[56] S. D. Watson, K. J. Lomas, and R. A. Buswell, “Decarbonising domestic heating: What is the peak GB demand?,” Energy Policy, vol. 126, pp. 533–544, 2019.

[57] P. McCallum et al., “A multi-sectoral approach to modelling community energy demand of the built environment,” Energy Policy, vol. 132, pp. 865–875, 2019, doi: 10.1016/j.enpol.2019.06.041.

[58] S. Eggimann, J. W. Hall, and N. Eyre, “A high-resolution spatio-temporal energy demand simulation to explore the potential of heating demand side management with large-scale heat pump diffusion,” Appl Energy, vol. 236, pp. 997–1010, 2019, doi: 10.1016/j.apenergy.2018.12.052.

[59] A. Bruce-Konuah, R. V Jones, A. Fuertes, and P. de Wilde, “Central heating settings and heating energy demand in low energy social housing in the United Kingdom,” Energy Procedia, vol. 158, pp. 3658–3663, 2019.

[60] H. Bruhns, “Identifying determinants of energy use in the UK nondomestic stock,” 2008.

[61] V. Goodright, “Estimates of heat use in the United Kingdom in 2013,” DECC Statistics, 2014.

[62] R. Sansom and G. Strbac, “The impact of future heat demand pathways on the economics of low carbon heating systems,” in BIEE-9th Academic conference, 19-20 September 2012, 2012.

[63] Z. Liu et al., “Accuracy analyses and model comparison of machine learning adopted in building energy consumption prediction,” Energy Exploration & Exploitation, vol. 37, no. 4, pp. 1426–1451, 2019.

[64] A. Mosavi, M. Salimi, S. Faizollahzadeh Ardabili, T. Rabczuk, S. Shamshirband, and A. R. Varkonyi-Koczy, “State of the art of machine learning models in energy systems, a systematic review,” Energies (Basel), vol. 12, no. 7, p. 1301, 2019.

[65] J.-P. Lai, Y.-M. Chang, C.-H. Chen, and P.-F. Pai, “A survey of machine learning models in renewable energy predictions,” Applied Sciences, vol. 10, no. 17, p. 5975, 2020.

[66] L. Zhang et al., “A review of machine learning in building load prediction,” Appl Energy, vol. 285, p. 116452, 2021.

[67] S. Singaravel, P. Geyer, and J. Suykens, “Component-based machine learning modelling approach for design stage building energy prediction: weather conditions and size,” in Proceedings of the 15th IBPSA conference, 2017, pp. 2617–2626.

[68] M. M. Singh, S. Singaravel, and P. Geyer, “Machine learning for early stage building energy prediction: Increment and enrichment,” Appl Energy, vol. 304, p. 117787, 2021.

[69] T. Kurek et al., “Heat demand forecasting algorithm for a Warsaw district heating network,” Energy, vol. 217, p. 119347, 2021.

[70] H. Deng, D. Fannon, and M. J. Eckelman, “Predictive modeling for US commercial building energy use: A comparison of existing statistical and machine learning algorithms using CBECS microdata,” Energy Build, vol. 163, pp. 34–43, 2018.

[71] S. Chen, Y. Ren, D. Friedrich, Z. Yu, and J. Yu, “Sensitivity analysis to reduce duplicated features in ANN training for district heat demand prediction,” Energy and AI, vol. 2, p. 100028, 2020.

[72] K. Amasyali and N. El-Gohary, “Machine learning for occupant-behavior-sensitive cooling energy consumption prediction in office buildings,” Renewable and Sustainable Energy Reviews, vol. 142, p. 110714, 2021.

[73] R. Olu-Ajayi, H. Alaka, I. Sulaimon, F. Sunmola, and S. Ajayi, “Building energy consumption prediction for residential buildings using deep learning and other machine learning techniques,” Journal of Building Engineering, vol. 45, p. 103406, 2022.

[74] H. Ghoddusi, G. G. Creamer, and N. Rafizadeh, “Machine learning in energy economics and finance: A review,” Energy Econ, vol. 81, pp. 709–727, 2019.

[75] Z. W. Geem and W. E. Roper, “Energy demand estimation of South Korea using artificial neural network,” Energy Policy, vol. 37, no. 10, pp. 4049–4054, 2009.

[76] X. Liu, B. Moreno, and A. S. García, “A grey neural network and input-output combined forecasting model. Primary energy consumption forecasts in Spanish economic sectors,” Energy, vol. 115, pp. 1042–1054, 2016.

[77] X. J. Luo, L. O. Oyedele, A. O. Ajayi, and O. O. Akinade, “Comparative study of machine learning-based multi-objective prediction framework for multiple building energy loads,” Sustain Cities Soc, vol. 61, p. 102283, 2020.

[78] E. Elbeltagi and H. Wefki, “Predicting energy consumption for residential buildings using ANN through parametric modeling,” Energy Reports, vol. 7, pp. 2534–2545, 2021.

[79] Z. Li, J. Dai, H. Chen, and B. Lin, “An ANN-based fast building energy consumption prediction method for complex architectural form at the early design stage,” in Building Simulation, Springer, 2019, pp. 665–681.

[80] L. Kannari, J. Kiljander, K. Piira, J. Piippo, and P. Koponen, “Building heat demand forecasting by training a common machine learning model with physics-based simulator,” Forecasting, vol. 3, no. 2, pp. 290–302, 2021.

[81] F. Bünning, P. Heer, R. S. Smith, and J. Lygeros, “Improved day ahead heating demand forecasting by online correction methods,” Energy Build, vol. 211, p. 109821, 2020.

[82] Y. Parfenenko, V. Shendryk, S. Vashchenko, and N. Fedotova, “The forecasting of the daily heat demand of the public sector buildings with district heating,” in Information and Software Technologies: 21st International Conference, ICIST 2015, Druskininkai, Lithuania, October 15-16, 2015, Proceedings 21, Springer, 2015, pp. 187–198.

[83] A. Li, F. Xiao, C. Fan, and M. Hu, “Development of an ANN-based building energy model for information-poor buildings using transfer learning,” in Building simulation, Springer, 2021, pp. 89–101.

[84] S. Seyedzadeh, F. P. Rahimian, I. Glesk, and M. Roper, “Machine learning for estimation of building energy consumption and performance: a review,” Visualization in Engineering, vol. 6, pp. 1–20, 2018.

[85] S. Singaravel, J. Suykens, and P. Geyer, “Deep-learning neural-network architectures and methods: Using component-based models in building-design energy prediction,” Advanced Engineering Informatics, vol. 38, pp. 81–90, 2018.

[86] A. Nutkiewicz, Z. Yang, and R. K. Jain, “Data-driven Urban Energy Simulation (DUE-S): A framework for integrating engineering simulation and machine learning methods in a multi-scale urban energy modeling workflow,” Appl Energy, vol. 225, pp. 1176–1189, 2018.

[87] S. Fathi, R. Srinivasan, A. Fenner, and S. Fathi, “Machine learning applications in urban building energy performance forecasting: A systematic review,” Renewable and Sustainable Energy Reviews, vol. 133, p. 110287, 2020.

[88] S. Seyedzadeh, F. P. Rahimian, P. Rastogi, and I. Glesk, “Tuning machine learning models for prediction of building energy loads,” Sustain Cities Soc, vol. 47, p. 101484, 2019.

[89] P. Potočnik, P. Škerl, and E. Govekar, “Machine-learning-based multi-step heat demand forecasting in a district heating system,” Energy Build, vol. 233, p. 110673, 2021.

[90] P. Zhang, “A novel feature selection method based on global sensitivity analysis with application in machine learning-based prediction model,” Appl Soft Comput, vol. 85, p. 105859, 2019.

[91] K.-Q. Shen, C.-J. Ong, X.-P. Li, and E. P. V Wilder-Smith, “Feature selection via sensitivity analysis of SVM probabilistic outputs,” Mach Learn, vol. 70, pp. 1–20, 2008.

[92] H. Sulieman and A. Alzaatreh, “A supervised feature selection approach based on global sensitivity,” Arch. Data Sci. Ser. A (Online First), vol. 5, no. 3, 2018.

[93] W. Becker, P. Paruolo, and A. Saltelli, “Variable Selection in Regression Models Using Global Sensitivity Analysis,” Journal of Time Series Econometrics, vol. 13, no. 2, pp. 187–233, 2021.

[94] Y. Guo et al., “Machine learning-based thermal response time ahead energy demand prediction for building heating systems,” Appl Energy, vol. 221, pp. 16–27, 2018.

[95] A. T. Eseye and M. Lehtonen, “Short-term forecasting of heat demand of buildings for efficient and optimal energy management based on integrated machine learning models,” IEEE Trans Industr Inform, vol. 16, no. 12, pp. 7743–7755, 2020.

[96] Z. Li, D. Friedrich, and G. P. Harrison, “Demand forecasting for a mixed-use building using agent-schedule information with a data-driven model,” Energies (Basel), vol. 13, no. 4, p. 780, 2020.

[97] S. Salcedo-Sanz, L. Cornejo-Bueno, L. Prieto, D. Paredes, and R. García-Herrera, “Feature selection in machine learning prediction systems for renewable energy applications,” Renewable and Sustainable Energy Reviews, vol. 90, pp. 728–741, 2018.

[98] T. Ahmad, H. Chen, and Y. Huang, “Short-term energy prediction for district-level load management using machine learning based approaches,” Energy Procedia, vol. 158, pp. 3331–3338, 2019.

[99] T. Ahmad et al., “Supervised based machine learning models for short, medium and long-term energy prediction in distinct building environment,” Energy, vol. 158, pp. 17–32, 2018.

[100] D. Geekiyanage and T. Ramachandra, “A model for estimating cooling energy demand at early design stage of condominiums,” Journal of Building Engineering, vol. 17, pp. 43–51, May 2018, doi: 10.1016/j.jobe.2018.01.011.

[101] A. Vaghefi, M. A. Jafari, E. Bisse, Y. Lu, and J. Brouwer, “Modeling and forecasting of cooling and electricity load demand,” Appl Energy, vol. 136, pp. 186–196, Jan. 2015, doi: 10.1016/j.apenergy.2014.09.004.

[102] N. Aghdaei, G. Kokogiannakis, D. Daly, and T. McCarthy, “Linear regression models for prediction of annual heating and cooling demand in representative Australian residential dwellings,” in Energy Procedia, Elsevier Ltd, 2017, pp. 79–86. doi: 10.1016/j.egypro.2017.07.482.

[103] M. Waite, E. Cohen, H. Torbey, M. Piccirilli, Y. Tian, and V. Modi, “Global trends in urban electricity demands for cooling and heating,” Energy, vol. 127, pp. 786–802, 2017, doi: 10.1016/j.energy.2017.03.095.

[104] J. Wang, N. C. F. Tse, T. Y. Poon, and J. Y. C. Chan, “A practical multi-sensor cooling demand estimation approach based on visual, indoor and outdoor information sensing,” Sensors (Switzerland), vol. 18, no. 11, Nov. 2018, doi: 10.3390/s18113591.

[105] E. Dulce-Chamorro and F. Javier Martinez-De-Pison, “Parsimonious Modelling for Estimating Hospital Cooling Demand to Improve Energy Efficiency,” Log J IGPL, vol. 30, no. 4, pp. 635–648, Aug. 2022, doi: 10.1093/jigpal/jzab008.

[106] M. C. Leung, N. C. F. Tse, L. L. Lai, and T. T. Chow, “The use of occupancy space electrical power demand in building cooling load prediction,” Energy Build, vol. 55, pp. 151–163, Dec. 2012, doi: 10.1016/j.enbuild.2012.08.032.

[107] K. Huang, K. P. Hallinan, R. Lou, A. Alanezi, S. Alshatshati, and Q. Sun, “Self-learning algorithm to predict indoor temperature and cooling demand from smart wifi thermostat in a residential building,” Sustainability (Switzerland), vol. 12, no. 17, Sep. 2020, doi: 10.3390/su12177110.

[108] C. Koo, S. Park, T. Hong, and H. S. Park, “An estimation model for the heating and cooling demand of a residential building with a different envelope design using the finite element method,” Appl Energy, vol. 115, pp. 205–215, Feb. 2014, doi: 10.1016/j.apenergy.2013.11.014.

[109] D. yeon Seo, C. Koo, and T. Hong, “A Lagrangian finite element model for estimating the heating and cooling demand of a residential building with a different envelope design,” Appl Energy, vol. 142, pp. 66–79, Mar. 2015, doi: 10.1016/j.apenergy.2014.12.051.

[110] J. Chambers et al., “Evaluating the electricity saving potential of electrochromic glazing for cooling and lighting at the scale of the Swiss non-residential national building stock using a Monte Carlo model,” Energy, vol. 185, pp. 136–147, Oct. 2019, doi: 10.1016/j.energy.2019.07.037.

[111] X. Li, J. Chambers, S. Yilmaz, and M. K. Patel, “A Monte Carlo building stock model of space cooling demand in the Swiss service sector under climate change,” Energy Build, vol. 233, Feb. 2021, doi: 10.1016/j.enbuild.2020.110662.

[112] M. Jakubcionis and J. Carlsson, “Estimation of European Union residential sector space cooling potential,” Energy Policy, vol. 101, pp. 225–235, Feb. 2017, doi: 10.1016/j.enpol.2016.11.047.

[113] M. Jakubcionis and J. Carlsson, “Estimation of European Union service sector space cooling potential,” Energy Policy, vol. 113, pp. 223–231, Feb. 2018, doi: 10.1016/j.enpol.2017.11.012.

[114] G. Falchetta and M. N. Mistry, “The role of residential air circulation and cooling demand for electrification planning: Implications of climate change in sub-Saharan Africa,” Energy Econ, vol. 99, Jul. 2021, doi: 10.1016/j.eneco.2021.105307.

[115] H. S. Laine, J. Salpakari, E. E. Looney, H. Savin, I. M. Peters, and T. Buonassisi, “Meeting global cooling demand with photovoltaics during the 21st century,” Energy Environ Sci, vol. 12, no. 9, pp. 2706–2716, Sep. 2019, doi: 10.1039/c9ee00002j.

[116] T. E. Morakinyo et al., “Estimates of the impact of extreme heat events on cooling energy demand in Hong Kong,” Renew Energy, vol. 142, pp. 73–84, Nov. 2019, doi: 10.1016/j.renene.2019.04.077.

[117] A. R. Day, P. G. Jones, and G. G. Maidment, “Forecasting future cooling demand in London,” Energy Build, vol. 41, no. 9, pp. 942–948, Sep. 2009, doi: 10.1016/j.enbuild.2009.04.001.

[118] P. Bezerra et al., “Impacts of a warmer world on space cooling demand in Brazilian households,” Energy Build, vol. 234, Mar. 2021, doi: 10.1016/j.enbuild.2020.110696.

[119] M. Rehfeldt, T. Fleiter, and F. Toro, “A bottom-up estimation of the heating and cooling demand in European industry,” Energy Effic, vol. 11, no. 5, pp. 1057–1082, Jun. 2018, doi: 10.1007/s12053-017-9571-y.

[120] S. Werner, “European space cooling demands,” Energy, vol. 110, pp. 148–156, Sep. 2016, doi: 10.1016/j.energy.2015.11.028.

[121] N. Pardo, K. Vatopoulos, A. K. Riekkola, and A. Perez, “Methodology to estimate the energy flows of the European Union heating and cooling market,” Energy, vol. 52, pp. 339–352, Apr. 2013, doi: 10.1016/j.energy.2013.01.062.

[122] J. Sachs, D. Moya, S. Giarola, and A. Hawkes, “Clustered spatially and temporally resolved global heat and cooling energy demand in the residential sector,” Appl Energy, vol. 250, pp. 48–62, Sep. 2019, doi: 10.1016/j.apenergy.2019.05.011.

[123] G. Pappaccogli, L. Giovannini, F. Cappelletti, and D. Zardi, “Challenges in the application of a WRF/Urban-TRNSYS model chain for estimating the cooling demand of buildings: A case

study in Bolzano (Italy)," Sci Technol Built Environ, vol. 24, no. 5, pp. 529–544, May 2018, doi: 10.1080/23744731.2018.1447214.

[124] J. Xiong, S. Guo, Y. Wu, D. Yan, C. Xiao, and X. Lu, "Predicting the response of heating and cooling demands of residential buildings with various thermal performances in China to climate change," Energy, vol. 269, Apr. 2023, doi: 10.1016/j.energy.2023.126789.

[125] R. A. Cox, M. Drews, C. Rode, and S. B. Nielsen, "Simple future weather files for estimating heating and cooling demand," Build Environ, vol. 83, pp. 104–114, Jan. 2015, doi: 10.1016/j.buildenv.2014.04.006.

[126] J. Allegrini, V. Dorer, and J. Carmeliet, "Analysis of convective heat transfer at building façades in street canyons and its influence on the predictions of space cooling demand in buildings," Journal of Wind Engineering and Industrial Aerodynamics, vol. 104–106, pp. 464–473, 2012, doi: 10.1016/j.jweia.2012.02.003.

[127] M. De Rosa, V. Bianco, F. Scarpa, and L. A. Tagliafico, "Impact of wall discretization on the modeling of heating/cooling energy consumption of residential buildings," Energy Effic, vol. 9, no. 1, pp. 95–108, Jan. 2016, doi: 10.1007/s12053-015-9351-5.

[128] J. Li, B. Zheng, K. B. Bedra, Z. Li, and X. Chen, "Evaluating the effect of window-to-wall ratios on cooling-energy demand on a typical summer day," Int J Environ Res Public Health, vol. 18, no. 16, Aug. 2021, doi: 10.3390/ijerph18168411.

[129] M. N. I. Maruf, G. Morales-España, J. Sijm, N. Helistö, and J. Kiviluoma, "Classification, potential role, and modeling of power-to-heat and thermal energy storage in energy systems: A review," Sustainable Energy Technologies and Assessments, vol. 53, Oct. 2022, doi: 10.1016/j.seta.2022.102553.

[130] H. L. Von Cube and F. Steimle, Heat pump technology. Elsevier, 2013.

[131] M. C. Barma, R. Saidur, S. M. A. Rahman, A. Allouhi, B. A. Akash, and S. M. Sait, "A review on boilers energy use, energy savings, and emissions reductions," Renewable and Sustainable Energy Reviews, vol. 79, pp. 970–983, 2017.

[132] M. Manni, A. Nicolini, and F. Cotana, "Performance assessment of an electrode boiler for power-to-heat conversion in sustainable energy districts," Energy Build, vol. 277, p. 112569, 2022.

[133] D. S. Sowmy and R. T. A. Prado, "Assessment of energy efficiency in electric storage water heaters," Energy Build, vol. 40, no. 12, pp. 2128–2132, 2008.

[134] B. R. Hughes, H. N. Chaudhry, and S. A. Ghani, "A review of sustainable cooling technologies in buildings," Renewable and Sustainable Energy Reviews, vol. 15, no. 6, pp. 3112–3120, 2011.

[135] B. Mitterrutzner, C. Z. Callegher, R. Fraboni, E. Wilczynski, and S. Pezzutto, “Review of heating and cooling technologies for buildings: A techno-economic case study of eleven European countries,” Energy, p. 129252, 2023.

[136] J. D. Boyes and N. H. Clark, “Technologies for energy storage. Flywheels and super conducting magnetic energy storage,” in 2000 Power Engineering Society Summer Meeting (Cat. No. 00CH37134), IEEE, 2000, pp. 1548–1550.

[137] M. M. Rahman, A. O. Oni, E. Gemechu, and A. Kumar, “Assessment of energy storage technologies: A review,” Energy Convers Manag, vol. 223, p. 113295, 2020.

[138] V. A. Boicea, “Energy storage technologies: The past and the present,” Proceedings of the IEEE, vol. 102, no. 11, pp. 1777–1794, 2014.

[139] D. B. Crawley et al., “EnergyPlus: creating a new-generation building energy simulation program,” Energy Build, vol. 33, no. 4, pp. 319–331, 2001, doi: https://doi.org/10.1016/S0378-7788(00)00114-6.

[140] “EnergyPlus™ Version 22.1.0 Documentation Engineering Reference,” 2022.

[141] J. Li, J. Cheng, J. Shi, and F. Huang, “Brief introduction of back propagation (BP) neural network algorithm and its improvement,” in Advances in Computer Science and Information Engineering: Volume 2, Springer, 2012, pp. 553–558.

[142] P. Wate, V. Coors, M. Iglesias, and D. Robinson, “Uncertainty assessment of building performance simulation: An insight into suitability of methods and their applications,” in Urban Energy Systems for Low-Carbon Cities, Elsevier, 2019, pp. 257–287.

[143] S. Indolia, A. K. Goswami, S. P. Mishra, and P. Asopa, “Conceptual Understanding of Convolutional Neural Network- A Deep Learning Approach,” Procedia Comput Sci, vol. 132, pp. 679–688, 2018, doi: https://doi.org/10.1016/j.procs.2018.05.069.

[144] R. Schmidt, Recurrent Neural Networks (RNNs): A gentle Introduction and Overview. 2019.

[145] Z. Xu and J. Y. Leung, “A novel formulation of RNN-based neural network with real-time updating – An application for dynamic hydraulic fractured shale gas production forecasting,” Geoenergy Science and Engineering, vol. 233, p. 212491, 2024, doi: https://doi.org/10.1016/j.geoen.2023.212491.

[146] D. B. Crawley, L. K. Lawrie, C. O. Pedersen, and F. C. Winkelmann, “Energy plus: energy simulation program,” ASHRAE J, vol. 42, no. 4, pp. 49–56, 2000.

[147] N. R. of Scotland, “Estimates of Households and Dwellings in Scotland, 2017,” 2018, National Records of Scotland.

[148] T. Boermans and C. Petersdorff, “U-Values. For better energy performance of buildings,” 2007.

[149] T. Loga, B. Stein, and N. Diefenbach, “TABULA building typologies in 20 European countries—Making energy-related features of residential building stocks comparable,” Energy Build, vol. 132, pp. 4–12, 2016.

[150] P. Baker, “Technical Paper 10: U-values and traditional buildings-In situ measurements and their comparisons to calculated values,” 2011.

[151] W. H. Organization, “Housing, energy and thermal comfort: a review of 10 countries within the WHO European Region,” 2007.

[152] A. J. Thomas, M. Petridis, S. D. Walters, S. M. Gheytassi, and R. E. Morgan, “On predicting the optimal number of hidden nodes,” in 2015 International Conference on Computational Science and Computational Intelligence (CSCI), IEEE, 2015, pp. 565–570.

[153] D. Stathakis, “How many hidden layers and nodes?,” Int J Remote Sens, vol. 30, no. 8, pp. 2133–2147, 2009.

[154] D. for Communities and L. Government, “English housing survey (Household report 2009–10),” 2011.

[155] S. Wales, “Dwelling stock estimates by local authority and tenure,” 2018.

[156] F. Filippidou, N. Nieboer, and H. Visscher, “Effectiveness of energy renovations: a reassessment based on actual consumption savings,” Energy Effic, vol. 12, no. 1, pp. 19–35, 2019.

[157] I. G. Hamilton, P. J. Steadman, H. Bruhns, A. J. Summerfield, and R. Lowe, “Energy efficiency in the British housing stock: Energy demand and the Homes Energy Efficiency Database,” Energy Policy, vol. 60, pp. 462–480, 2013.

[158] I. G. Hamilton, A. J. Summerfield, D. Shipworth, J. P. Steadman, T. Oreszczyn, and R. J. Lowe, “Energy efficiency uptake and energy savings in English houses: A cohort study,” Energy Build, vol. 118, pp. 259–276, 2016.

[159] S. N. Justine Piddington Helen Garrett Matthew Custard, “The Housing Stock of The United Kingdom,” BRE Trust, Watford, 2020.

[160] V. economics, “Energy innovation needs assessment: Building fabric,” 2019.

[161] C. Smith, “Energy Performance of Buildings Certificates Statistical, Release January to March 2021, England and Wales,” 2021.

[162] C. Watts, M. F. Jentsch, and P. A. B. James, “Evaluation of domestic Energy Performance Certificates in use,” Building Services Engineering Research and Technology, vol. 32, no. 4, pp. 361–376, 2011.

[163] S. D. Brenda Boardman Gavin Killip Mark Hinnells Christian N. Jardine Jane Palmer and Graham Sinden, “Chapter 5: Building fabric and housing stock,” Environmental Change

Institute, University of Oxford, Oxford, 2005. [Online]. Available: https://www.eci.ox.ac.uk/research/energy/downloads/40house/40house.pdf

[164] A. M. C. Tony Key Vicki Law, "The Size and Structure of the UK Property Market: End-2018 Update," IPF, London, 2019.

[165] "Facts and figures about the UK commercial property industry to year-end 2016," Property Industry Alliance, London, 2017.

[166] J. Chen, J. Yang, J. Zhao, F. Xu, Z. Shen, and L. Zhang, "Energy demand forecasting of the greenhouses using nonlinear models based on model optimized prediction method," Neurocomputing, vol. 174, pp. 1087–1100, 2016.

[167] G. Ramos Ruiz and C. Fernandez Bandera, "Validation of calibrated energy models: Common errors," Energies (Basel), vol. 10, no. 10, p. 1587, 2017.

[168] N. G. E. S. Operator, "National grid ESO: Historic demand data," 2020, UK. [Online]. Available: https://data.nationalgrideso.com/data-groups/demand

[169] "Future Energy Scenarios 2020 Interactive - August 2020," National Grid ESO, Warwick, 2020.

[170] ofgem, "Easy guide to heat pumps," 2018.

[171] J. Allison et al., "Assessing domestic heat storage requirements for energy flexibility over varying timescales," Appl Therm Eng, vol. 136, pp. 602–616, 2018.

[172] D. W. Patterson, "Artificial Neural Networks: Theory and Applications," Prentice Hall, Englewood Cliffs, 1996.

[173] S. Shanmuganathan, Artificial neural network modelling: An introduction. Springer, 2016.

[174] J. Cai, J. Luo, S. Wang, and S. Yang, "Feature selection in machine learning: A new perspective," Neurocomputing, vol. 300, pp. 70–79, 2018.

[175] G. Chandrashekar and F. Sahin, "A survey on feature selection methods," Computers & Electrical Engineering, vol. 40, no. 1, pp. 16–28, 2014.

[176] A. Saltelli et al., Global sensitivity analysis: the primer. John Wiley & Sons, 2008.

[177] P. Schober, C. Boer, and L. A. Schwarte, "Correlation coefficients: appropriate use and interpretation," Anesth Analg, vol. 126, no. 5, pp. 1763–1768, 2018.

[178] S. Parker, "Energy Consumption in the UK (ECUK) 1970 to 2020," Department for Business, Energy & Industrial Strategy, London, 2021.

[179] "Scottish Energy Statistics Hub: Energy Efficiency-End use of energy consumption." [Online]. Available: https://scotland.shinyapps.io/sg-scottish-energy-statistics/?Section=EnergyEfficiency&Subsection=DemandReduction&Chart=HHoldEnConsumption

[180] Wikimedia Commons contributors, “File:London-boroughs.svg,” Wikimedia Commons. Accessed: May 17, 2023. [Online]. Available: https://commons.wikimedia.org/w/index.php?title=File:London-boroughs.svg&oldid=530603825

[181] C. & L. G. (MHCLG) Ministry of Housing, “London Local Authority Housing Stock.” Accessed: May 17, 2023. [Online]. Available: https://data.london.gov.uk/dataset/local-authority-housing-stock

[182] “Creating benchmarks for cooling demand in new residential developments,” London, Jul. 2015.

[183] F. Zhou, C. Shen, G. Ma, and X. Yan, “Power usage effectiveness analysis of a liquid-pump-driven hybrid cooling system for data centers in subclimate zones,” Sustainable Energy Technologies and Assessments, vol. 52, Aug. 2022, doi: 10.1016/j.seta.2022.102277.

[184] Á. Andrade, Á. Restrepo, and J. E. Tibaquirá, “EER or Fcsp: A performance analysis of fixed and variable air conditioning at different cooling thermal conditions,” Energy Reports, vol. 7, pp. 537–545, Nov. 2021, doi: 10.1016/j.egyr.2020.12.041.

[185] H. & C. M. of H. C. & L. G. Department for Levelling Up, “A guide to air conditioning inspections in buildings.”